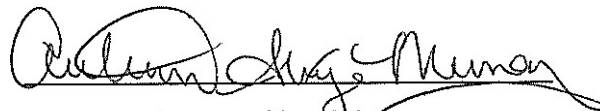
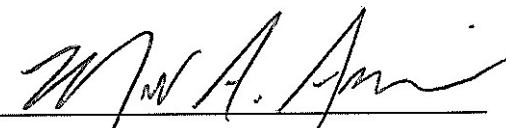


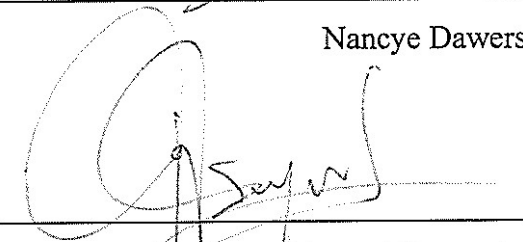
WATER EXCHANGE IN NEAR-SURFACE MARSH STRATA OF BARATARIA
BASIN, LOUISIANA AND THE IMPLICATIONS FOR SUBSIDENCE

AN ABSTRACT SUBMITTED ON THE 12th DAY OF JUNE 2020
TO THE DEPARTMENT OF EARTH AND ENVIRONMENTAL SCIENCES
IN PARTIAL FULFILLMENT OF THE REQUIRMENTS
OF THE SCHOOL OF SCIENCE AND ENGINEERING
OF TULANE UNIVERSITY
FOR THE DEGREE
OF
MASTER OF SCIENCE
BY


Autumn Skye Murray

APPROVED: 
Mead A. Allison (M.S. Director)


Nancye Dawers


Torbjörn E. Törnqvist

ABSTRACT

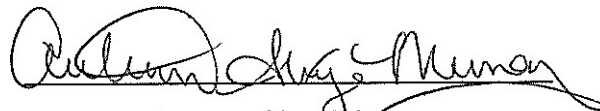
Louisiana's deltaic wetlands are threatened in the 21st century by rapid sediment subsidence that compounds climate-driven rising sea levels. Much of the coastal wetlands that fringe the Mississippi Delta are underlain by 1-2 m of an organic-rich and highly compressible surficial marsh mat substrate, where shallow subsidence is controlled by the interrelated factors of mineral and organic loading-induced compaction and the vertical accretion rate, as well as subsidence occurring deeper in the sediment column through a variety of drivers. The supply of organic and mineral sediment varies dependent on local elevation, marsh type, and hydrologic connectivity with riverine and turbid estuarine water bodies that supply mineral sediment. Shallow subsidence is thought to be a major factor driving coastal wetland land loss in the Mississippi Delta compounding other factors such as disconnection with riverine sediment sources, prolonged inundation resulting in marsh drowning, and marsh fragmentation through canal dredging. An analysis of delta-wide Coastwide Reference Monitoring Systems (CRMS), rod- surface elevation table (R-SET) data illustrates that there is also a relationship between mineral and organic loading to subsidence.

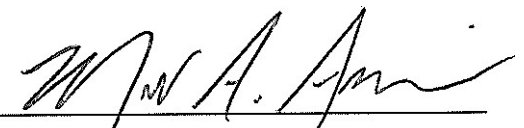
Continuously recording surface elevation tables (CR-SET) were deployed at four different marsh ecotypes within Barataria Basin, Louisiana to examine mechanisms that influence marsh surface elevation change. The CR-SET's are located adjacent to long-term CRMS stations that record vertical accretion and surface elevation change. This study examines (1) the impact of seasonal and daily meteorological changes on water levels and marsh surface elevation, aims to (2) directly measure subsidence in the wetland layer over a water year, and (3) examine the interrelationship of these factors

with marsh stratigraphy. Results show that marsh elevation fluctuations are correlated with subsurface groundwater levels controlled by water level in nearby canals. The most organic-rich site showed a higher correlation with water levels and larger fluctuations of the surface elevation on diel and monthly timescales. Surface fluctuations are a direct response to lateral draining and filling of the marsh vadose zone, with frequency and degree of water exchange and surface elevation variation controlled by distance from the nearest canal edge and subsurface stratigraphy. Shallow subsidence rates calculated by previous studies from CRMS vertical accretion and total elevation change measurements, are revised for the fresh, intermediate, brackish, and saline marsh study sites using a normalization for a mean water level—the revised subsidence rates are not greatly influenced by the marsh expansion-contraction process. Marsh fragmentation through canal cutting and interior ponding increases linear extent of marsh edge, creating increased vadose spatial extent and frequency of exposure to air-filled pores in a given marsh. A hypothesis is explored herein that suggest that this increase in marsh edge in Barataria and other degrading Mississippi Delta sub-basins can result in increased peat oxidation that may have increased compactional subsidence in recent decades.

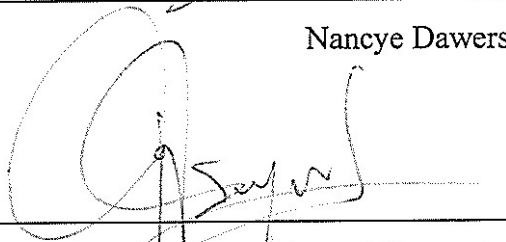
WATER EXCHANGE IN NEAR-SURFACE MARSH STRATA OF BARATARIA
BASIN, LOUISIANA AND THE IMPLICATIONS FOR SUBSIDENCE

AN ABSTRACT SUBMITTED ON THE 1st DAY OF AUGUST 2020
TO THE DEPARTMENT OF EARTH AND ENVIRONMENTAL SCIENCES
IN PARTIAL FULFILLMENT OF THE REQUIRMENTS
OF THE SCHOOL OF SCIENCE AND ENGINEERING
OF TULANE UNIVERSITY
FOR THE DEGREE
OF
MASTER OF SCIENCE
BY


Autumn Skye Murray

APPROVED: 
Mad A. Allison (M.S. Director)


Nancye Dawers


Torbjörn E. Törnqvist

ACKNOWLEDGEMENTS

I would like to thank the Department of Earth and Environmental Sciences and the Department of River Coastal Science and Engineering for giving me the opportunity to study Earth processes at Tulane University. I would also like to thank Dr. Mead Allison for his continued support and tireless effort throughout this project. I could not have asked for better mentor. Thank you for pushing me to become a better scientist.

I would like to give a very special thanks to Marie Mathews for her overwhelming support with field work and all things graduate school. She has been a great friend and colleague throughout this experience. I would also like to thank the graduate students of Earth and Environmental Sciences for everlasting friendships and great memories in New Orleans that I will carry with me throughout my life.

I want to dedicate this thesis to my wonderful parents, Todd and Angela Murray, my boyfriend Clay Jordan, my best friend Sydney Pozzuto and to the rest of my family. Mom and Dad, I cannot thank you enough for instilling me with courage, determination, and natural curiosity. Clay, thank you for supporting me not only through graduate school but throughout our lives together. You are selfless, caring, and one of my main motivators. Sydney, you always pick me up when I am down and fuel me when I am up.

Thank you.

TABLE OF CONTENTS

| | |
|--|----|
| ACKNOWLEDGEMENTS..... | ii |
| LIST OF TABLES..... | v |
| LIST OF FIGURES..... | vi |
| 1. INTRODUCTION..... | 1 |
| 2. BACKGROUND..... | 6 |
| 2.1 Subsidence in Coastal Louisiana..... | 6 |
| 2.2 Controls on Marsh Productivity and Sustainability..... | 8 |
| 3. BARATARIA BASIN STUDY AREA | 12 |
| 3.1 Geologic Evolution of the Basin..... | 12 |
| 3.2 Accretion and Subsidence Rates in Barataria Basin..... | 16 |
| 3.3 Confinement of the Mississippi River..... | 20 |
| 3.4 Meteorology and Hydrodynamics..... | 22 |
| 3.4.1 Astronomical and Meteorological Tides..... | 22 |
| 3.4.2 Ecoregions and Historical Wetland Loss in Barataria Basin | 24 |
| 4. METHODS..... | 28 |
| 4.1 Site Selection..... | 28 |
| 4.2 Continuously Recording Rod Sediment Elevation Table (CR-SET) | 30 |
| 4.3 Calculating Site Marsh Elevation..... | 37 |
| 4.4 Sediment Coring..... | 39 |
| 4.5 Laboratory Methods..... | 40 |
| 4.5.1 Core Bulk Properties..... | 40 |
| 4.5.2 Granulometry..... | 41 |
| 4.5.3 Organic Analysis..... | 42 |
| 4.5.4 Sediment Accumulation Rates..... | 42 |
| 4.6 CRMS Surface Elevation Correction..... | 44 |
| 5. RESULTS..... | 45 |
| 5.1 Marsh CR-SET Elevation Sensors..... | 45 |
| 5.1.1 Seasonal and Diel Fluctuations to the Marsh Surface..... | 54 |

| | |
|--|-----|
| 5.1.2 Water Level Statistics..... | 56 |
| 5.2 Soil Properties and Stratigraphy..... | 59 |
| 5.2.1 Core Stratigraphy..... | 59 |
| 5.2.2 Soil Properties..... | 63 |
| 5.2.3 Radionuclide-derived Sediment Accumulation Rates..... | 66 |
| 6. DISCUSSION..... | 70 |
| 6.1 Marsh Expansion and Contraction: Mechanisms and Controls..... | 70 |
| 6.2 Implications for Subsidence in Louisiana Coastal Wetlands..... | 84 |
| 7. CONCLUSIONS..... | 102 |
| APPENDICES..... | 103 |
| APPENDIX A: Ultrasonic Sensor Experiment..... | 103 |
| APPENDIX B: Marsh Surface Elevation Interpretation..... | 105 |
| APPENDIX C: 2018 Vertical Accretion Measurements..... | 109 |
| APPENDIX D: Distance from CR-SET to CRMS Water Level Gauge.... | 114 |
| APPENDIX E: Core Descriptions..... | 118 |
| APPENDIX F: D50 Grain Size..... | 122 |
| APPENDIX G: Total Organic Matter, Detrital, and Live Rooting..... | 126 |
| APPENDIX H: Lead-210 and Cesium-137 Activity and Errors..... | 130 |
| LITERATURE CITED..... | 134 |

LIST OF TABLES

Table 1. Surface Elevation Change (SEC), Vertical Accretion rate (VA), Shallow Subsidence rate (SS), and Relative Sea Level Rise rates, and R-SET Foundation Depth depths for the Four sites.

Table 2. Monthly and Hourly Marsh Elevation Ranges and Standard Deviation at the four study sites.

Table 3. CR-SET/CRMS site distances from the nearest canal and from the NOAA Grand Isle Gauge

Table 4. Longer-Term (WY 2012-2019) and Short-Term (WY 2019) Average Water Elevations at the four study sites within Barataria Basin

Table 5. Organic Sedimentary Facies of Cores taken in Barataria Basin, Louisiana

Table 6. Organic Matter Content (%) for the Four Study sites in Barataria Basin

Table 7. Lead-210, Cesium-137, and CRMS VA rates compared linearly, consolidated to 75% porosity assuming 25% mineral at 2.65 g/cm^3 , and 75% consolidation of porosity assuming 25% is organic (1.24 g/cm^3) and mineral sediment

Table 8. Bulk Properties Potentially Affecting the Permeability of Marsh Soils

Table 9. Corrected Surface Elevation Change (SEC) measurements and Shallow Subsidence (SS) rates

Table 10. Core stratigraphy sectioned into; the surficial VA (0-6 cm), the Vadose Zone (6 cm to 5th percentile water elevations from 2012-2019), and the Phreatic Zone (base of Vadose zone to end of 87 cm core) at each site

LIST OF FIGURES

- Figure 1.** CRMS Vertical Accretion vs. Shallow Subsidence Rates
- Figure 2.** Geologic Map of Barataria Basin, Louisiana
- Figure 3.** Late Holocene evolution of the Mississippi River Delta Plain
- Figure 4.** Surficial Peat Isopach Map
- Figure 5.** Vertical Accretion Rates in Barataria Basin
- Figure 6.** Shallow Subsidence Rates in Barataria Basin
- Figure 7.** Shifts in Wetland Ecotypes in Barataria Basin
- Figure 8.** Progressive Land Loss Map of Barataria Basin
- Figure 9.** Study Sites and Wetland Habitats in Barataria Basin
- Figure 10.** Schematic of High Resolution CR-SET Design
- Figure 11.** CR-SET Sensor Specifications
- Figure 12.** Photograph of CR-SET
- Figure 13.** Marsh Elevation Interpretation
- Figure 14.** Hourly Marsh Surface Elevations plotted against Water Elevation
- Figure 15.** Flooding Events recorded by Linear Position Sensor
- Figure 16.** Cold Fronts at the Saline Site
- Figure 17.** Cold Fronts at the Intermediate Site
- Figure 18.** Diurnal Tidal Signal vs. Cold Front Signal at the Brackish Site
- Figure 19.** Linear Relationship between Water Level and Marsh Elevation
- Figure 20.** Marsh Elevation Response at the Fresh Site
- Figure 21.** Monthly Averaged Marsh Elevation
- Figure 22.** Hourly Averaged Marsh Elevation
- Figure 23.** Monthly Averaged Water Elevations (WY 2019)
- Figure 24.** Monthly Averaged Water Elevations (2012-2019)
- Figure 25.** Stratigraphic Columns of the D₅₀ Granulometry
- Figure 26.** Stratigraphic Columns of Organic Matter Content
- Figure 27.** Downcore Porosity at each site
- Figure 28.** Relationship between Detrital Organic Matter, Live Rooting, and Mineral Content with Depth at the Four Study Sites

Figure 29. Downcore activities and accumulation rates derived from radionuclide dating of ^{210}Pb and ^{137}Cs for the Fresh and Intermediate sites

Figure 30. Downcore activities and accumulation rates derived from radionuclide dating of ^{210}Pb and ^{137}Cs for the Brackish and Saline sites.

Figure 31. Schematic Representation of Internal Water Exchange during Marsh Filling

Figure 32. Schematic Representation of Internal Water Exchange while Marsh is submerged

Figure 33. Schematic Representation of Internal Water Exchange during Marsh Draining

Figure 34. Variability in Marsh Surface Elevation

Figure 35. The Interpreted Filling, Buoyancy, and Draining Phases of the Marsh at the Saline Site recorded by the Linear Position Sensor

Figure 36. Corrected CRMS Surface Elevation Change (SEC) at the four study sites

Figure 37. Weekly Averaged and Normalized Surface Elevation Change CR-SET Measurements throughout the study period for the Fresh and Intermediate sites

Figure 38. Weekly Averaged and Normalized Surface Elevation Change CR-SET Measurements throughout the study period for the Brackish and Saline sites

Figure 39. Long-term (WY 2012-2019) and Short-Term (WY 2019) Site-Specific Water Elevation Statistics for the Fresh and Intermediate sites from CRMS Water Gauges

Figure 40. Long-term (WY 2012-2019) and Short-Term (WY 2019) Site-Specific Water Elevation Statistics for the Brackish and Saline sites from CRMS Water Gauges

Figure 41. Detrital Organic Matter Storage Rate compared with the Mineral Flux at the four sites

Figure 42. Schematic plots of Organic Stratigraphy and Percent Organic Matter compared with Water Elevation Statistics

Figure 43. Land-Water Area Difference Maps from 1932-1956, 1956-1977, 1977-1987, and 1987-2016 from USGS Data

1. INTRODUCTION

Deltaic wetlands are some of the most resilient and dynamic ecosystems on the planet. These unique environments host an array of exclusive species in swamps and marshes that form the main subaerially emergent environments in the growth of deltas in the late Holocene (Stanley and Warne, 1994). In the Mississippi Delta in Louisiana, these diverse ecosystems are threatened in the 21st century by natural drivers such as subsidence, sea level rise, and storm erosion (Cahoon and Reed, 1995; Törnqvist et al., 2008; Yuill et al. 2009; Kolker et al., 2011; Morton and Barras, 2011; Allison et al., 2016). These negative factors are compounded by a host of deleterious anthropogenic activities which have incised the marsh surface for access and navigation, limited river-delivered sediment supply, increased rates of relative sea level rise, and drained and converted wetlands for settlement and agriculture. Freshwater to saline marsh wetlands make up 41% of coastal wetlands in Louisiana and have experienced ~5,000 km² of land loss since 1932 (Turner and Gosselink, 1975; Couvillion et al., 2011). These unique ecosystems provide important services to coastal communities including commercial and recreational fishing (Coastal Protection and Restoration Authority of Louisiana, 2017), and provide a buffer on the impact of extreme storms by slowing water velocities, damping waves, and decreasing storm surge heights (Craig et al., 1979).

Within the Mississippi Delta, there is presently a negative balance in the combined mineral and organic accretion to the relative rate of sea level rise (Reed, 1989; Kesel, 1989; Cahoon and Reed, 1995). Subsidence, coupled with accelerating sea level rise, which together define the rate of relative sea level rise, is recognized as a major mechanism responsible for transforming Louisiana deltaic marshes to open water.

However, of the four key mechanisms that define marsh sustainability mentioned above (e.g., mineral accretion rate, organic accretion rate, subsidence rate, and rising ocean level), ocean levels are the only parameter that is at all constrained at a site-specific level in coastal Louisiana (Syvitski et al., 2009; Kolker et al., 2011). Mineral and organic accretion rates are plant species-specific and highly spatially and temporally variable due to the microtopography of the local marsh, which influences the hydroperiod (Hatton et al., 1983; Nyman et al., 1990; Cahoon and Reed, 1995; Reed, 2002; McKee et al., 2011), proximity of the marsh to water bodies (sediment sources), seasonal resuspension of sediments through storms and cold fronts (Cahoon et al., 1995; Booth et al., 2000), and variable stem densities that trap suspended sediments (Gleason et al., 1979; Stumpf, 1983). In general, however, increased flooding causes a complex response in that it provides increased mineral sediment supply, and also supplies increased nutrients that can stimulate autochthonous aboveground (stems and leaves) and belowground (roots) organic deposition rate, but can also cause plant stress. Previous studies have shown that when relative sea level (RSL) rise exceeds the long-term rate of mineral and organic accretion, a tipping point occurs and marshes transition to drowning and fragmentation (Nyman et al., 1993; DeLaune et al., 1994; Cahoon and Reed, 1995). RSL rise rates from a paleo marsh record indicate that ancient Holocene marshes of the Mississippi River Delta (MRD) were unable to keep pace with RSL rise rates greater than 3 mm per year causing marshes to disappear within 200 years (coupled with the tidal regime and subsidence that hinders elevation capital; Törnqvist et al., 2020).

Subsidence, coupled with altered hydrology due to canalization and limited sediment supply from levees and flood control structures, is thought to have magnified land loss

rates throughout coastal Louisiana (Reed, 1989; Blum and Roberts, 2009). Methods for calculating subsidence rates in these wetland areas, however, are not well constrained and evidence to date suggests considerable variability in space and time. Site-specific measurements of subsidence rates to date using continuously operating reference (CORS) GPS stations (Morton and Bernier, 2010; Byrnes et al., 2019) provide incomplete measurements of total subsidence by excluding (shallow) subsidence occurring above the benchmark foundation depth which can be 10's of meters in the Mississippi Delta region (Keogh and Törnqvist, 2019). Shallow subsidence measurement methods such as the use of rod-surface elevation tables (R-SET; Jankowski et al., 2017; Nienhuis et al., 2017) potentially capture shallow subsidence from the sediment interval above their foundation depth but exclude deep subsidence and are difficult to use for spatial mapping due to variable foundation depths from site-to-site. Repetitive aerial and satellite surveys by light detection and ranging (LiDAR) or interferometric synthetic aperture radar (InSAR) provide wide spatial coverage of high-resolution ground elevation change and have proven useful for measuring subsidence in high backscatter urban areas like greater New Orleans (Dixon et al., 2006; Jones et al., 2016). However, these methods have difficulties in wetlands induced by (1) low backscatter intensity wetland surfaces, (2) presence of seasonally variable vegetation canopies, (3) temporally variable water inundation, and (4) ground elevation is impacted by accretion and erosion as well as subsidence (Couvillion et al., 2013; Couvillion et al., 2017).

Another complicating factor in understanding the importance and linkage between subsidence and organic + mineral accretion and marsh sustainability in coastal Louisiana is the role of canal cutting through wetlands that was widely practiced in the 1930's

through the 1970's. Construction of relatively deep canals was conducted for oil and gas exploration activities such as canal dredging for pipeline installment and access to drilling sites (Deegan et al., 1984). Navigation canals were also cut through wetlands to improve navigation to community's further inland. Canal cutting and marsh fragmentation through interior ponding (Penland et al., 2002) are hydrologically altering the coast and are believed to be responsible for accelerating marsh deterioration from natural mechanisms such as marsh edge erosion from waves (Hatton et al., 1983; Salinas et al., 1986). From 1955 to 1978, Deegan et al., 1984 found that 25-39% of land loss in the Mississippi Delta Plain was directly related to canal and spoil construction, and to slumping-induced lateral expansion of canals. Increasing water levels and altered hydrology has caused salinity intrusion into the upper reaches of the coast affecting bald cypress swamps (Chambers et al., 2000), which has led to restoration projects, e.g., the Davis Pond and Caernarvon Freshwater Diversions, aimed at counteracting saltwater intrusion. To counteract land loss in Barataria Basin the State of Louisiana has authorized and is moving forward with the design and permitting of a large sediment diversion (Mid-Barataria Sediment Diversion) that will deliver river water, sediment, and nutrients into degraded brackish-saline marshes.

What remains poorly constrained in Barataria Basin and other Louisiana coastal wetland areas is the role that the organic-rich coastal marsh layer, that is typically 1-2 m thick across this interdistributary deltaic basin, plays in subsidence. A goal of the present thesis is to test whether a significant portion of the overall subsidence rates at four different marsh ecotypes is occurring within this shallowest portion of the sediment column. Preliminary results from CRMS data show a correlation between vertical

accretion and subsidence within the near-surface of Barataria Basin (Figure 1). If loading of organic and mineral material causes compaction of near-surface sediments, it is also important to understand the sedimentological properties of the vertical accretion that cause compaction. It is hypothesized for the present study that differing plant communities, flooding frequencies and depths, and soil types control both the organo-mineralic sediment supply and preservation, and the resulting compactional subsidence. Further, it is hypothesized that the historical changes in riverine hydrologic connectivity, canalization, and progressive degradation of once-continuous wetland areas, has potentially altered subsidence rates in the shallow subsurface. It is particularly key to understand these effects now prior to the opening of a major coastal restoration project (i.e., The Mid-Barataria Sediment Diversion) in the Basin to gauge how existing wetlands in the receiving area will respond to the additional mineral loading and changing flooding frequency and magnitude. A significant portion of the predicted benefit of the Mid-Barataria Sediment Diversion (and other riverine sediment diversions in coastal Louisiana) is that over the project's 50-year lifespan, in addition to new emergent land, the project will also rejuvenate existing wetlands that would have disappeared under predicted relative sea level rise rates without the increased mineral sediment accretion that will be produced by the diversion (Coastal Protection and Restoration Authority of Louisiana, (2017).

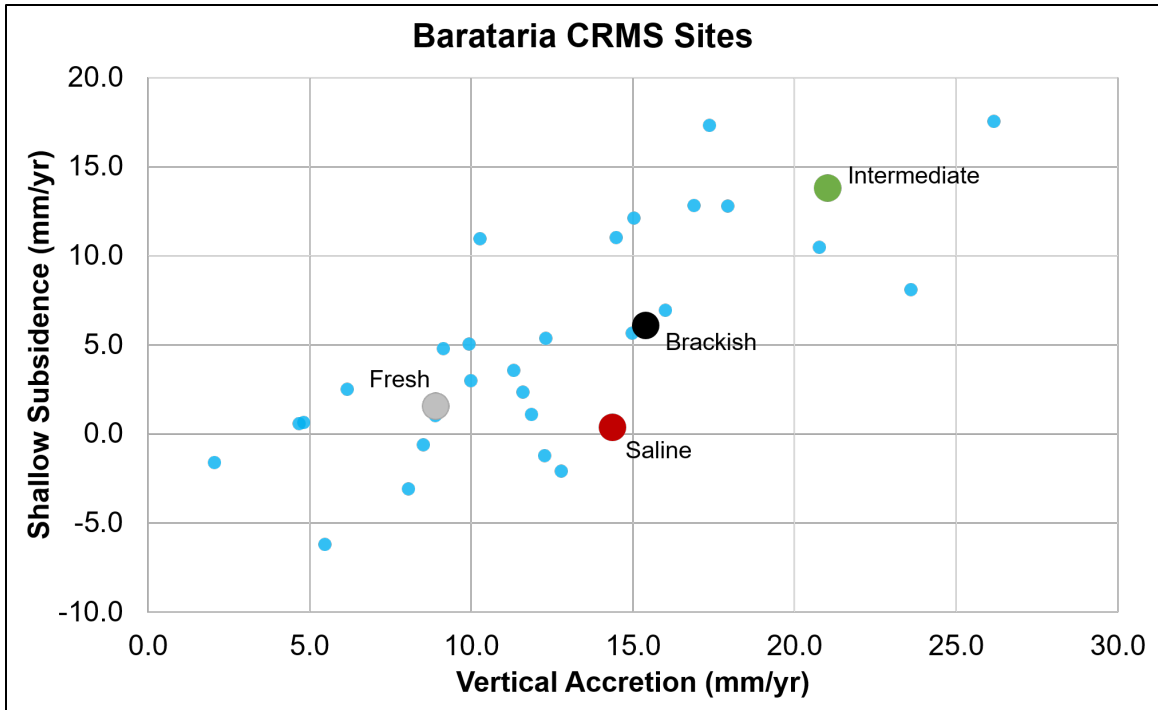


Figure 1. Vertical accretion rates and shallow subsidence rates calculated from data collected by the Coastal Reference Monitoring Station (CRMS) network within Barataria Basin, Louisiana. The four numbered sites refer to the locations occupied in the present study and are represented by their CRMS station number. These calculated rates follow the methods described in Jankowski et al. (2017).

2. BACKGROUND

2.1. Subsidence in Coastal Louisiana

Land loss throughout coastal Louisiana is influenced by subsidence from both anthropogenic and natural geologic processes that contribute to accelerated relative sea level rise (Dokka, 2006; Allison et al., 2016; Jones et al., 2016). Dividing the major contributor(s) to land loss through a particular subsidence mechanism is often difficult and highly debated due to the juxtaposition between physical, chemical, and biologic processes that drive or influence land subsidence. Subsidence is complex because multiple mechanisms occur within different depth intervals and operate over a wide range of time periods (Yuill et al., 2000; Allison et al., 2016). These mechanisms range from

deep geologic processes such as glacial isostatic adjustment, tectonic subsidence, and faulting (Dokka et al., 2006; Yuill et al., 2000; Gagliano et al., 2003; Dokka et al., 2011; Shen et al., 2016), to sediment compaction of thick and highly porous, organic-rich late Holocene deltaic sediments (Penland et al., 1990; Roberts et al., 1994; Törnqvist et al., 2008). Anthropogenic-related subsidence such as deep subsurface fluid withdrawal of hydrocarbons (Morton et al., 2002) and shallower groundwater withdrawal (Jones et al., 2016) are also argued to have increased subsidence rates in certain areas of the Mississippi Delta. Kolker et al. (2011) also point out a temporal association between peak wetland loss rates and peak hydrocarbon mining in the wetlands in the late 20th century from tide gauge records.

Initial attempts to map subsidence throughout coastal Louisiana (Nienhuis et al., 2017) have suggested that multiparameter subsidence, combined with stratigraphic differences on local scales, may be responsible for observed high spatial variability in shallow subsidence rates (e.g., subsidence within the Holocene sediment interval). Dewatering of organic-rich soils due to overburden loading of the Holocene sediment package are thought to be a main driver of subsidence rates in the Delta (Roberts et al., 1994; Byrnes et al., 2019), although Bridgeman et al. (2018) demonstrate that a 40-meter-thick Holocene core in Barataria Basin has a long-term subsidence rate of only 0.4 mm per year, and Jankowski et al., (2017) show how the spatial variability in subsidence rates across the Mississippi River Delta and Chenier Plain is not well correlated with Holocene sediment thickness. Tide gauge records have also been utilized to quantify rates of sea-level rise and infer subsidence rates across the coast (Morton and Bernier, 2010; Kolker et al., 2011; Keogh and Törnqvist, 2019) although tide gauges are benchmarked at

variable (> 10 m) or unknown depths that only capture subsidence processes below the foundation depth (Keogh et al., 2019). Tide gauges do illustrate that sea levels fluctuate on seasonal and interannual timescales due to atmospheric pressure and thermal expansion of GOM waters (Kolker et al., 2011). Together this evidence suggests that on short (years to centuries) timescales, subsidence of Holocene deposits in coastal Louisiana is influenced by multiple processes related to sediment composition and loading rates, but may also be influenced by water loading on diel, seasonal and interannual timescales; and cyclic water level changes may play a role in all these.

2.2 Controls on Marsh Productivity and Sustainability

Coastal marshes are resilient systems that are able to keep pace up to a point with sea level rise through landward facies transgression, and vertical accretion of organic and trapped mineral materials (Kosters, 1989). The sustainability of coastal marshes relies on the accretion rate of organic and inorganic sediments at rates equivalent to, or faster than, the rate of relative sea level rise (Kennish, 2001; Reed, 2002; DeLaune et al., 2002). Surface elevation gain is directly influenced by the local hydrology which serves as a major mechanism for sediment deposition, resuspension of fine-grained sediments, and biomass production (DeLaune et al., 2002). Furthermore, mineral sediment deposition promotes root growth through supplying nutrients, contributes to the overall allochthonous and autochthonous accretion, and influences organic matter decomposition rates by increasing soil aeration (DeLaune et al., 1981; Baldwin et al., 1998; Mitsch and Gosselink, 2015). In general, marshes in equilibrium with local sea level are capable of increased vertical accretion in rising sea level conditions through the additional flooding

stimulating biomass production and trapping increased quantities of nutrient-rich mineral particles. These accretion processes are variable between marsh communities and depend upon factors such as hydroperiod, tidal range, and salinity (Cahoon and Reed, 1995; Morris et al., 2002; DeLaune et al., 2003). Marshes can “drown” when relative sea level rise rates, even with the stimulating effects of increased hydroperiod nutrient supply on organic and mineral accretions, still exceeds the total vertical accretion rate (Törnqvist et al., 2020).

The rate of autochthonous organic matter accumulation defines the vertical accretion of a marsh in concert with detrital mineral sediment and allochthonous organic matter deposition during marsh flooding. Autochthonous biomass production takes place both aboveground and belowground. Above ground biomass is the mass of leaves and stems per area for a specific plant species (Mitsch and Gosselink, 2015). Below ground biomass production is the live root mass: as roots grow they can also potentially increase marsh surface elevation by displacing the soil laterally. In coastal Louisiana, both above and below-ground biomass production show a strong seasonal component but vary in amount with species composition (Hopkinson et al., 1978).

The sustainability of coastal marshes is threatened by the compaction of organic-rich near- surface sediments (peat) that can account for 5 mm/yr of subsidence on millennial time scales, and up to 10 mm/yr on timescales of a decade to a century (Meckel et al., 2006; Törnqvist et al. 2008; Syvitski et al., 2009; Cahoon et al., 2011). Subsidence related to peat compaction is highly variable and depends on the type of peat, rate of decomposition, density (dependent on plant fiber content) and thickness of peat layers (Mitsch and Gosselink, 2015), draining depth, climate, and land use history

(Schothorst, 1982; Stewart, 1994; Wösten et al., 1997). In the MRD, early settlers transformed coastal Louisiana from swamps (containing bottomland hardwood forests) into agricultural land by the drainage of organic-rich soils (Conner and Day, 1987), therefore, the consolidation, compaction, oxidation, and shrinkage of organic soils resulting from these practices could be ongoing.

Species distributions in coastal Louisiana marshes are spatially heterogeneous due to centimeter-scale changes in elevation that influence the frequency and duration of inundation between within each marsh ecotype (LA CWCS, 2005). Fresh marshes in coastal Louisiana have water salinities under 2 ppt (average 0.5-1 ppt) and the most dominate plant species is *Panicum hemitomon* (maidencane) whereas, other species include *Alternanthera philoxeroids* (alligator weed), *Eleocharis* (spikesedge), and *Spartina Patens* (wire grass) (LA CWCS, 2005). Fresh marshes of coastal Louisiana contain the highest amounts of soil organic matter (Chabreck, 1972). Intermediate and brackish marshes are species diverse due to the range of salinities (2 to 10 ppt) and irregular tidal regimes (Chabreck, 1972). Dominant plant species include *Spartina patens*, along with a mix of fresh and brackish species. Brackish marshes contain many salt-tolerant species such as *Spartina patens*, *Distichlis spicata* (salt grass), *Spartina alteriflora* (smooth cordgrass), and *S. cynosuroides* (big cordgrass) (Hatton et al., 1983; LA CWCS, 2005). Saline marshes are regularly tidally flooded, and are dominated by salt grasses such as *Spartina alteriflora*, *S. patens*, and *Batis maritima* (salt wort). Mean salinities in this marsh type are 16 ppt (6- 22 ppt) (LA CWCS, Dec 2005) and contains the lowest soil organic matter content (Chabreck, 1972).

Coastal marshes are most productive when there is also sufficient terrigenous sediments (delivered by riverine input) to provide mineral material, promoting aboveground (and belowground) vegetation growth which further increases sediment trapping efficiencies by decreasing tidal water velocities (Stumpf, 1983). Local hydrologic conditions are largely correlated with fluctuations in surface elevation from the shrink and swell of organic-rich soils and rates of sediment deposition (Cahoon et al., 2011). The rate of mineral sediment deposition is temporally and spatially complex in coastal Louisiana due to seasonal changes in sediment supply from winter fronts, episodic hurricanes, and riverine flooding (Baumann, 1980; Cahoon and Turner, 1987; Reed, 1989). Historical changes to the basin's tidal range through bay expansion as marshes have retreated with rising sea level and wetland edge erosion (Fitzgerald et al., 2007) has altered mineral sediment deposition and hydroperiod, which in turn is an increasing stressor potentially causing marsh collapse (Hatton et al., 1983; Reed, 1995).

Differing marsh plant species are tolerant of certain salinity and inundation regimes which are related to the local marsh elevation, and thus controls the rate of above and below ground biomass production (DeLaune et al., 1983; Nyman et al., 1990; Mitsch and Gosselink, 2015). Marshes below Mean Water Level (MWL) are most susceptible to marsh collapse and deterioration through increased inundation frequency and salinities. Couvillion and Beck (2013) find a range of water depths can lead to a potential for marsh collapse. The range of water depths, according to MWL derived from NAVD88 water levels from CRMS data, varies from 30.7 to 35.8 cm for an intermediate marsh, to 20 to 25.6 cm for a brackish marsh, and 16.9 to 23.5 cm MWL for a saline marsh. Therefore,

marshes that maintain MWL above these ranges should be resilient enough to battle rising relative sea level (ocean level + subsidence).

To add more complexity to marsh productivity and sustainability, other factors have been identified in coastal Louisiana such as lateral retreat of marshes associated with canal expansion (Penland et al., 2002), marsh edge erosion from storms (Wilson and Allison, 2008), and pond creation and expansion from increased tidal prisms in which wind- fetch waves erode marsh shorelines further exaggerates land loss (FitzGerald et al., 2007; Ortiz et al., 2017). Large hurricanes such as Rita and Katrina experienced in 2005 have shown to erode vast amounts of marshes contributing to a total loss of 562 km² with storm surges 5.5 and 8.0, respectively (Barras et al., 2006).

3. BARATARIA BASIN STUDY AREA

3.1 Geologic Evolution of the Basin

Barataria Basin is a deltaic interdistributary basin located in southeastern Louisiana, south of New Orleans, bounded on the east by the Mississippi River and on the west by the abandoned Lafourche distributary lobe. Connectivity with the Gulf of Mexico (GOM) is through a degraded barrier island chain across southern Barataria Bay, (Figure 2). Mississippi Delta interdistributary basins are relatively low energy, shallow (<10 m) environments that receive mineral sediment episodically by strong storms and riverine (overbanking and crevasse) flood pathways (Frazier et al., 1967; Hatton et al., 1983). Seasonal flushing of water and sediment through a series of inlets exchange large amounts of water and sediment with the inner shelf (Fitzgerald et al., 2004). Barataria Pass is the main inlet and exports over 8,800 t of suspended sediment within one tidal cycle, and exchanges 66% of the total water entering, and exiting the estuary (Marmer,

1948; Fitzgerald et al., 2004; Li et al., 2011). The Basin was created by the deposition and subsidence of stacked deltaic complexes from the St. Bernard delta lobe (4.0-1.7 kya), the Lafourche delta (1.6-0.6 kya), and by the present-day Plaquemines-Balize delta (Kosters et al., 1993; Hijma et al., 2017; Bomer et al., 2019) (Figure 3).

During deglaciation of the Last Glacial Maximum at about 18-20 kya, incision of the Mississippi Valley by the Mississippi River served as a conduit for post-glacial sediments and meltwater into the GOM (Blum and Roberts, 2012). Once sea level began to rise at about 12 kya, the Mississippi River transformed from a braided river system into a meandering river system and began infilling previously incised river channels and the present continental shelf was transgressed. Holocene deltaic formation began around 7.5 kya (Hijma et al., 2017), coincident with a slowdown in the rate of sea level rise with the progradation of the multiple deltaic complexes that are relic landscape features of the present delta plain.

Barataria Basin is composed of Quaternary alluvium that is present in the northwestern regions of the basin and through distributary networks (Figure 2). The underlying stratigraphy of Barataria Basin is stacked, compressible organic-rich marsh deposits and sandy to clay-rich terrigenous distributary deposits as a result of autogenic and allogenic drivers of delta avulsion which cause channel abandonment, shifts in the depocenters of sediment deposition, and land subsidence/marsh accretion (Frazier et al., 1967; Kosters et al., 1993). When the main river channel avulses, progradation of delta front facies, composed of fine-grained silts and clays are deposited into low elevation shallow bays. Distributary channels deposit well-sorted mouth-bar sands atop of the delta front deposits. The mouth bar sands are generally overlaid with fine-grained overbank

deposits, which are then capped with marsh sediments comprised of intercalated silts, clays, peats, nonorganic floodplain and natural levee deposits (Fitzgerald et al., 2004; Chamberlain et al., 2018; Frazier 1967; Bommer et al., 2019).

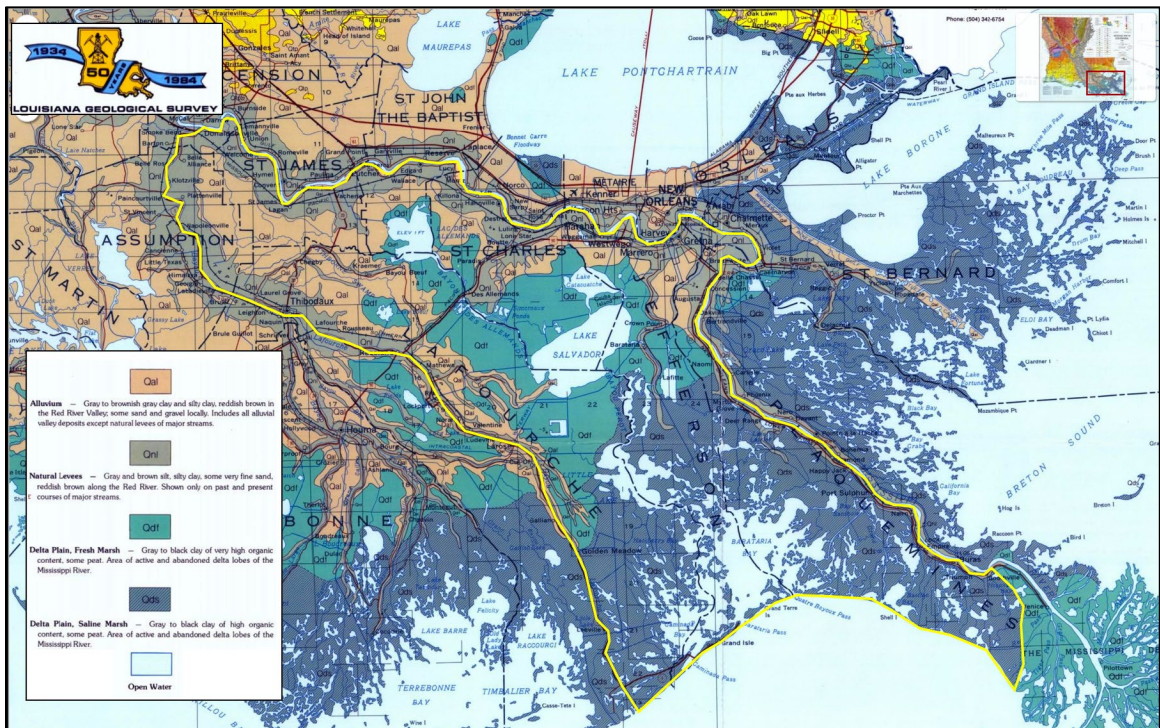


Figure 2. Geologic map of Barataria Basin (outlined in yellow). Map is modified from the Louisiana State Geological Survey (1984). Surficial Quaternary sediments across Barataria Basin are comprised of alluvial silts, sands, and gravels within the Northwestern parts of the basin in abandoned distributary channels and relict natural levees (Qal and Qnl). Further to the southeast, these grade into interdistributary wetland highly organic silts and clays mixed with peats (Qdf). The southern-most reaches of the Basin is comprised of bay bottom highly organic clays and peats (Qds).

Natural levee deposits are found within the vicinity of abandoned distributary channel networks, specifically around the Lafourche distributary and along the Mississippi River. From the center of the basin, extending towards the southeast, the basin is composed a mixture of organic-rich marsh sediments. Each subdelta has a specific thickness due to the amount of sediment supply and changes to base level.

Holocene deltaic deposits within Barataria Basin (BB) range from maximum thicknesses of 60 meters near Grand Isle to a minimum of 8 meters in the northern reaches of the basin (Kosters et al., 1993; Byrnes et al., 2019). During interdistributary phase such as the present, organic-rich marsh sediments accumulate between natural levee deposits of varying thicknesses. The spatial pattern of organic-rich facies (>75% organic matter) are the greatest in the northern parts of the basin from Lake Salvador through Little Lake, and decrease towards the GOM (Kosters et al., 1993). The distribution of organic-rich marsh/wetland surficial layer in BB is laterally discontinuous as the accumulation of peat relies on subsidence rate, sediment deposition rate, and inundation (Bailey, 1983). Peat accumulates in areas that are relatively isolated from clastic sedimentation, where the thickest deposits occur in the central portions of interdistributary bays (Frazier, 1967; Kosters 1988) (Figure 4).

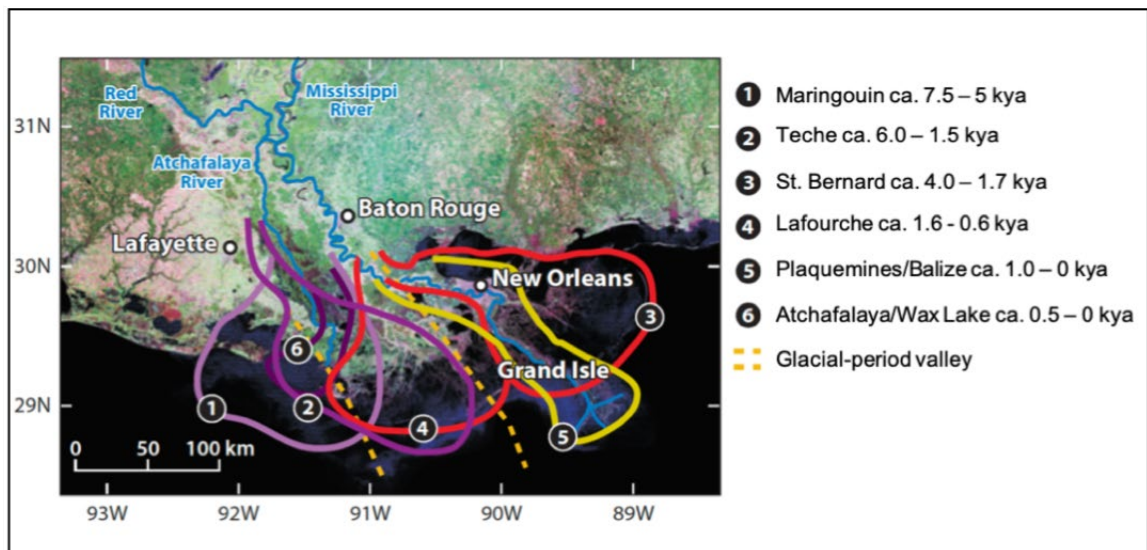


Figure 3. Late Holocene evolution of the Mississippi River deltaic plain. (Modified from Blum and Roberts, 2012 with adjusted dates from Hijma et al. (2017).

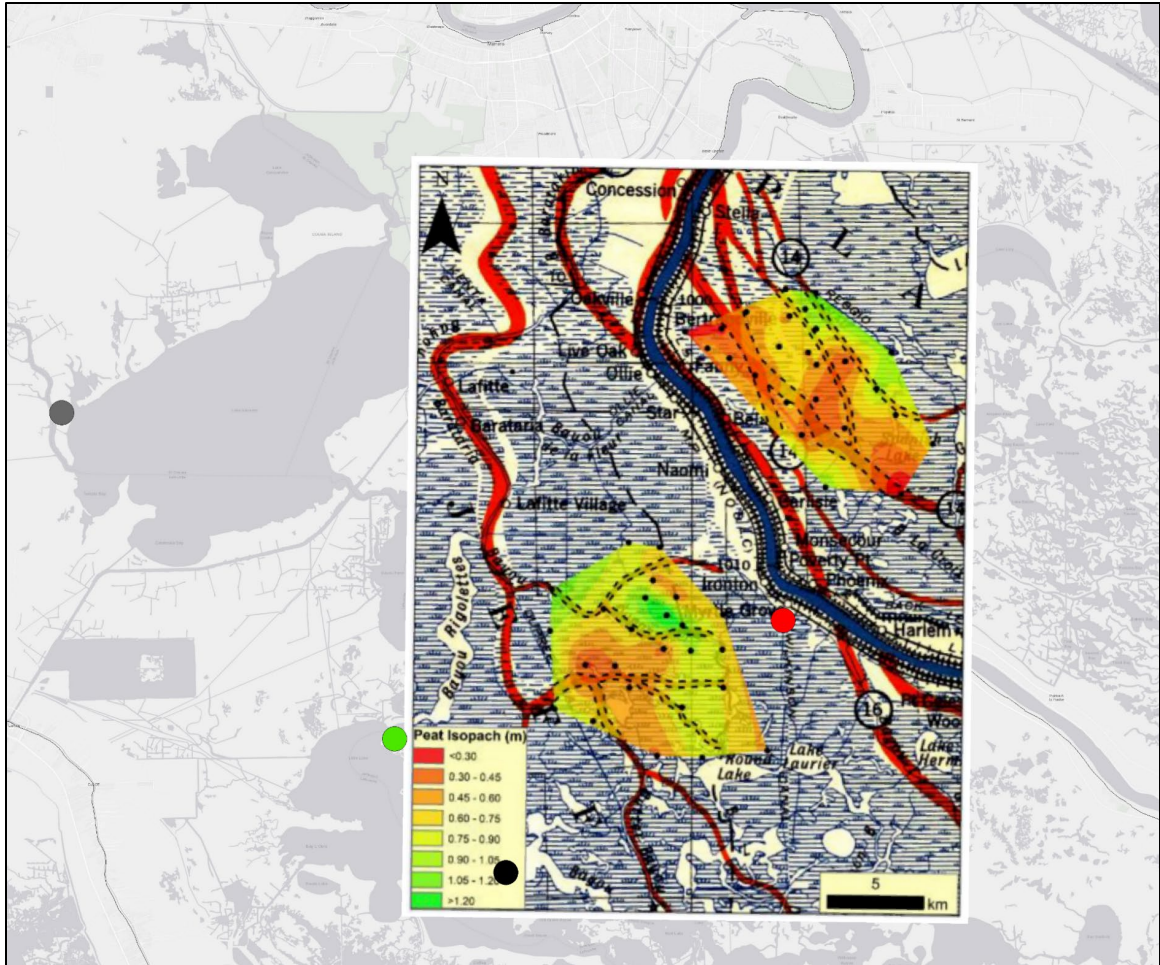


Figure 4. Surficial peat isopach map overlaid on historical map of paleo-distributaries of the Plaquemines-Modern delta from Fisk, (1944). Modified from Bomer et al., (2019). Colored dots (4 in number) represent locations for the present study.

3.2 Accretion and Subsidence Rates in Barataria Basin

Soil accretionary processes are complex, with organic matter accumulation and production as an important component of accretionary processes within Louisianan marshes. Therefore understanding the rate of vertical accretion (VA) compared with subsidence is important for wetland sustainability. Organic matter production and decomposition are dependent on marsh type (Stagg et al., 2017), and therefore VA (mineral + organic) rates should show trends in marsh type (fresh, intermediate, brackish, and saline).

The State of Louisiana has 390+ CRMS stations across the coast that collect accretion measurements in wetlands using feldspar marker horizons, and total surface elevation change (SEC) recorded by rod-surface elevation tables (R-SET). Measurements are generally collected twice per year by site visit (Todd et al., 2014) during normal water level conditions (hence, data is not collected during storms or drought conditions). R-SET depths vary widely—in the Barataria Basin sites they range from 25.5-26.9 m (Table 1). VA rates from these sites have been compiled by Jankowski et al. (2017) and show spatial variability throughout Barataria Basin ranging from 2 to 64 mm/yr with no definable relationship to marsh type (Figure 5). Within Barataria Basin (BB), Jankowski et al., (2017) utilized the difference between the rates of VA and SEC to calculate a shallow subsidence (SS) rate above the foundation depth of each site's R-SET: SS varied from -0.06 cm/yr to +6.0 cm/yr from 2006 to 2015. Nienhuis et al. (2017) used this data combined with GPS-derived measurements and calculated a delta-wide average total subsidence rate (integrating both deep and shallow processes) of 9 ± 1 mm per year (Figure 6). This methodology does not capture deep subsidence at a site, defined in this case as any subsidence occurring at a depth below the R-SET foundation.

Particle-reactive radiotracers have also been utilized in Louisiana wetlands to measure marsh accretion of soils using a range of short-term and long-term isotopes such as ^7Be , ^{137}Cs , and ^{210}Pb . DeLaune et al. (1978) calculated sediment accumulation rates since the onset of ^{137}Cs fallout from atmospheric thermonuclear testing in 1954 and find marshes near tidal channels vertically accrete mineral sediment at an average rate of 1.35 cm/yr compared to inland marshes (0.75 cm/yr). Similarly, Hatton et al. (1983) found that VA rates vary by 1.3 cm/yr in levee areas and 0.7 cm/yr in “back marshes” within BB.

More recent VA rates using ^{137}Cs show that deteriorating marshes vertically accrete more than stable marshes (Nyman et al., 2006). It should be noted that these radiotracer rates represent time averages over longer time intervals (decades to a century) than CRMS R-SET/feldspar plot rates that have been measured only over the last 6-10 years.

Byrnes et al. (2019) quantified subsidence rates in BB using high-resolution, continuously recording GPS benchmarks supplemented by USGS, NOAA, and USACE water level gauges. This method quantified subsidence rates based on a series of GPS stations, where foundation depths of those that are known range from 14.6 to 32.9 m into the subsurface. Although this method is useful for quantifying deeper subsidence mechanisms, the near surface (shallow subsidence above the benchmark foundation depth) is neglected from calculated subsidence rates using the GPS elevation record, underestimating total subsidence rates for BB. The R-SET and marker horizon (MH) methodology — called SET-MH — allows for a precise measurement of expansion and contraction of the wetland layer, provides a comparison of surface elevation and accretion relative to tidal frame, and can be used to calculate local rates of RSLR (Cahoon et al., 2020).

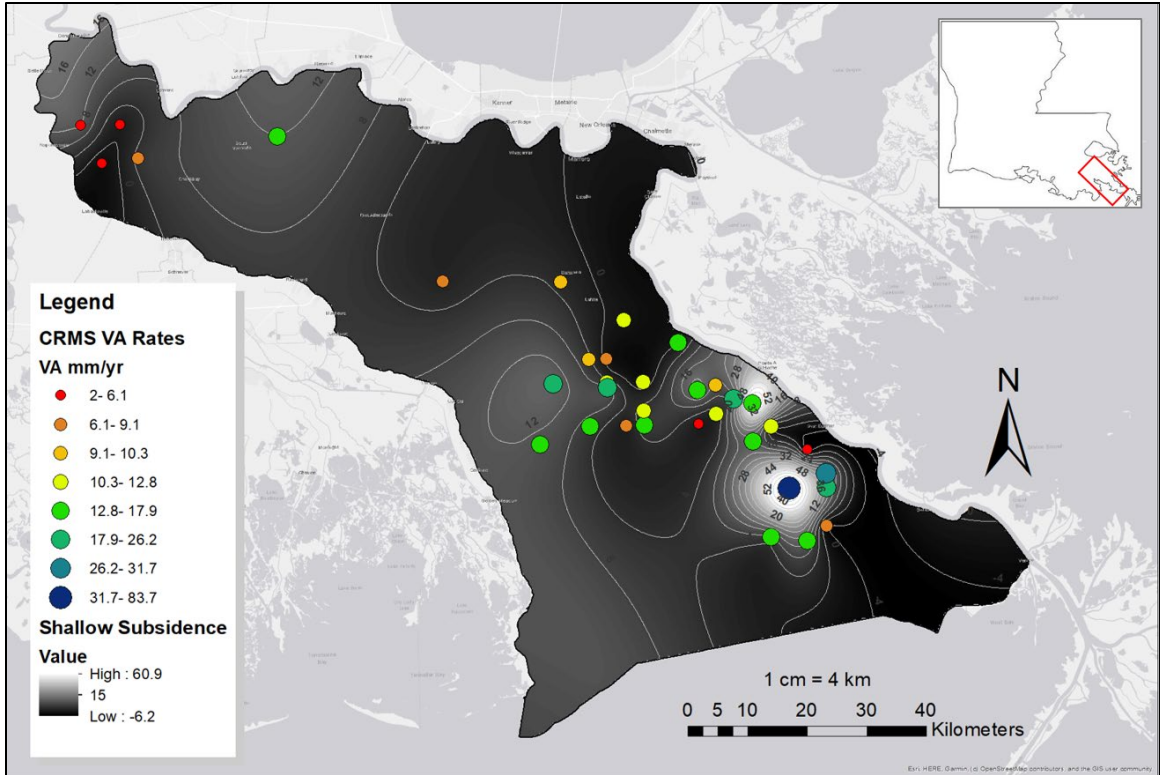


Figure 5. Vertical accretion (VA) rates (points) and shallow subsidence rates (VA-Surface Elevation Change) in Barataria Basin from CRMS stations plotted from rates by Jankowski et al. (2017).

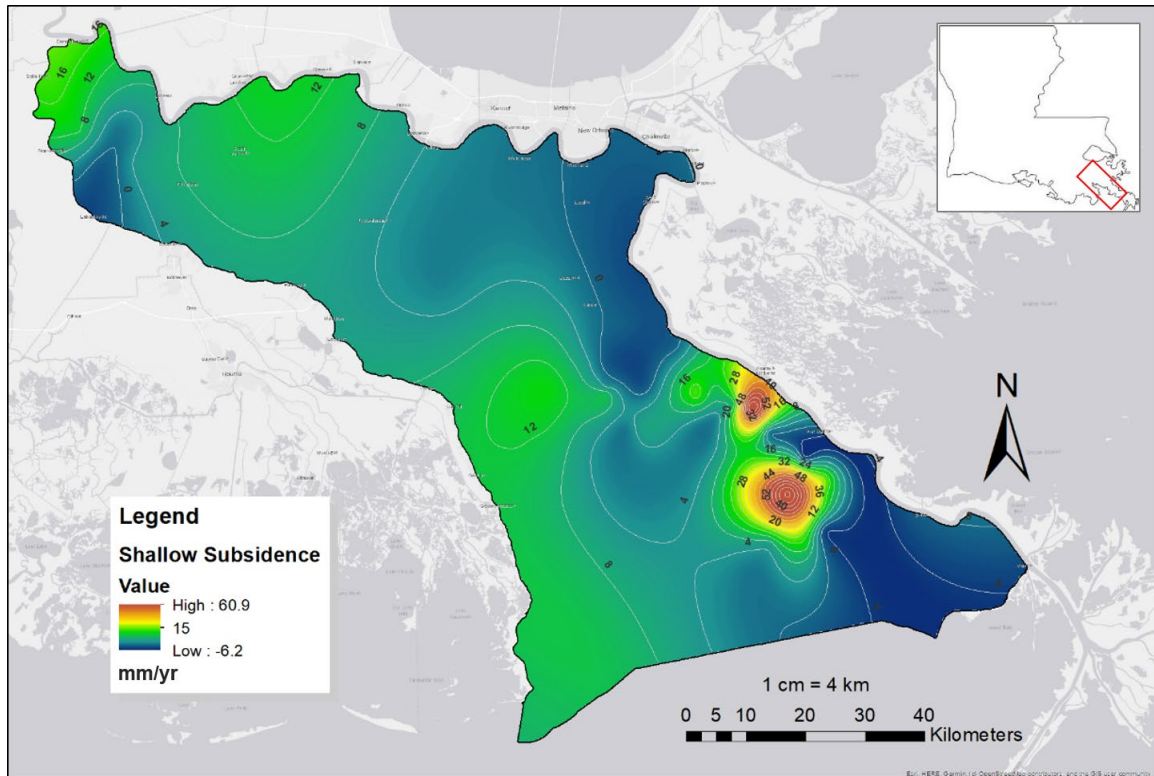


Figure 6. Map of shallow subsidence (SS) rates in Barataria Basin plotted from data in Jankowski et al. (2017). Shallow subsidence rates are derived by subtracting site-specific CRMS measured vertical accretion (VA) rate (collected by feldspar markers) from the rate of surface elevation change (SEC) measured by rod-surface elevation tables. Rates are derived from site-establishment data in 2006 to the Fall of 2015.

3.3 Confinement of the Mississippi River

Barataria Basin in the late Holocene and even the early historical period received terrigenous sediment from the bounding Mississippi River and Bayou Lafourche through overbank deposition and crevassing (Hatton et al., 1983; Shen et al., 2015; Chamberlain et al., 2018). The Lafourche subdelta was primarily active from 1.6 to 0.6 ka and shared water and sediment with the Mississippi River until about 0.6 ka when channel abandonment of Bayou Lafourche avulsed to the Atchafalaya River (Shen et al., 2015; Törnqvist et al., 1996; Hijma et al., 2017). Bayou Lafourche was finally totally sealed off from Mississippi River water in 1902 (Conner and Day, 1987). Early pioneers settled on

the natural levees of Bayou Lafourche and the Mississippi River and utilized the fertile floodplains for agriculture (Conner and Day, 1987). These peoples were the first to begin building artificial levees to protect their homes built on the natural levee of the rivers dating back to the 1700's.

For flood protection and navigation purposes, BB first became isolated from Mississippi River sediment, water, and nutrient input beginning with the US Government's "Levee's Only" policy of 1885. This policy allowed for the initial confinement of the river channel by the construction of a levee system stretching from New Orleans, Louisiana to Cairo, Illinois (Conner and Day, 1987). It was not until the Great Flood of 1927, that Congress saw the need for flood protection for the City of New Orleans and surrounding communities and implemented the Flood Control Act of 1928 which establishing the Mississippi River and Tributaries (MR&T) Project. By the 1930's into the 40's, extensive levee systems were constructed along the Mississippi River as well as many bypass floodways were constructed (such as the Old River Control (Red River Landing) and the Bonnet Carrie Spillway to limit the water flow passing through New Orleans to less than 1,250,000 cfs (35,986 cms). The Old River Control structure was built in 1961-63 to divert 30% of the Mississippi + Red River flow and sediment load into the Atchafalaya Riverto keep the river from avulsing (Rogers, 2008). The combined effect of these engineering works was to seal off BB from direct riverine terrigenous sediment input given that a continuous earthen levee bounding BB was constructed to Venice, LA, although turbid river-derived water can still enter via the shelf through the inlets in the bay mouth barrier island chain.

Due to massive rates of land loss throughout the coast, many restoration projects have been constructed to counteract saltwater intrusion and land loss. Those that have reintroduced a limited amount of river water directly to BB include the Naomi and West Pointe a la Hache siphons, and the Davis Pond Diversion (DP) (Inoue et al., 2008). The siphons pump water from the Mississippi River into BB at $60 \text{ m}^3/\text{s}$ while DP diverts freshwater at $300 \text{ m}^3/\text{s}$. The DP diversion was constructed in 2002 and located near river mile 118. This diversion structure contains seven man-made channels extending from the structure to the top of Lake Cataouatche (Keogh et al., 2019) in upper BB: DP is only operated in the spring at discharge rates up to $300 \text{ m}^3/\text{s}$. Other planned projects, such as the Mid-Barataria Diversion, are projected greatly increase Mississippi River input into the Basin to help reverse wetland loss.

3.4 Meteorology and Hydrodynamics

3.4.1 Astronomical and Meteorological Tides

Barataria Basin is a tidal system and exhibits a mean diurnal astronomical tidal signal of about 30-40 cm, with a maximum astronomical tidal amplitude of 62 cm (Fitzgerald et al., 2004; Payandeh et al., 2019). Supplementing the astronomical tide are wind-driven (meteorological) water level changes. The basin experiences two distinct seasonal wind directions that are influenced by changes in atmospheric pressure within the Northern Gulf of Mexico (GOM). Fall and Winter experience frontally dominated conditions that alternate between SE-to-SW (pre-frontal) and northwesterly (post-frontal) while Spring and Summer months are characterized by a strong southeasterly component (Conner and Day, 1987 Kolker et al., 2011). Seasonal and interannual changes in

atmospheric pressure over the GOM region have been shown to create significant differences in tide gauge water levels (Kolker et al., 2011). Sea surface temperatures also vary annually, where warmer Spring and Summer GOM and bay temperatures drive higher water levels compared to the fall and winter months (Conner and Day et al., 1987). Rainfall is relatively consistent on a seasonal basis throughout coastal Louisiana, although it is closely linked to seasonal wind directions: maximum rainfall occurs during July and the minimum in October (Conner and Day, 1987).

Meteorological events such as cold fronts and tropical storms are the basin's main mechanisms of freshwater input, causing sediment resuspension and deposition because the basin is relatively shallow (~ 2 m deep; Conner and Day, 1987). Individual cold front post-frontal wind events can raise water levels as much as 1-2 meters on an average of every 3 to 8 days in the October – April period, while a typical tidal cycle raises water levels about 0.6 meters (Poyandeh et al., 2019). Tropical storms and hurricanes have heavily altered BB marshes from increased wind-wave fetch erosion of marsh bay edges and by causing saltwater intrusion into fresher marsh zone (Barras, 2005; Wilson and Allison, 2008). Tropical system landfalls occur between 1 June – 30 November and have a northwest trajectory through the state. Conner et al., (1989) report that over 40,000 tropical storms have occurred in the Northern GOM since the beginning of the Holocene. Storm surges associated with these tropical storms have been reported as high as 1-2 meters during Hurricane Andrew (Cahoon et al., 1995).

3.4.2 Ecoregions and Historical Wetland Loss in Barataria Basin

Salinity and elevation define the ecological communities that make up the wetland ecoregions of the basin (Visser et al., 2002). The lowest salinity marshes and swamp forests are found in the northwest near various large lakes such as Lake Salvador, Lake Cataouatche, and Lac des Allemandes. Between the salinity extremes are intermediate marshes beginning around Bayou Perot and Bayou Rigolettes (Figure 7). Moving southward, brackish marshes occur through Bay Dosgris and Little Lake. The highest salinities occur in the south around Barataria Bay. Elevations within the basin are generally highest in the northern reaches (~1 m) and decrease towards the coast, with elevation decreasing by about 1 cm every 1 km (Conner and Day, 1987; Nelson et al., 2002).

Ecoregions of Barataria Basin were first identified by O'Neil, 1949, and have shifted through time (Figure 6). Vegetative shifts through time show the transformation of fresh marshes into intermediate and brackish marshes through the Bayou Perot and Bayou Rigolettes region. Marsh loss has been greatest in areas where fresh marshes were subject to higher salinities from 1945-1980 (Sasser et al., 1986). As a restoration effort to reverse the effects of saltwater intrusion, the David Pond Fresh Water Diversion supplies fresh water from the Mississippi River into northern BB at a maximum discharge of 300 m³/s (Das et al., 2012). Although salinity is an important control on marsh sustainability, BB's annual salinity pattern is projected to increase by ~3 ppt for saline marshes and 1 ppt for intermediate marshes with current projected sea level rise scenarios (Wiseman et al., 1990; Swenson, 2000).

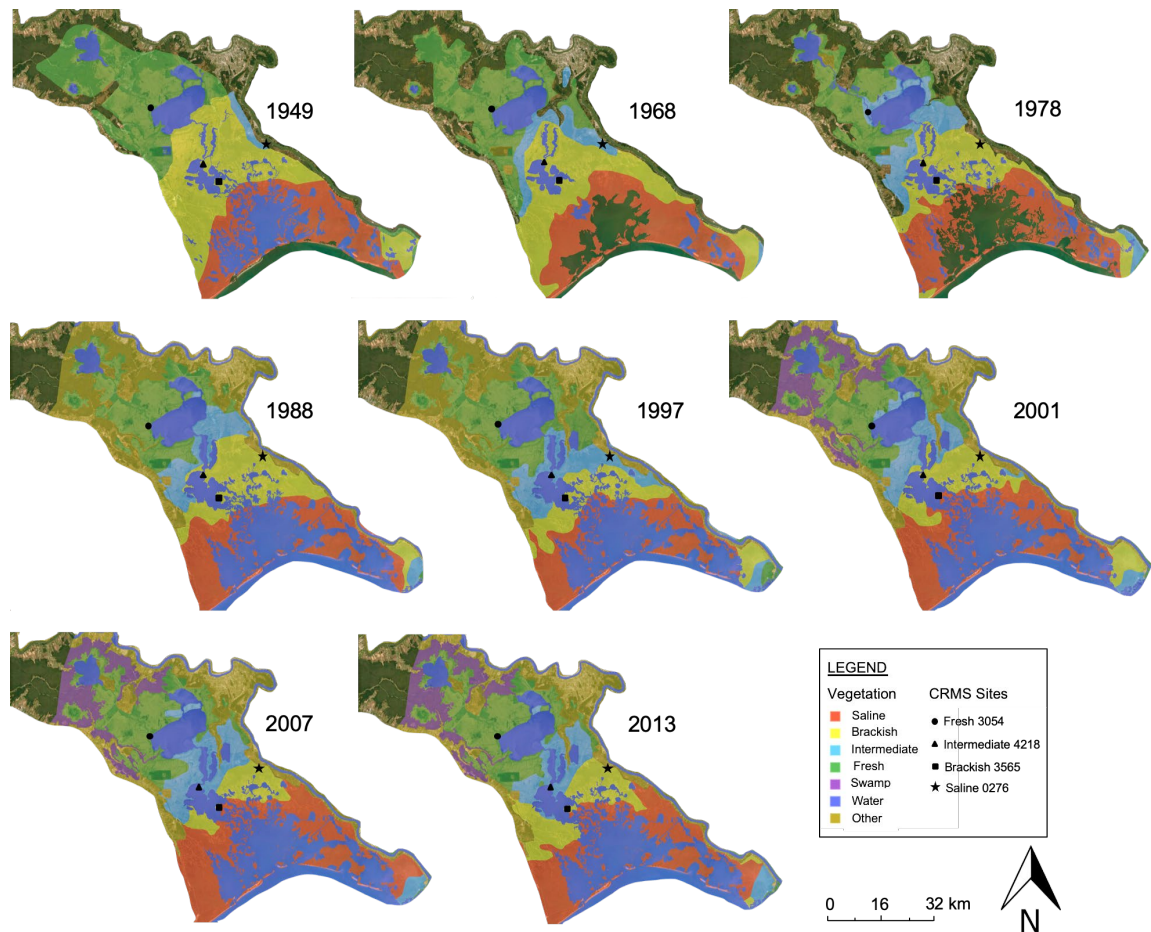


Figure 7. Shifts in wetland ecotype in Barataria Basin between 1949 and 2013. Digitized vegetation is based on data from multiple publications including; O’Neil (1949), Chabreck et al. (1968, 1978, 1988, and 1997), Linscombe et al. (2001), and Sasser et al. (2002 and 2013).

Wetlands within Barataria Basin have experienced the highest rates of land loss of any hydrologic basin in coastal Louisiana (Salinas et al., 1986). Barataria Basin has lost 29-31% of its wetland area since 1932 (Couvillion et al., 2017, Figure 8). Craig et al. (1979) analyzed land loss rates within Barataria Basin and found a total of 337 ha/year of loss in saline marshes from 1890-1960, 371 ha/year for brackish marshes, and 77 ha/year for fresh marshes. In a study by Evers et al., (1992), they find that land loss rates within Barataria Basin increased from 1945 to 1985, and begin to decline after 1980. As discussed earlier, there are a multitude of reasons for this, including widespread canal

cutting in BB. Deegan et al. (1984) found from analysis of multiple quadrangles of the delta plain that large areas of marsh are likely to withstand erosion and experience lower rates of land loss (1955-1978) than marshes that are fragmented by canal cutting or other mechanisms (e.g., interior subsidence ponding).

Dredging canals has been common practice throughout coastal Louisiana for almost a century. Land loss rates since 1956 have been shown to be directly correlated with canal cutting and spoil banks (along with other human-induced activities): 2.85 ha of open water was formed with each ha of canal dredged (Bass and Turner, 1997).

Hydrologic alterations to the basin from subsidence and sea level rise have also negatively impacted marshes that have been heavily fragmented through canalization.

Canals affect drainage patterns and influence saltwater intrusion to marshes, and hence ecotype, by allowing water to access parts of the marsh that would otherwise not experience water level fluctuations (Davis 1973; Craig et al., 1979; Sasser et al., 1986).

Widening of canals also occurs at alarming rates due to wave erosion and increased water flow to highly organic soils (Craig et al., 1979). Not only do canals widen post-construction, but interior ponding also occurs due to canal construction spoil deposits along canal margins that limit the amount of inundation and mineral sediment the central area of the marsh receives (Craig et al., 1979; Deegan et al., 1984).

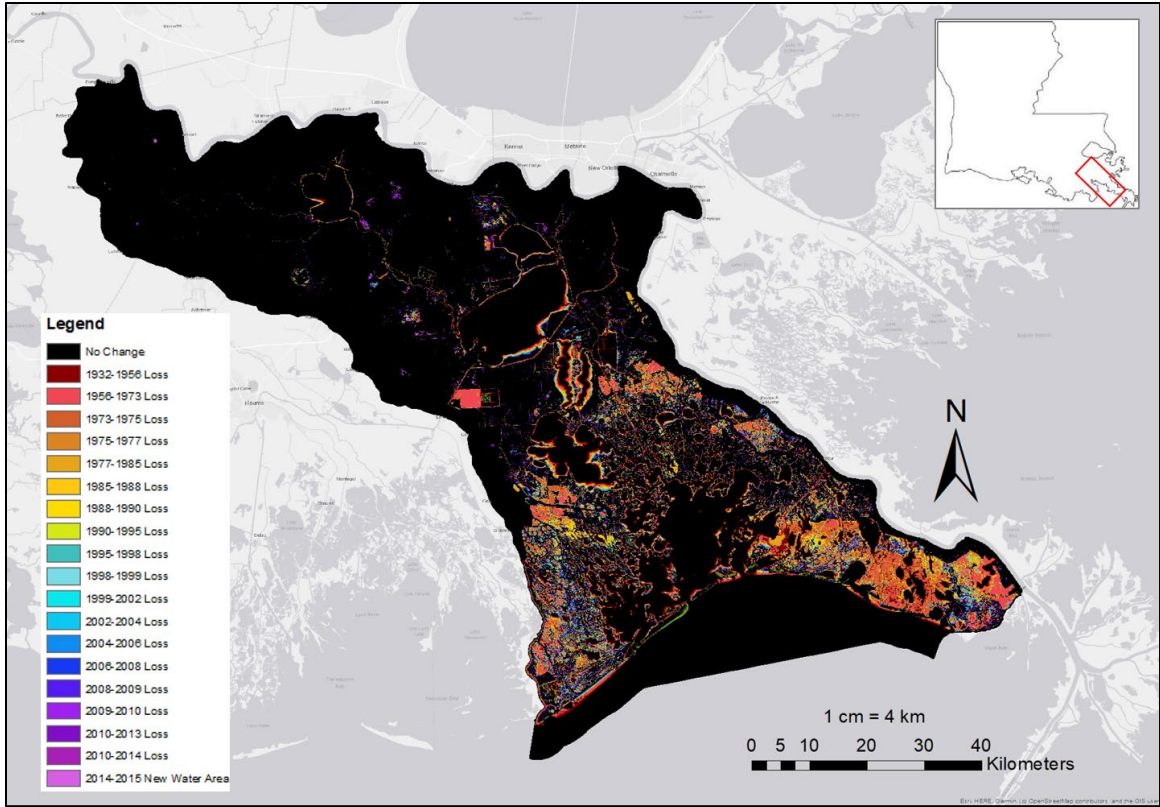


Figure 8. Progressive land loss map of Barataria Basin for the period between 1930 and 2016 (modified from Couvillion et al., 2017).

4. METHODS

4.1 Site Selection

Study sites were selected within Barataria Basin co-located (<500 m) with sites from the State of Louisiana's CRMS network: one site was selected each in areas classified based on dominant species as fresh, intermediate, brackish, and saline marsh (CRMS 3054, 4218, 3565, and 0276; Figure 8). The CRMS data from each site provides ancillary information for the present study on a wide range of marsh ecological and soil conditions including, soil porewater pressure, surface elevation change, vertical accretion rate, salinity, plant species composition and abundance, local land to water ratio, and other soil characteristics, as well as real-time water level and salinity from a gauge located in a nearby canal or bayou (CRMS-Factsheet, 2010). Vertical accretion is measured at CRMS sites using feldspar marker horizons which are sampled semi-annually a cryogenic sample corer (Cahoon and Turner, 1989; Cahoon et al., 1996). The marsh surface elevation is recorded approximately semi-annually by rod surface elevation table (R-SET) where pin heights are measured and referenced to NAVD88 vertical datum (Cahoon et al., 2002). R-SET's have the foundation rod hammered manually "to refusal" resulting in most foundations at 10-30 m, often above the base of the Holocene section. CRMS records hourly canal water levels at each site.

The four different marsh ecotypes utilized for the present study were selected to examine the relative effects of elevation, vegetation type, substrates, and tidal range on marsh elevation changes. Specific CRMS locations to deploy R-SETs for the present study (see below) were also chosen to exhibit a range in calculated CRMS vertical accretion, surface elevation change, and shallow subsidence rates as derived by

Jankowski et al. (2017) (Table 1) — as well as time length of CRMS record and site accessibility. The saline site for the present study (CRMS 0276) was also selected to be co-located with a subsidence “superstation” measuring rates and drivers of subsidence using continuously operating reference stations (GPS) and extensometers buried to three depths (38.7 m, 25 m, 10 m) in the Holocene substrate (Bridgeman, 2018).

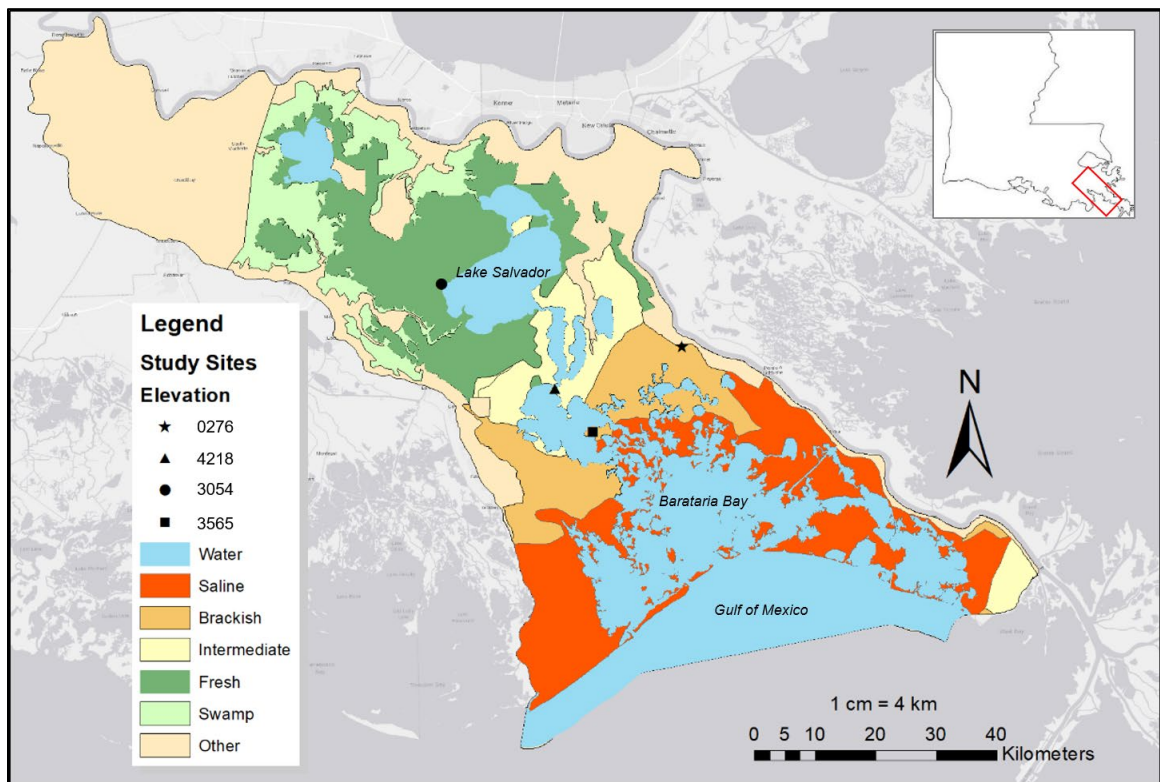


Figure 9. Wetland habitats in Barataria Basin relative to salinity regime from Sasser et al., (2013). The locations for the four study sites are also noted with their corresponding CRMS station numbers.

Table 1. Site characteristics for the four CRMS sites chosen for the present study. Surface elevation change (SEC), vertical accretion rate (VA), shallow subsidence rate (SS), and relative sea level rise rates are reported from Jankowski et al. (2017). R-SET foundation depth are found within CRMS Survey Reports during site construction (available at lacoast.gov/crms/).

| CRMS Sites | SEC (mm/yr) | VA (mm/yr) | SS (mm/yr) | Rate of Relative Sea-Level Rise (mm/yr) | R-SET Foundation Depth NAVD88 (m) |
|--------------------------|-------------|------------|------------|---|-----------------------------------|
| Fresh 3054 | 7.3 | 8.9 | 1.6 | 7.4 | 25.5 |
| Intermediate 4218 | 7.2 | 21.0 | 13.8 | 20.2 | 26.6 |
| Brackish 3565 | 9.3 | 15.4 | 6.1 | 12.7 | 26.9 |
| Saline 0276 | 14.0 | 14.4 | 0.4 | 6.6 | 26.5 |

4.2 Continuously Recording Rod Sediment Elevation Table (CR-SET)

Traditional methods of measuring marsh vertical accretion rate (organic and mineral) and surface elevation change are often too infrequent to capture the seasonal and event-based variability in mineral sediment deposition and allochthonous and autochthonous (aboveground and belowground) organic accretion. These methods include the feldspar marker horizons method utilized at CRMS sites where vertical accretion is calculated based on the amount of sediment accumulated atop of the white feldspar layer and collected semi-annually (Cahoon et al., 1995). Topographic surveys using theodolite instruments have also used to quantify surface elevation change but are relatively inaccurate due to the compressibility of marsh soils, soil compaction (Cahoon et al., 2000), and are often infrequent and have a short period-of-record. Other methods that measure vertical accretion use a combination of feldspar marker horizons and surface erosion tables (SET) that measure the change in elevation from an anchored benchmark to the sediment surface (Boumans and Day, 1993). High-resolution, rod-surface elevation tables, marker horizons (SET-MH) were developed (Cahoon et al., 1995; Cahoon et al.,

2020) as a low-cost, fixed method of capturing the surface elevation change, and, when coupled with vertical accretion measurements by feldspar accretion (Cahoon and Turner, 1989) or another method, can be used to deconvolve the portion of surface elevation change (SEC) that is subsidence or uplift independent of vertical accretion or erosion (Jankowski et al., 2017). The SET-MH method utilized on the CRMS stations follows Cahoon et al. (1995), and uses a series of downward-pointing, fixed pins that are lowered to the sediment surface and then distance of burial or exposure is measured at time intervals of site visit (pins are reset to the sediment surface after each site reading). Multiple pins over a 365 cm² area allow quantification of small-scale spatial variability in SEC. As outlined by Jankowski et al. (2017), the depth of foundation for the CRMS's R-SET's is critical for determining what depth interval they are integrating SEC, and by calculation (VA-SEC), shallow subsidence rate (SS). The CRMS method of R-SET measurement of SEC is limited to semi-annual site visits.

Cahoon et al. (2011) developed a continuous elevation sensor, consisting of a down-looking ultrasonic sensor mounted on a frame with a shallow foundation depth (2 m) and self-recording marsh surface elevation changes on a timescale of minutes-to-hours. This methodology was used as a model to develop the high resolution, continuously recording (CR-SET) surface elevation tables for the present study. The CR-SET frames were constructed from hollow aluminum pipes (0.03 m OD) configured into an H-shaped, square 0.61 m x 0.61 m platform with aluminum fittings, with the legs anchored at a depth of 1.5 m into the subsurface (Figures 8, 9, 10, and 11). The depth was selected as it was below the organic-rich surficial marsh mat at the four sites. Each of the four site CR-SETs were equipped with a Banner (T30UXIA-Q8) ultrasonic sensor.

The ultrasonic sensors were attached and leveled to the CR-SET frame approximately 0.5 m above the marsh surface and were housed inside a 0.15 m (6") diameter perforated PVC cover and top (Figures 10 and 12) designed to reduce interference from floating vegetation and limit solar heating of the electronics. Within each PVC housing, a PVC circular target for the ultrasound (10.2 cm in diameter) was anchored by three legs to a depth of 15 cm into the substrate and stands 10 cm above the sediment surface (Figure 10). The ultrasonic sensor has a maximum beam diameter of 7 cm at 70 cm from the sensor (5.7°). The purpose of this target is to provide a stable, reflective target for the ultrasound pulse and follows the methods of Cahoon et al. (2011). Hence, the CR-SET ultrasonic design, as deployed, measures changes in elevation integrated between depths of 15 cm (target foundation depth) to 1.5 m (frame foundation depth) and continues recording the sediment surface when the site is inundated by up to 10 cm of water, at which point the sensor begins to track the water surface.

At CRMS Site 0276 (Saline site), two other elevation measuring methods were also deployed on the CR-SET frame to test additional methodologies: a Banner Engineering laser sensor (Model Q4XTILAF500), and a Turck inductive linear positioning sensor (Model L1500P1-Q25LM0-LIU5X3-H1151) (Figure 11). The laser sensor was deployed with the same target-shroud configuration as the ultrasonic sensors, while the linear position sensor was a rod mounted to a circular target (10.2 cm diameter) resting on the sediment surface that was anchored in the substrate to a depth of 1 cm (Figure 11). Hence, the linear position sensor measured surface elevation change as influenced over the entire 0-to-150 cm CR-SET foundation depth interval, and continues measuring at marsh surface submergences of >10 cm. The Linear Position sensor was

mounted approximately 32 cm from the soil surface. The Laser sensor was mounted approximately 33 cm from the surface. The Ultrasonic sensor was mounted approximately 40 cm from the sediment surface at the Saline site, ~60 cm at the Brackish site, 50 cm at the Intermediate site, and ~52 cm at the Fresh site. Each platform was geolocated using a real-time kinematic GPS sensor (Trimble model R8 RTK) to acquire latitude and longitudinal position, and ground surface elevation at the time of installation to an accuracy of about +/-3 cm. Multiple topographic points were acquired by continuously recording position and elevation over a period of minutes. The horizontal datum of the survey points was acquired in Universal Transverse Mercator (UTM) Zone 15N in the North American Datum of 1983 (NAD83). The vertical datum was recorded in North American Datum of 1988 (NAVD88) and uses the 2012A Geoid.

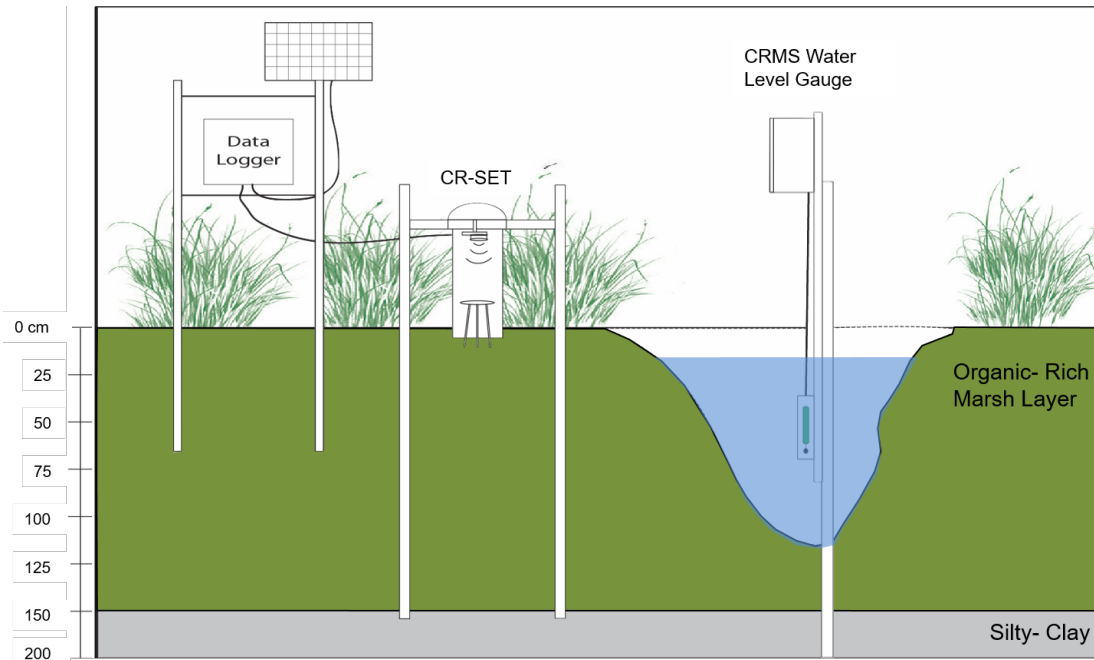


Figure 10. Schematic of high- resolution CR-SET design utilized in the present study. The CR-SET foundation (four legs) was driven to a standard depth of 1.5 m for all four sites: this was sufficient to penetrate the entire organic-rich marsh layer as observed from site coring. The data logger and solar power array was mounted on a separate foundation. The CRMS water level gauge was located in a tidal creek or other open water body <1 km from the CR-SET sites.

Each sensor of the three types has an analog output and was wired in a 4-20 mA loop with a Campbell Scientific CR800 data logger. Each sensor has individual sensing resolution and specifications (Figure 11). The sensors were installed through a 10 Ω shunt (resistor) that allows the data logger to relate the change in voltage to a distance. The sensors were powered by Campbell Scientific 12V batteries recharged by a 10W solar panel- with the exception of the Saline site which required 24V batteries that are wired in series and is recharged by a 20W solar panel to handle the load of three sensors. The data logger was programmed with Campbell Scientific’s Logger Net software to collect distance measurements every 2 seconds for a full minute (60 seconds), then averaged and stored these 30 data points as a single value (1 sample/min).

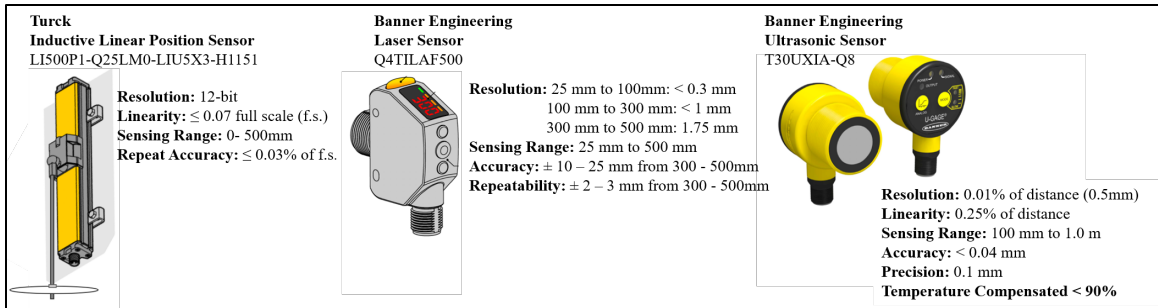


Figure 11. CR-SET sensor specifications deployed at the four Barataria Basin study sites. The ultrasonic sensor was deployed at all four sites, while all three sensor types were deployed at the saline site CRMS 0276. These three analog sensors collect continuous measurements by converting a change in voltage to a distance (and position). Errors associated with outputs across different sensing ranges are expressed in the sensor's linearity and resolution. The resolution is the smallest incremental change in voltage the sensor can detect. The linearity is the error associated with the deviation of the measured distance outputs from a straight line at a fixed voltage (and temperature for the ultrasonic sensor). Accuracy and Precision for the ultrasonic sensor were measured in lab (Appendix A).

The Turck linear positioning sensor is unique compared to the ultrasonic and laser sensors because it uses both a sensor and a positioning element that allows the system to measure and convert the measured variable into a length and position (Turck manual, 2018). The positioning element on the sensor was engineered to be manually pushed by the surface itself by attaching a ~40 cm long threaded aluminum rod with a 10.2 cm diameter disk that sits on the ground surface (Figure 11). This positioning element moves the sensor up and down when surface elevation changes. The Banner Engineering laser sensor has the highest resolution of the three sensor types deployed in the present experiment, with a visible red Class 1 laser (655 nm) that can detect submillimeter distance changes--but it also has the lowest sensing distance range (25 mm – 500 mm). Banner Engineering's ultrasonic sensor is temperature compensated which reduces the error due to temperature by about 90% (Banner Engineering manual, 2016). The sensor emits a pulse of ultrasonic energy to the target, the sensor then reads the reflected energy that travels back to the sensor. The sensor manually measures the total two-way travel

time required for the energy to reach the target and back to the sensor. The distance of the target to the sensor is calculated by using the following formula:

$$D = ct \div 2 \quad (1)$$

Where, D = distance from the sensor to the target, c = speed of sound in air, and t = transit time for ultrasonic pulse.



Figure 12. Photograph of the CR-SET deployment at the Fresh site (CRMS 3054) in November 2018.

CR-SET's were deployed in late autumn of 2018. The period of record from each site varies due to different deployment dates and due to damage caused by Hurricane

Barry on July 12, 2019. The Saline site was first deployed on 17 September 2018 without a target and PVC shroud for the ultrasonic sensor to conduct preliminary testing. The PVC shroud and targets were installed on December 15, 2019 at the site. The Saline site record extends until 22 June 2019, the last date the site was visited, and data downloaded prior to Barry. The Fresh site was deployed on 7 November 2018 and the record extends until 25 September 2019. This was the only site where the electronics module on the separate frame were not damaged by water inundation (>1 m) by Hurricane Barry. The Intermediate and Brackish sites were both deployed on 30 November 2018. Both sites electronics were damaged by water inundation by Barry. At the Intermediate site, the data was recovered from the damaged electronics module, and therefore the record ends on 12 July 2019. Data from the Brackish site was not recoverable post-Barry, hence the record ends on the last site visit on 29 May 2019. Each site was visited about every six weeks for data collection and maintenance which involved cleaning nesting organisms off equipment and checking battery voltage.

4.3 Calculating Site Marsh Elevation

Marsh surface elevations for the four sites were determined utilizing the CRMS water level gauges located in nearby canals by pin-pointing the water elevation where water floods the 10 cm high target (Figure 13). This proved to be a more accurate method of determining site elevation of each sensor than the RTK spot measurements, although these generally varied by <10 cm from the water level method. The surface elevation data, when plotted against water elevations from the CRMS gauges that are referenced to a geodetic datum (NAVD88) show a distinct inflection point in the graph (Figure 13), which is the point where overtopped the target 10 cm above the marsh surface. This is the

point where the ultrasonic (and laser) sensors begin to track water level and not the marsh surface. Marsh elevations were corrected to NAVD88 using the raw elevation (range) data and the inflection point minus the target elevation above the marsh surface:

$$\text{Marsh Elevation (cm, NAVD88)} = (\text{ZeroRAW} - \text{RAW}) + \text{BASE} \quad (2)$$

Where, ZeroRAW = Raw distance to the target (in cm) at the point that the linear regression meets the water depth inflection point where the sensor begins to track the water surface. WATER = the NAVD88 canal water elevation (cm) where the marsh elevation values begin to track the water surface and not the marsh surface. TARGET = the height of the target above the marsh surface (10 cm in all cases), RAW = the uncorrected distance to target measurement from the ultrasonic (or laser sensor). BASE = WATER – TARGET.

The linear position sensor is referenced to the marsh surface elevation during initial site deployment because the linear position sensor does not have a target; instead it was equipped with a threaded aluminum rod with a circular PVC disc that sits at the marsh surface. The linear position sensor is referenced by using the first hourly measurement as a baseline (Equation 3).

$$\text{Linear Sensor Marsh Elevation (cm, NAVD88)} = \frac{(SE * ((BASE - \text{Raw}_{Data}) + BASE))}{BASE} \quad (3)$$

Where SE is the surface elevation recorded by the RTK during site deployment on 30 September 2018, BASE is the baseline value recorded within the first hour, and Raw_{Data} is the hourly data.

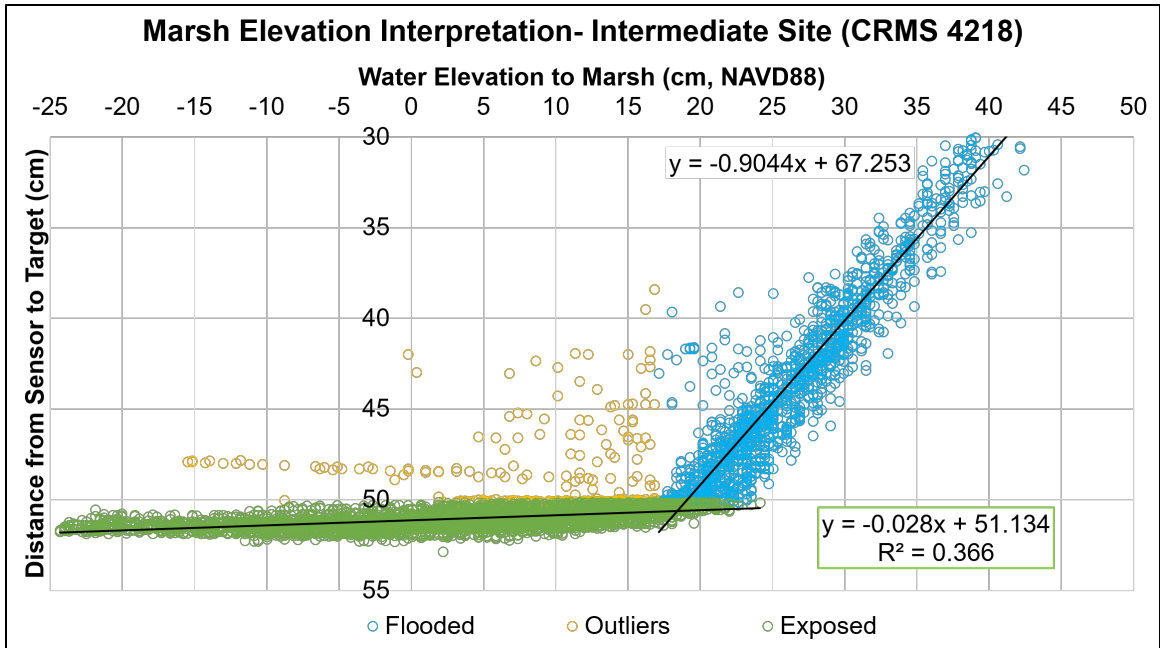


Figure 13. Marsh elevation (CR-SET) record during the study period plotted against hourly water elevation (recorded by the CRMS water level gauge). This comparison was utilized to measure 10 cm inundation (target height in NAVD88) above the marsh surface (inflection point). Water elevation are corrected so that the inflection point ($x=18.4$ cm) is the surface elevation of the marsh instead of the +10 cm target (which would have occurred at 28.4 cm prior to the correction). Green dots are the marsh elevation points below +10 cm NAVD88 above local marsh surface elevation. The blue dots are when the sensor begins to track water level. Yellow dots are outliers based on one standard deviation of the marsh elevation.

4.4 Sediment Coring

Sedimentological properties of the upper 1 to 2 m of the organic-rich marsh surficial strata were analyzed at each of the four sites to understand the geotechnical, sedimentological and organic properties that may influence differences in surface elevation change from site-to-site (e.g., between marsh types). Cores were collected with an Eijkelkamp 5 cm in diameter peat auger at each site within 3 m of the CR-SET. Cores were removed by spatula into PVC collection sleeves on site, wrapped in clear plastic wrap to reduce exposure to air, and transported within a few hours to Tulane’s River and Coastal Center in New Orleans for further laboratory analysis. To extend the cored horizon below the 1 m length of the auger barrel, the auger barrel after the initial section

was removed, was re-inserted into the hole and an extension rod utilized to collect up to 2 m length cores. Actual maximum core depth reflected geotechnical properties that allowed the core to be extracted from the substrate without breaking and sliding back into the core hole.

4.5 Laboratory Methods

4.5.1 Core Bulk Properties

In the laboratory, cores were subsampled into two cm increments for the first 0-10 cm of the core. After the first 10 cm, two cm subsamples were collected every five cm to the bottom of each core. Samples were placed in pre-weighed Whirlpak bags and weighed to determine the wet weight of each increment. Samples were freeze-dried and weighed to determine the dry weight and allow bulk properties to be calculated. Freeze-drying was conducted instead of heating to reduce alteration of the organic component of the sediment for analysis as described below. Sediment down core porosity was calculated from water content (wet – dry weight) assuming a sediment mineral grain density of 2.65 g/cm³ and an organic matter density of 1.24 g/cm³. To correct for organic matter content and porosity in these calculations the ratio of organic matter to mineral sediment from each sample was determined by using the Loss on Ignition (LOI) method to derive the relative mineral: organic ratio of each sample. The percentage of organic matter was calculated by the change in percent of pre and post sample weights heating for 14 hours to 550°C (Equation 4) (Wilson and Allison, 2008).

$$LOI (\%) = \frac{Pre-Post}{Pre} \times 100 \quad (4)$$

Porosity was then used in the consolidated bulk density calculation by determining the porosity of the sample including the organic and mineral bulk densities. Porosity is calculated from the saturated bulk density using the following equation:

$$Porosity = 1 - \left(\left(\frac{S_{BD} - 1.01}{2.65 \times (1 - LOI)} \right) + 1.24 \times LOI \right) \quad (5)$$

Where, S_{BD} is saturated bulk density and 1.01 g/cm^3 is the density of water, 2.65 g/cm^3 is the density of quartz, 1.24 g/cm^3 is the density of organic matter, and LOI is the decimal loss on ignition fraction.

4.5.2 Granulometry

Samples burned for LOI to remove organic material were then utilized for granulometric analysis using a Malvern Mastersizer 3000 unit. This unit uses laser diffraction and a HydroEV dispersion unit to analyze grain size. Samples were rehydrated in 0.1% sodium metaphosphate solution of deionized water for at least 24 hours and then sonicated for at least one hour in an ultrasonic bath before being introduced into the Malvern HydroEV cell. Grain size statistics (D_{10} , D_{50} , D_{90} , mean, skewness, and kurtosis) were calculated automatically by the Malvern from a combination of two 15 second measurements, one with a laser of 632.8 nm wavelength, and one with a laser of 470 nm wavelength. Samples were tested three times within the Malvern and the replicates were averaged to produce the final grain size statistics.

4.5.3 Organic Analysis

In addition to LOI analysis to determine bulk organic matter content, and to allow an examination of the allochthonous versus autochthonous organic matter at each site, a second core was collected at each site within 50 cm of the first core. These cores were transported and processed the same manner as the above-mentioned cores. Subsamples were freeze-dried and weighed to determine the total weight of dry sediment. Samples were then soaked in 0.1% sodium metaphosphate and sieved through a 63 μm and 120 μm screens. The 120- μm screen was placed atop of the 63- μm screen to capture the large particle organic fraction, while the 63- μm concentrated the sand-sized mineral fraction. Live and dead roots and were then hand-picked from the remaining (detrital) organic fragments from the 120- μm screen and dried in an oven to compare root weight to the total organic matter weight. To determine the ratio of root and detrital organic matter, the LOI measurements from the first core were utilized.

4.5.4 Sediment Accumulation Rates

Particle-reactive radiotracers (^{210}Pb and ^{137}Cs) were utilized to measure the long-term sediment accumulation rates (decades to a century) at each of the sites. Samples for radiochemical analysis utilized aliquots of the freeze-dried (mineral) sediment taken after LOI consumption of organic matter. ^{210}Pb is a naturally occurring uranium daughter isotope with decay half-life of 22.3 years (Nittrouer et al., 1979). Supported ^{210}Pb is the product of the in-situ decay of ^{226}Ra from uranium in the sediments (Lynch et al., 1989). Unsupported (excess of supported) ^{210}Pb is produced by the decay of the uranium daughter ^{222}Rn as this gas escapes the subsurface into the atmosphere and, following

decay to the Pb daughter, precipitates back to the land surface (He et al., 1996).

Accumulation rates derived from this method assume a constant rate of excess supply and average accumulation rates over the period where excess is present at measurable values—about 4-5 half-lives or ~ 100 years (Appleby & Oldfield, 1978). ^{137}Cs is an anthropogenic radionuclide produced by thermonuclear weapons testing between 1954 and the 1972 aboveground nuclear test ban treaty. (Lynch et al., 1989; He et al., 1996). Therefore, ^{137}Cs has a non-steady state input and declines with continued fallout from the upper atmosphere to the present. Accretion rates for ^{137}Cs are calculated assuming the depth of the greatest ^{137}Cs activity corresponded to the peak year (1963) of thermonuclear testing (Pennington et al., 1973; Lynch et al., 1989).

Aliquots from the freeze-dried cores samples were lightly ground with a mortar and pestle to disaggregate, then sealed in vials to sit for at least 21 days to allow ^{210}Pb supported levels to reach secular equilibrium (Lynch et al., 1989). Samples were then analyzed for total and supported ^{210}Pb activity and ^{137}Cs activity on well (vial) configuration, Canberra Low-Energy Germanium (LEG) gamma spectrometers for at least 24 hours. ^{210}Pb accumulation rates (mm/yr) are determined by fitting a best fit linear regression to the log transformed excess ^{210}Pb . ^{137}Cs accumulation rates were calculated using the sediment depth of the peak activity (that corresponds to the year 1963) subtracted from the year the core was collected (DeLaune et al., 1978). Errors for these two different methods differ. ^{210}Pb accumulation rates are calculated based on the fit of the regression equation, and errors for ^{137}Cs accumulation rates are calculated based on distance between the peak activity interval and depth intervals above and below the zone of peak activity (Wilson and Allison, 2008).

4.6 CRMS Surface Elevation Correction

CRMS R-SET surface elevation change (SEC) measurements are corrected by using a yearly averaged water elevation centered on the water level during CRMS site-sampling. The water levels during CRMS SEC sampling are corrected using the median marsh elevation and the linear relationship between marsh elevation and water elevation found within this study. The water elevation during SEC sampling is differenced from the yearly averaged water elevation and input into the linear regression equation- yielding the elevation difference of the marsh at different water levels. The elevation difference is added to the average surface elevation measurement (campaign). Detailed SEC methods can be found in Jankowski et al. (2017).

$$\text{Correction} = (\text{Median ME} - ((0.0041 * (\text{WE Diff}) + 23.555)) + \text{Campaign} \quad (6)$$

5. RESULTS

5.1 Marsh CR-SET Elevation Sensors

As outlined in the methods, the marsh surface elevation of four sites, each a different ecotype (e.g., fresh, brackish, intermediate, and saline) was recorded every minute with a down-looking ultrasonic sensor. In addition, the Saline site was equipped with two additional sensors (laser and linear position) to test multiple methods for recording marsh surface elevation change. For most analytical purposes reported herein, the high-frequency measures were averaged hourly using the median, and then referenced to NAVD88 vertical datum elevation by selecting the point at which the water level elevation (according to the NAVD88 datum from nearby CRMS water level gauge) rises above the 10 cm tall target. This is marked by an inflection point when the ultrasonic and laser sensors begin to track the water surface and not the marsh surface (Figure 13). Multiple linear regression lines were fit to pinpoint the exact elevation when water floods the target. The inflection point then marks the top of the target (elevation +10 cm NAVD88), therefore 10 cm is subtracted from the inflection point to acquire the average marsh surface elevation. Due to small scale differences in marsh topography and how the sensors are mounted relative to one another, a comparison of results from the ultrasonic and laser sensors show cm-scale differences of the inflection point. The inflection point chosen for the Saline site (Figure 13) is 13.2 cm which is recorded by the ultrasonic sensor, and therefore the laser is referenced to 13.2 cm NAVD88. The linear position sensor is referenced differently due to the different design of the sensor. The sensor is referenced using the RTK elevation recorded at the site during site deployment on 30 September 2018 at an elevation of 10.8 cm.

The marsh elevation versus water elevations of the saline site compared to the other four sites shows a similarity in the change in variability of marsh elevation as water levels rise and fall (Figure 14). The standard deviation of the calculated marsh surface elevations derived by the fit of the linear regressions of the “exposed” marsh surface (measured while the sensor was tracking the marsh surface, and not water levels) ranges from ± 0.23 cm (Fresh site) to ± 0.56 cm (Saline site). The site-specific surface elevation fluctuations are 1.72 cm for the Fresh site, 2.72 cm at the Intermediate site, 1.75 cm for the Brackish, and 2.11 cm at the Saline site. At the Saline site for example (additional figures equivalent to Figure 14 are shown in Appendix B), the ultrasonic and laser sensors indicate significant variability of the marsh surface elevation during the period when the sensor target is not water inundated (Figure 14). As water levels in adjacent canals rise, the marsh surface elevation also increases and the recorded variability (point scatter) at any one elevation around the best fit linear regression decreases up to target inundation depth (10 cm above the marsh surface), at which point the sensors begin to track water level. The linear position sensor also records the same change in variability of the marsh surface (Figure 14C) although the point scatter variability at a single water elevation is considerably smaller than that recorded by the laser and ultrasonic sensors. The linear position follows the same general trend with increasing water levels, although the slope of the linear regression line is lower compared with the laser and ultrasonic sensors at that site. This sensor also records the marsh surface elevation at water elevations greater than 10 cm above the marsh surface at this site. The linear position sensor captures multiple trend lines during flooding events shown in Figure 15.

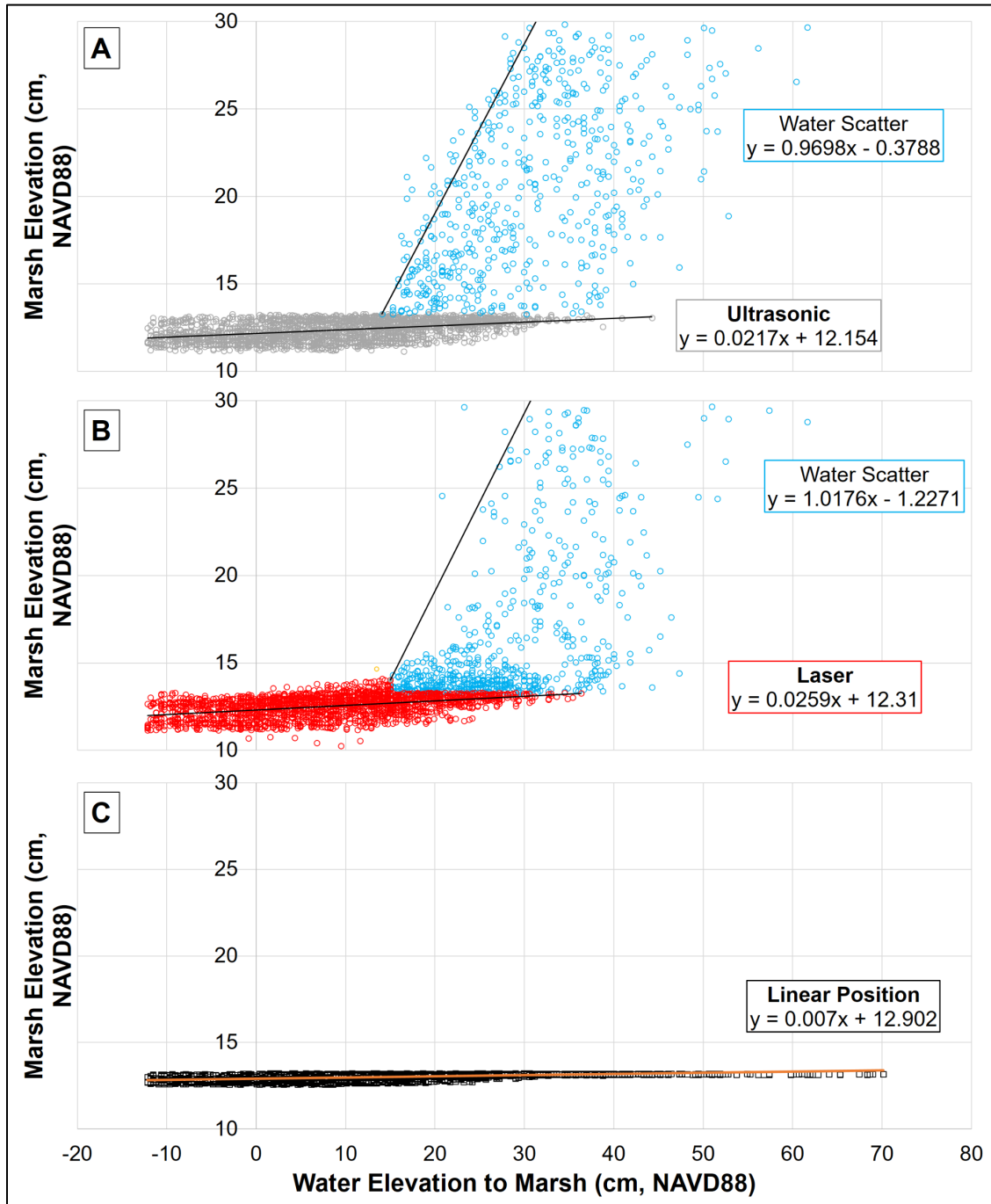


Figure 14. Hourly marsh surface elevations at the Saline site (CRMS 0276) for the entire period of record (15 Dec 2018 to 22 June 2019) for each of the three sensors (plots A, B, and C) plotted against the hourly water elevation in the adjacent canal as recorded by the CRMS 0276 gauge. The blue and purple regression lines mark the interpreted elevations where water elevation was greater than marsh surface +10 cm NAVD88 above local marsh surface elevation (where the sensors began to track the water surface instead of the marsh surface).

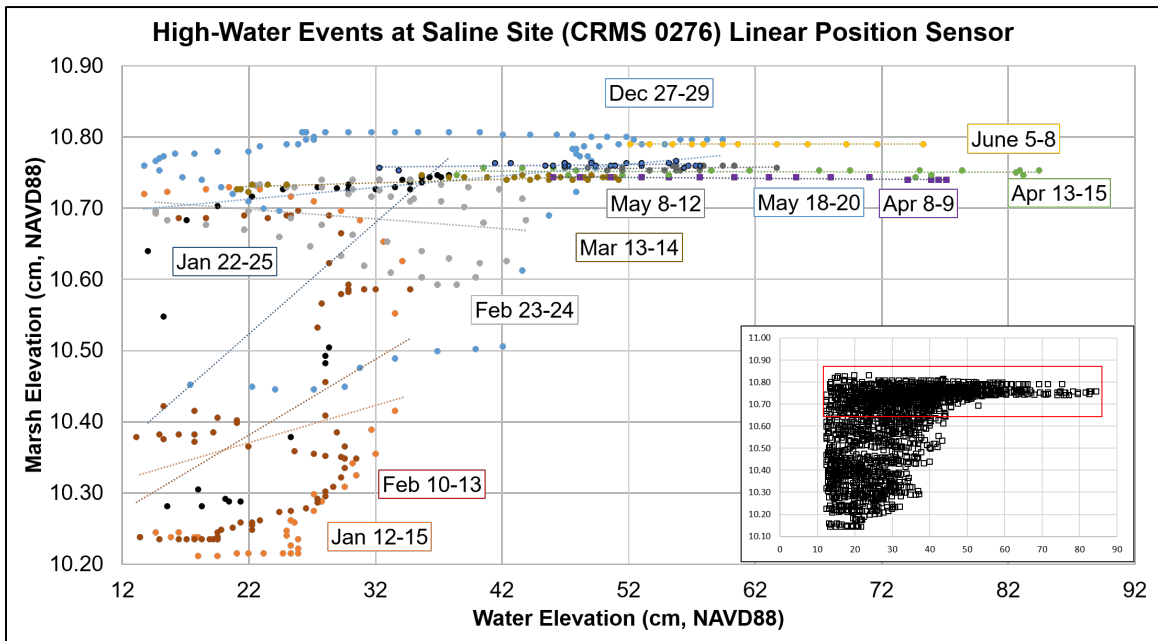


Figure 15. Selected flooding events at the Saline site (CRMS 0276) recorded by the linear position sensor. The linear position sensor is the only sensor able to record changes to the marsh surface during flooding events where water depths exceeded 10 cm. Linear position sensor is referenced to the marsh elevation during site deployment (10.8 cm).

During cold front events where canal water surface elevation changes sharply (deepening in pre-frontal onshore winds and shallowing post-frontal when winds shift), marsh elevation at the four sites respond similarly. Examples are shown in Figures 16, 17, and 18. It is also observed that the three different sensors at the Saline site capture similar fluctuations to the marsh surface elevation of up to ± 1 cm during frontal passage, and is shown in an example time segment from the 10th to 30th of January 2019 (Figure 16). When water levels in adjacent canals increase, the marsh surface begins to rise and after the front passes water levels sharply decrease, and the marsh elevation continues to decrease for several days until the onset of the next pre-frontal period of rising water levels (Figure 16). As shown in Figure 16, during passage of frontal events on the 13th, 18th -21st, 23rd, and the 29th of January 2019, the marsh surface elevation response lags by

several hours the beginnings of changes to canal water level (both rises and falls). When water levels drop low enough and for more than several days remain at low elevations, marsh surface elevations stabilize at a baseline value— about 12 cm NAVD88 in the example in Figure 16. The Intermediate site also shows similar fluctuations to frontal passage events where the surface responds almost immediately to water level changes. (Figure 17). Figure 18 shows the Brackish site responds similarly with a lag in the surface elevation response with passage of a cold front event on 15 March 2019 where the surface elevation does not respond to the water elevation change for about 24 hours (Figure 18B), and the Brackish marsh response to a normal tidal signal (Figure 18A).

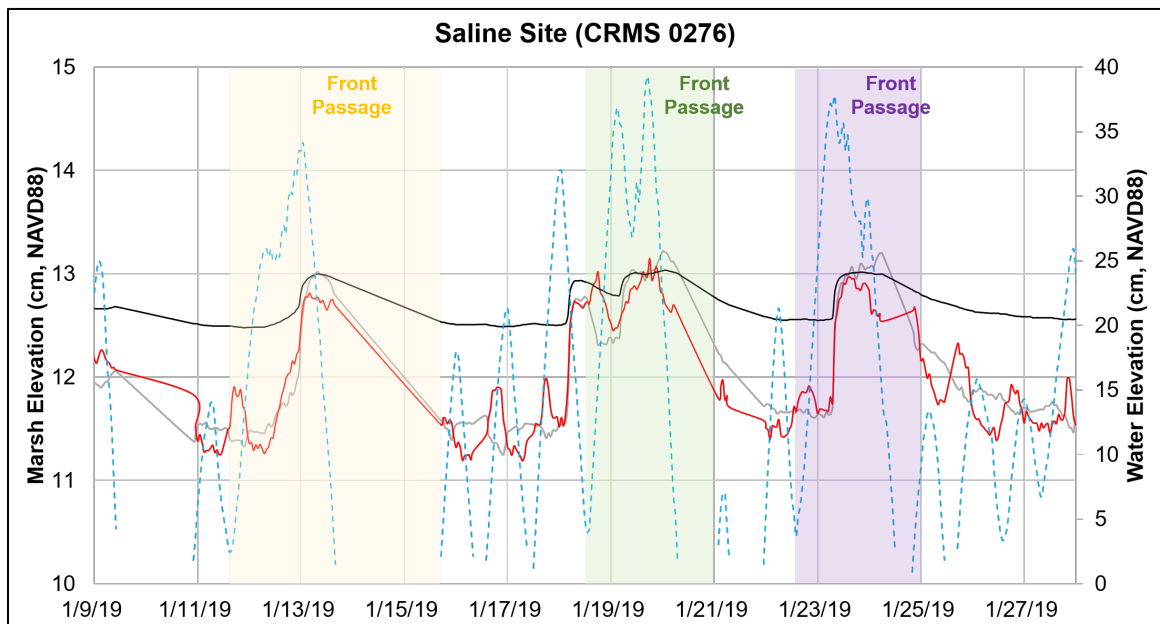


Figure 16. Time slice in January-February 2019 at the Saline site (CRMS 0276) showing the record of marsh surface elevation by the three sensors installed on the CR-SET (red line is laser, gray is ultrasonic, black is linear position). Water elevations on the nearby canal gauge at the CRMS station are also plotted at a different elevation scale (blue dotted line). Each of these plotted frontal events caused a water level response below +10 cm marsh elevation such that the sensors are not recording water elevation during this period. Note the time offset (hours) between the onset of water level pre-and post-frontal shifts and the onset of marsh rise and fall.

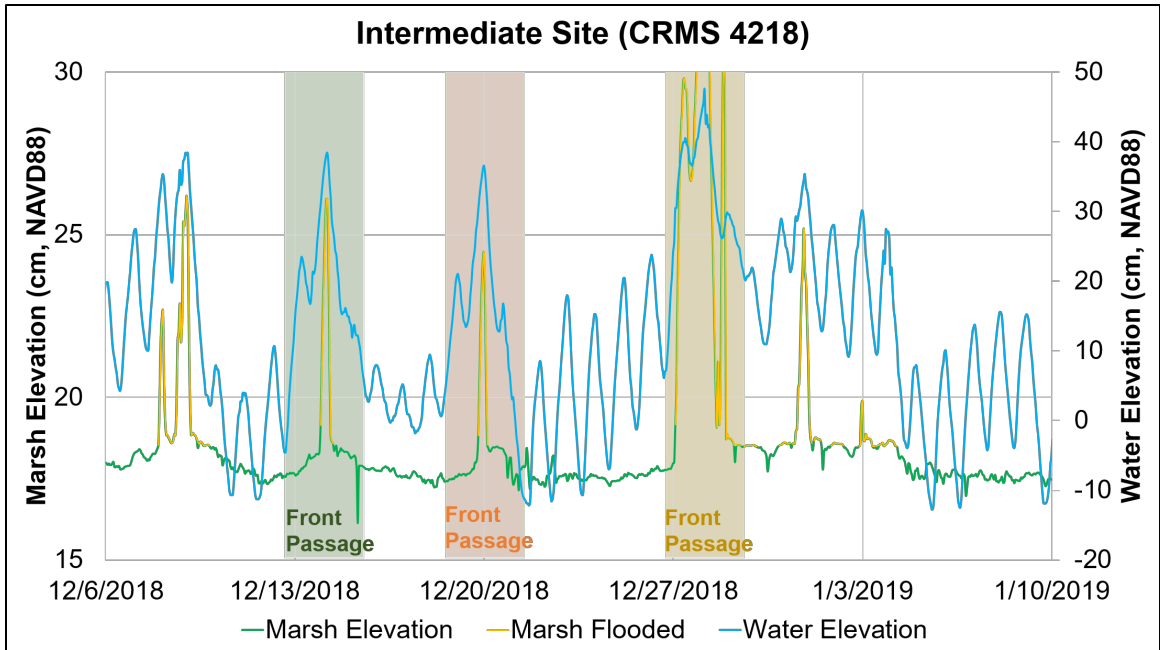


Figure 17. Marsh elevation as recorded by the ultrasonic sensor at Intermediate site (CRMS 4218) during the period of December 2018 to mid-January 2019. Also plotted are the canal water elevation as recorded by the CRMS gauge at the site (blue line). Flooding events over the +10 cm target are colored in yellow marking periods when the ultrasonic sensor was tracking the water surface and not the marsh surface.

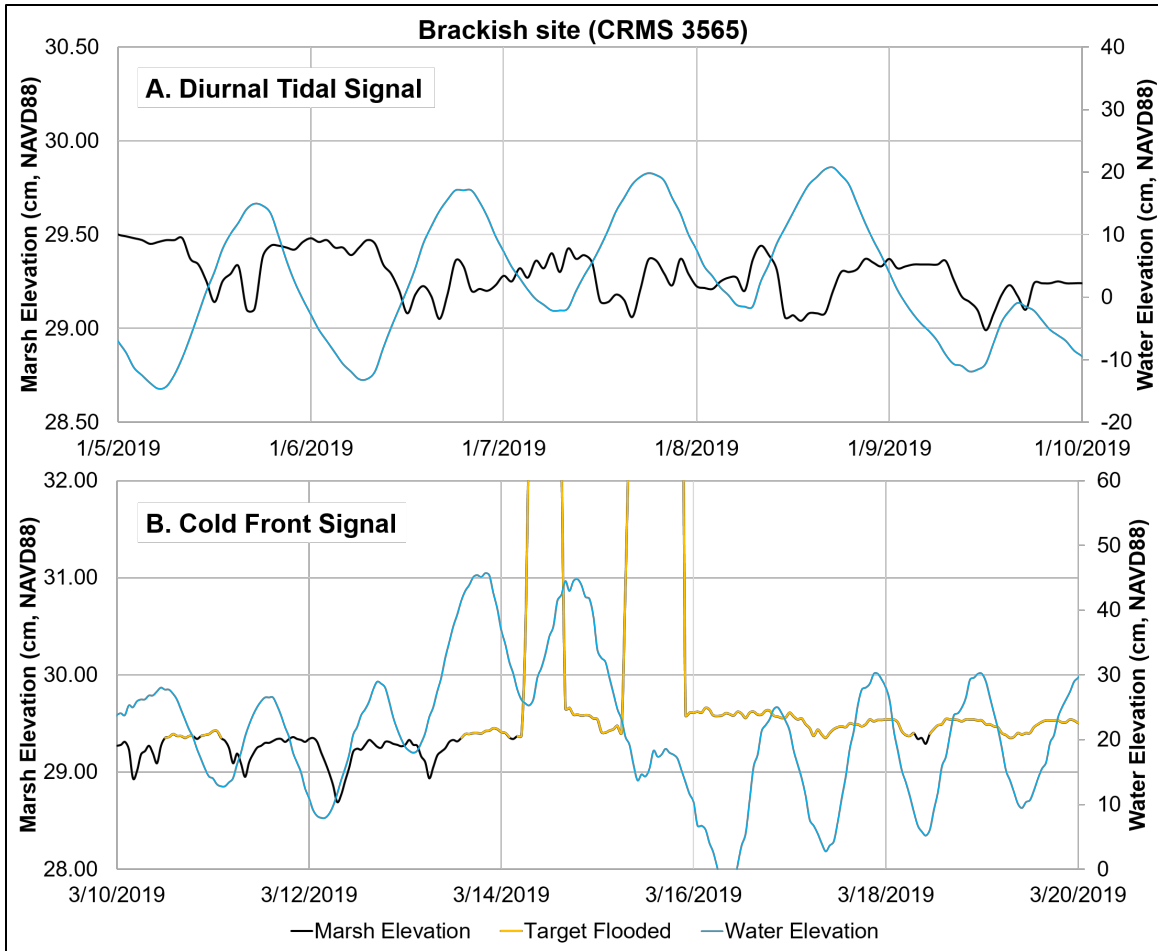


Figure 18. Marsh elevation (black and yellow line) as recorded by the ultrasonic sensor at the Brackish site (CRMS 3565). The top plot (A) shows the surface elevation response to normal tidal conditions (blue line) that do not flood the marsh surface during a period in January 2019. The bottom figure (B) shows the surface elevation response to a cold front. Also plotted are the canal water elevation as recorded by the CRMS gauge at the site. Flooding events over the +10 cm target are colored in yellow marking periods when the ultrasonic sensor was tracking the water surface and not the marsh surface.

To better understand the controlling factors on marsh elevation, the relative slope of the linear regressions is fitted to the marsh surface elevation relative to site-specific water elevation (Figure 19). Exposed marsh elevations (including +10 cm of water on the surface of the marsh) are derived by choosing the emergence point where the ultrasonic sensor begins to track water level (Figures 16, 17, and 18). Before fitting the regression, any marsh elevations above inundation +10 cm are removed as are outliers $>1 \sigma$ from the

mean. While R^2 fits remain poor (Figure 19), there are measurable differences in the degree of marsh contraction-expansion with water level between sites. The Intermediate site (CRMS 4218) has the highest slope and R^2 -value of the four sites and there is a general trend of increasing marsh response (slope) down basin.

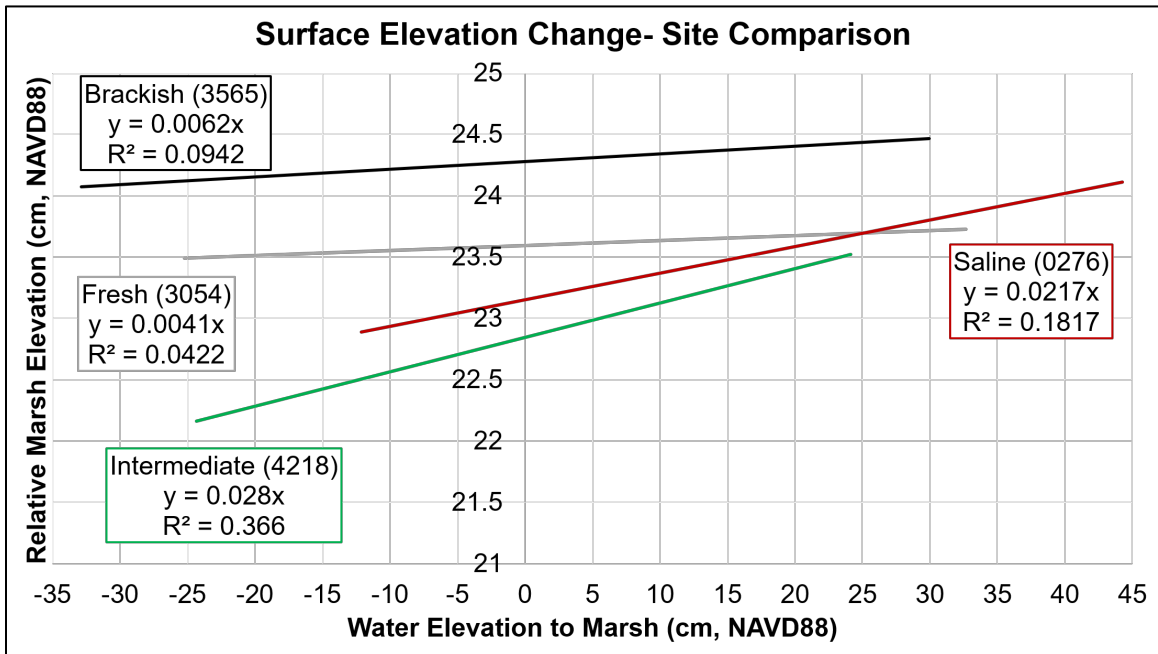


Figure 19. Best fit linear regression relationship between canal water level and marsh elevation as derived from the ultrasonic sensors for water elevations below marsh surface +10 cm. Each elevation is referenced to the Fresh site (CRMS 3054) for ease of comparison.

The direct correlation between rise and fall in canal water level and corresponding rise and fall of the marsh surface in CR-SET data, as well as the temporal lag in the marsh response, is not always observed at the Fresh site. At this site, which is located furthest away from the canal (67 m), the surface elevation does not respond to changes in water levels during a high-water event in the Fall 2018 (Figure 20A). However, during a similar high-water event in the Spring of 2019 the ultrasonic sensor responds to these flooding events on multiple occasions (Figure 20B). During the first event beginning on

24 November 2018- and extending through 26 November 2018, the marsh surface does not show a response to the ~25 cm change in water level. Comparing the same magnitude water level change over the same time period (~ 2 days) in the later event, the marsh surface shows a limited response before the target is flooded on 14 March 2019 (Figure 20B). It is not until a significant amount of time passes (~24 hours) until the marsh responds to the water level rise event occurring on 15 March 2019.

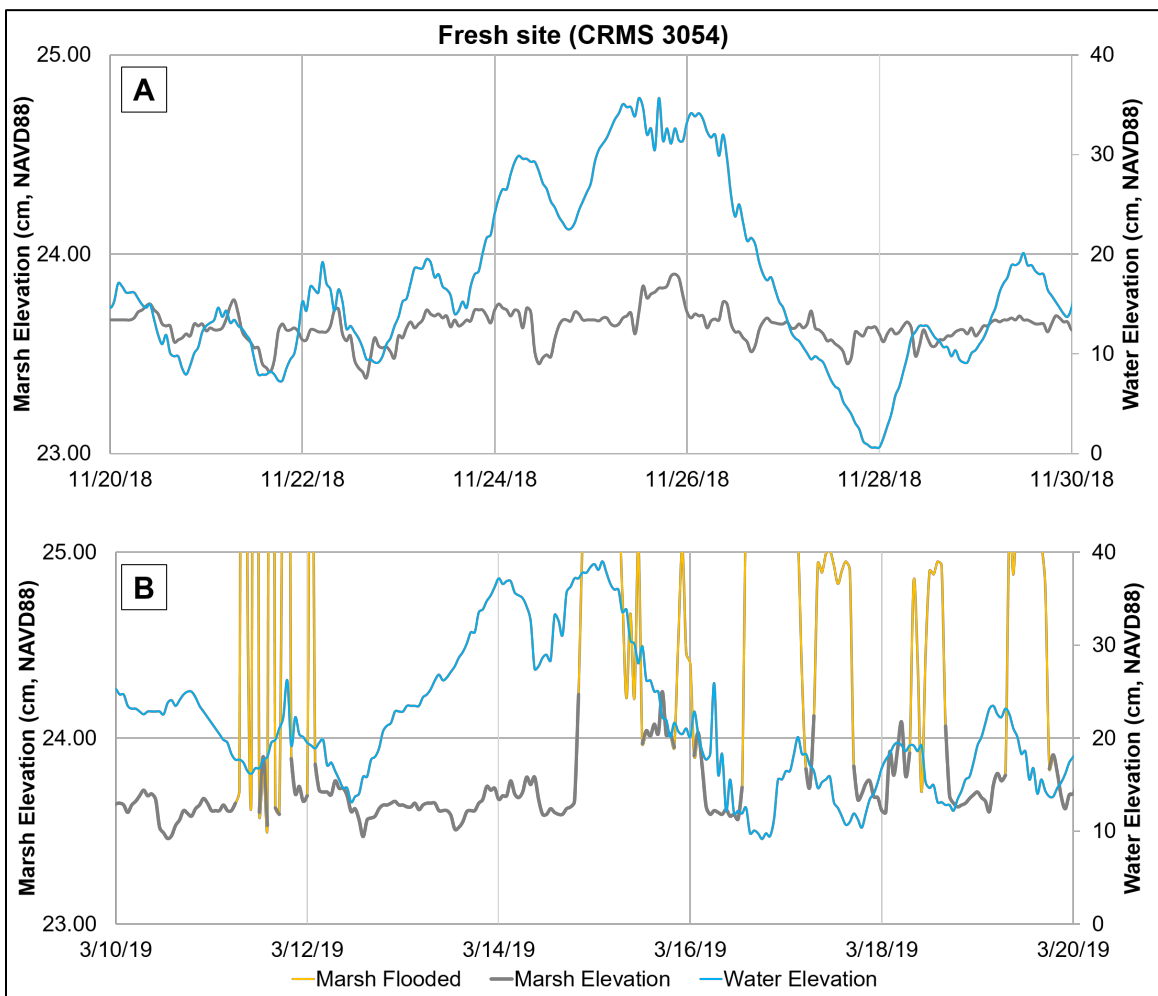


Figure 20. Marsh surface elevation response to water level changes in the canal at Fresh site (CRMS 3054) from the ultrasonic sensor. The upper plot (A) displays a water level change event in November 2018 with limited marsh response, while the lower plot (B) shows a period in March 2019 when the marsh elevation site responds like the other three sites—direct correlation between marsh level and water level.

5.1.1 Seasonal and Diel Fluctuations of the Marsh Surface

To further examine the relationship between canal water level changes at a site and the marsh surface elevation response, data were binned on daily and seasonal time scales. After removing data from canal local water elevations equivalent greater than +10 cm NAVD88 of water on the marsh surface and outliers beyond 1σ , monthly averages of ultrasonic sensor marsh elevations periods of record show higher elevations in the Spring and Summer versus lower elevations in the Fall/Winter. The magnitude of these seasonal marsh elevation changes is different between each site. The range of surface fluctuations for the longest period of record (Fresh site) exhibits little seasonal surface elevation (monthly range ± 0.22 cm). The most distinct seasonal difference is observed at the Intermediate site (monthly range ± 1.09 cm) where monthly averaged marsh surface elevation increases by almost 1 cm between March and May 2019 (Figure 21).

Diel elevation trends are consistent at three of the four sites where the marsh surface elevation decreases during day light hours and increases at night (Figure 22). The ultrasonic sensor at the Saline site shows the opposite trend and also has the smallest daily fluctuation in the surface elevation compared to the other three sites (Figure 22). Averaging the hours where the sun is above the horizon throughout the year (8 am through 4 pm) and the nighttime hours from 10 pm to 5 am, the marsh is on average 0.6 mm higher in nighttime at the Fresh, 0.7 mm at the Intermediate, -0.4 mm at the Brackish, and -0.1 mm at the Saline site.

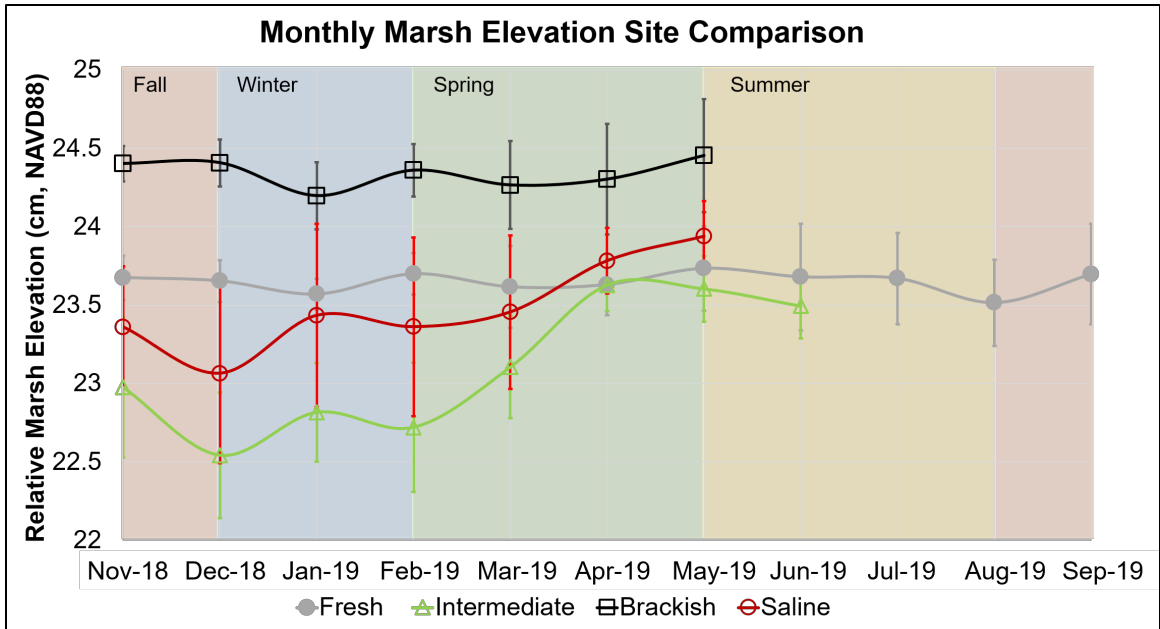


Figure 21. Monthly averaged marsh surface elevation compared between the four sites. Each site is referenced to the NAVD88 marsh elevation of the Fresh site (CRMS 3054) for graphing purposes. Error bars are 1σ from the mean monthly values.

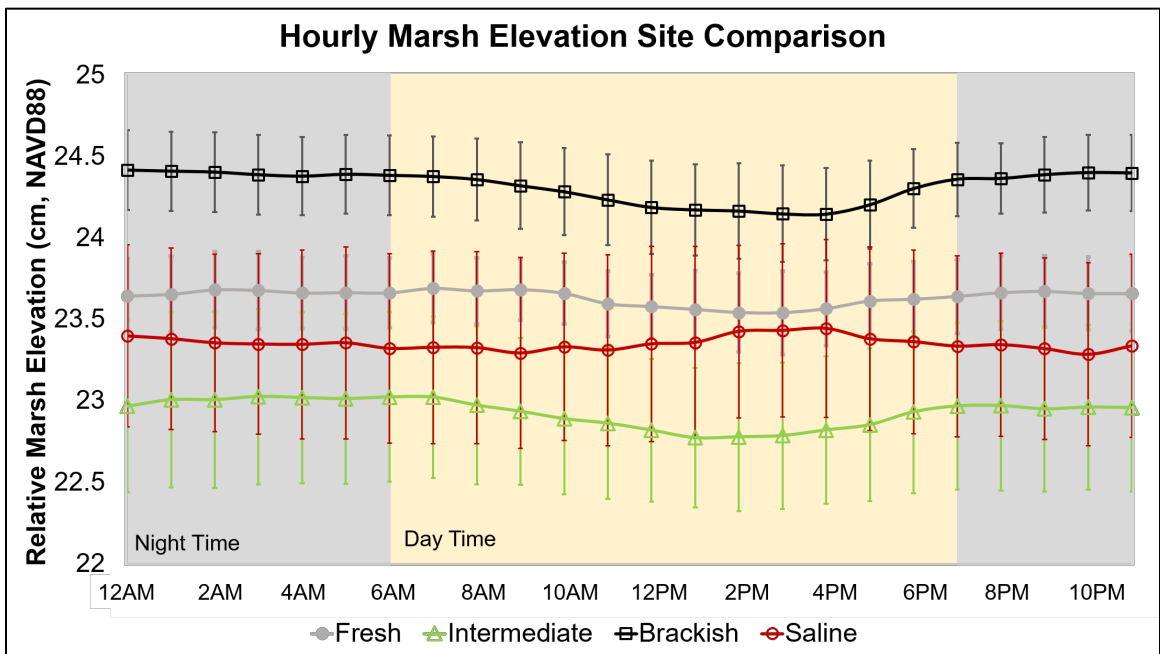


Figure 22. Hourly averaged surface elevation at each study site utilizing the ultrasonic sensors. Site-specific marsh elevations are referenced to Fresh site (CRMS 3054) for graphing purposes. Error bars are 1σ from the mean hourly values.

A summary of the monthly and hourly ranges of marsh surface elevation for the four sites is shown in Table 2. These observed ranges demonstrate that there are regular differences between marsh elevation between day and night and between seasons that explain much of the variability observed in the sensor data at a given canal water elevation (see Figure 14).

Table 2. *Monthly and Hourly Marsh Elevation Ranges and Standard Deviation at the four study sites. Hourly elevations are calculated based on daylight hours (8 am – 4 pm) and nighttime hours (10 pm to 5 am). Monthly averages are calculated by grouping fall and winter months separate from spring and summer months.*

| CRMS Sites | Average elevation difference between daylight and nighttime hours (mm) | Average elevation difference between seasons (mm) |
|--------------------------|---|--|
| Fresh 3054 | 0.6 ± 0.5 | 0.2 ± 0.6 |
| Intermediate 4218 | 0.7 ± 0.8 | 5.3 ± 4.2 |
| Brackish 3565 | -0.4 ± 0.9 | 0.0 ± 0.9 |
| Saline 0276 | -0.1 ± 0.4 | 3.5 ± 2.9 |

5.1.2 Water Level Statistics

As outlined in Section 5.2, there are seasonal patterns in the monthly fluctuations in marsh elevations at the four CR-SET sites (as well as diel variations). To examine whether there is a link in the seasonal signal to Gulf of Mexico levels, and the adjacent Barataria Bay and fringing wetlands where the sites are located, the monthly averaged water level plotted for the water year of 2018 (1 October 2018 through 30 September 2019) at the Grand Isle tidal gauge (NOAA gauge 8761724) and at the four study sites from CRMS water elevation records (Figure 23). Data are clipped to water levels between that the 5th and 95th percentiles and are based on hourly sampling frequency at both the NOAA and CRMS gauges. Both datasets demonstrate that water levels are

highest during the Spring/Summer months and lowest during the Fall/Winter (Figure 23). These trends correspond to those observed seasonally in marsh surface elevation changes (Figure 21) that is, a higher Gulf of Mexico and Barataria Bay water level is seasonally correlated with higher water levels and higher marsh surface elevations during the Summer than Winter.

Previous studies (Turner, 1991; Kolker et al., 2011) have shown that the seasonal water level change at Grand Isle and the Gulf is primarily driven by thermal expansion, changes in sea water density, atmospheric pressure, and other steric effects in the warmer, and higher solar insolation period. These seasonal water levels trends described by these previous studies generally match longer- term (WY 2012-2019) monthly water elevations calculated in the present study for the CR-SET/CRMS sites and the Grand Isle gauge (Figure 24). These trends are only partly associated with the distance between the CR-SET/CRMS sites from ocean-sourced tide and Barataria Bay (Table 3) but it should be noted that meteorologically driven water level variations are also present in these monthly averages and have elements that are seasonally distinct (e.g., the cold front season from October-April, for instance). An ANOVA of the four study sites shows there is a statistically significant difference between the short term (WY 2019) and longer-term (WY2012-2019) variation in water level except at the Intermediate site where there is no difference between the long term and short-term average (Table 4).

Table 3. CR-SET/CRMS site distances from the nearest canal and from the NOAA Grand Isle Gauge (calculated from Google Earth imagery). Maps provided in Appendix D.

| CRMS Sites | Linear Distance from NOAA Grand Isle Gauge | Linear Distance from CR-SET Platform to Nearest Water Body |
|-------------------|--|--|
| Fresh 3054 | 64.1 km | 67.3 m |
| Intermediate 4218 | 38.8 km | 11.8 m |
| Brackish 3565 | 29.6 km | 23.2 m |
| Saline 0276 | 39.4 km | 5.7 m |

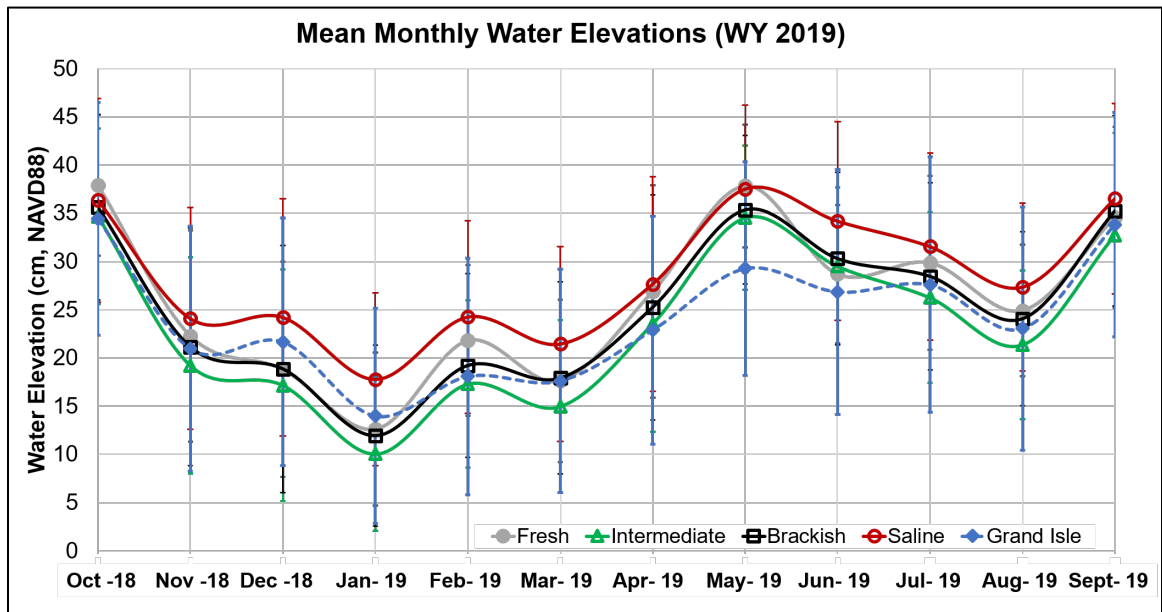


Figure 23. Monthly averaged water levels at each CR-SET site (from the adjacent CRMS gauge) and at the tide gauge at the mouth of Barataria Bay (NOAA gauge 8761724, Grand Isle, Louisiana) from October 2018 through September 2019. Error bars are 1σ of the data within the 5th and 95th percentile.

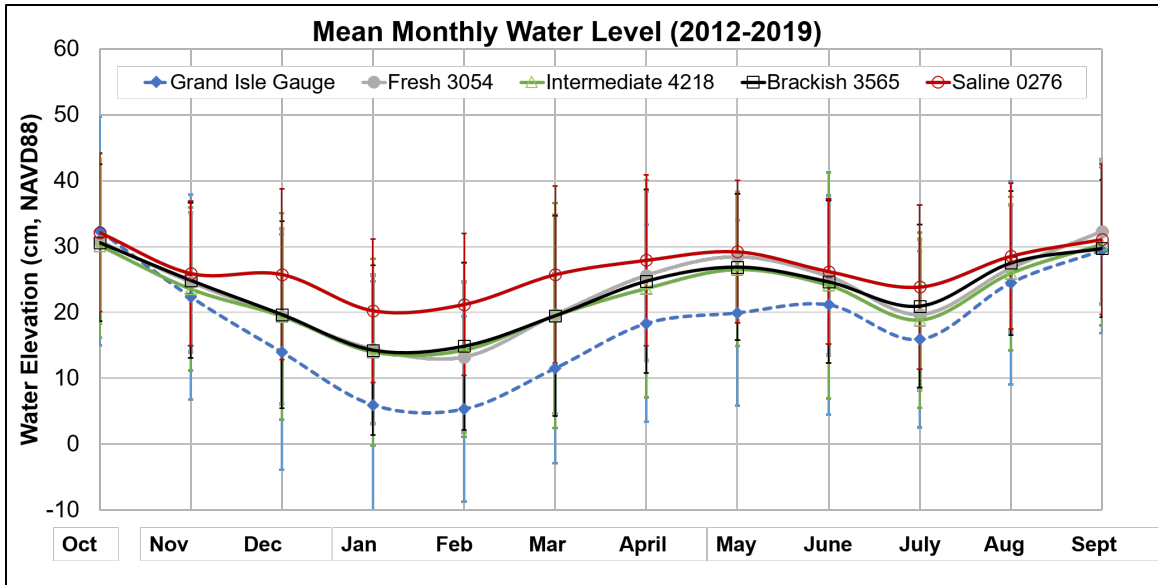


Figure 24. Monthly averaged CRMS and Grand Isle gauge (NOAA gauge 8761724) water elevations from WY 2012 - 2019, excluding years 2013-2014 where the water year records are incomplete.

Table 4. Longer-term (WY 2012-2019) and short-term (WY 2019) average water elevations at the four study sites within Barataria Basin.

| CRMS Site | Av. Water Elevation (cm) WY 2012-2019 | Av. Water Elevation (cm) WY2019 |
|--------------------------|---------------------------------------|---------------------------------|
| Fresh 3054 | 22.4 ± 16.2 | 26.3 ± 14.6 |
| Intermediate 4218 | 23.6 ± 16.6 | 23.8 ± 16.1 |
| Brackish 3565 | 24.0 ± 17.6 | 25.6 ± 16.6 |
| Saline 0276 | 26.0 ± 14.5 | 29.8 ± 15.8 |

5.2 Soil Properties and Stratigraphy

5.2.1 Core Stratigraphy

Stratigraphic columns derived from the auger cores at the study site are shown in Figures 25 and 26. The mineral granulometric values were obtained from the core descriptions and laboratory analysis of granulometry of sampled intervals (Figure 25) after LOI removal of organic components. The cores from all four sites contain a down core mineral mixture of silty clays and clayey silts in the organic-rich, surficial marsh layer that is captured throughout the cored intervals. The Brackish and Saline sites

contain the coarsest mineral sediments: coarse silt is the dominant component in the upper 24 cm of the Brackish site and the upper 2 cm of the Saline site. No clear trend of down core coarsening or fining of the mineral fraction is observed at any of the four study sites.

Organics are categorized into facies based on percent organic matter (through the LOI proxy) following the designations of Kusters et al. (1989) and Wilson and Allison (2008) (Table 5). Using this definition, the Fresh, Intermediate, and Brackish sites showed intervals of true peat intervals ranging from 5-25 cm thick, but all site cores were dominantly a combination of organic-rich and organic poor muds (Figure 26). In the 0-87 cm depth interval that was reached in cores at all four study sites, average organic matter content was $23\% \pm 16$ for the saline site, $41\% \pm 21$ for the brackish, $47\% \pm 18$ for the intermediate site, and $40\% \pm 27$ for the fresh site (Table 5).

Table 5. Organic sedimentary facies of cores taken in Barataria Basin, Louisiana as defined by Kusters et al. (1989) and observed porosity and organic matter (LOI) contents for each of the four study sites from 0-87 cm.

| Facies | OM % \pm SD | Porosity \pm SD | Facies |
|--------------------------|---------------------------------|-------------------------------------|---|
| Fresh 3054 | 42 ± 27 | 82 ± 9.4 | 4.6 % True Peat 72.4 % Organic- Poor 23 % Organic- Rich |
| Intermediate 4218 | 47 ± 18 | 87 ± 1.8 | 28 % True Peat 33% Organic- Poor 37% Organic-Rich |
| Brackish 3565 | 41 ± 21 | 84 ± 6.7 | 0% True Peat 20% Organic- Poor 80% Organic- Rich |
| Saline 0276 | 23 ± 16 | 80 ± 1.0 | 0% True Peat 85% Organic-Poor 15% Organic- Rich |

Mineral Stratigraphic Columns

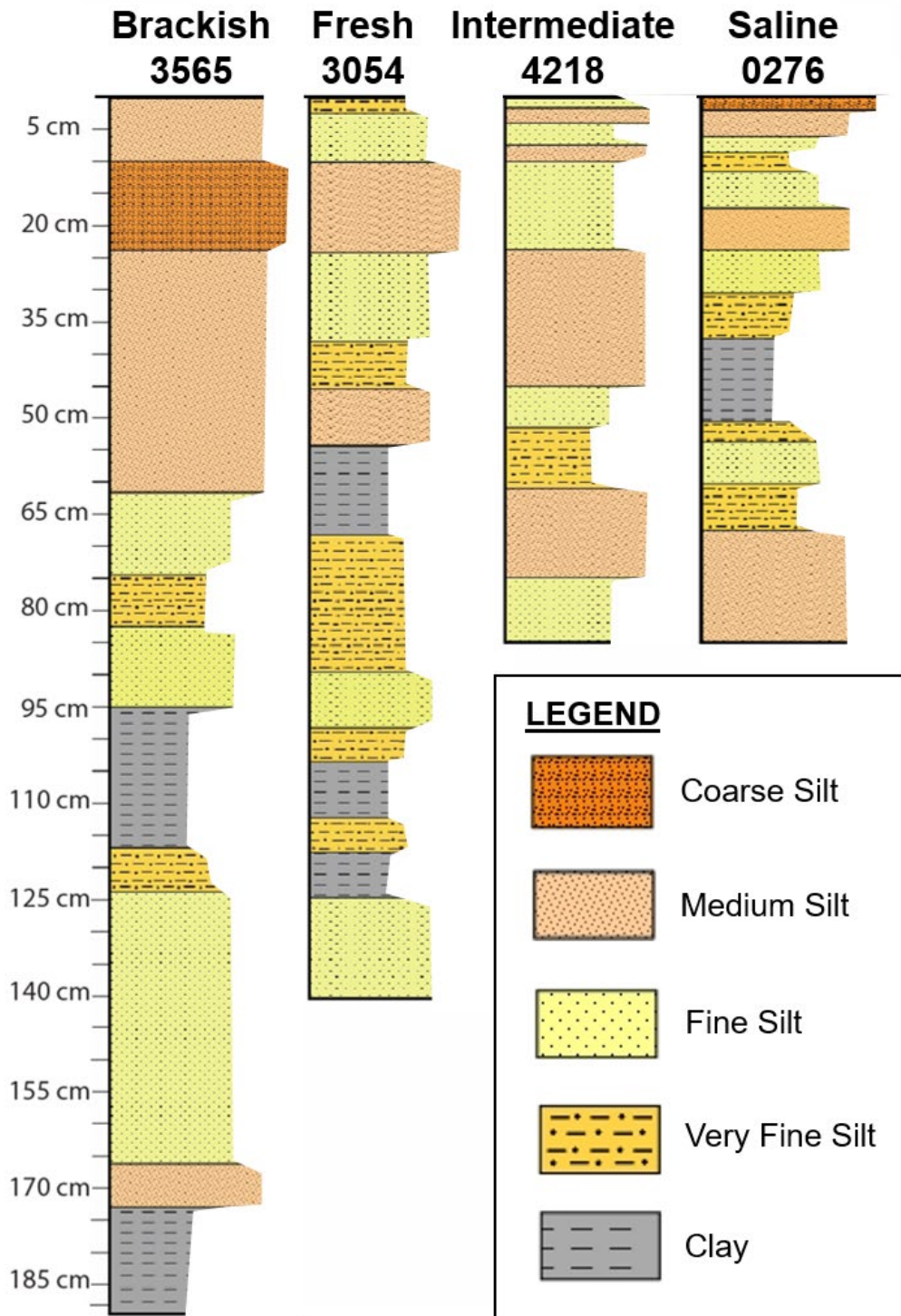


Figure 25. Stratigraphic columns of the D_{50} (median) granulometry from auger cores collected at each site. The D_{10} , D_{50} , and D_{90} grain size is measured at all subsampled intervals using the Malvern Mastersizer 3000. Core descriptions are available in Appendix E.

Organic Stratigraphic Columns

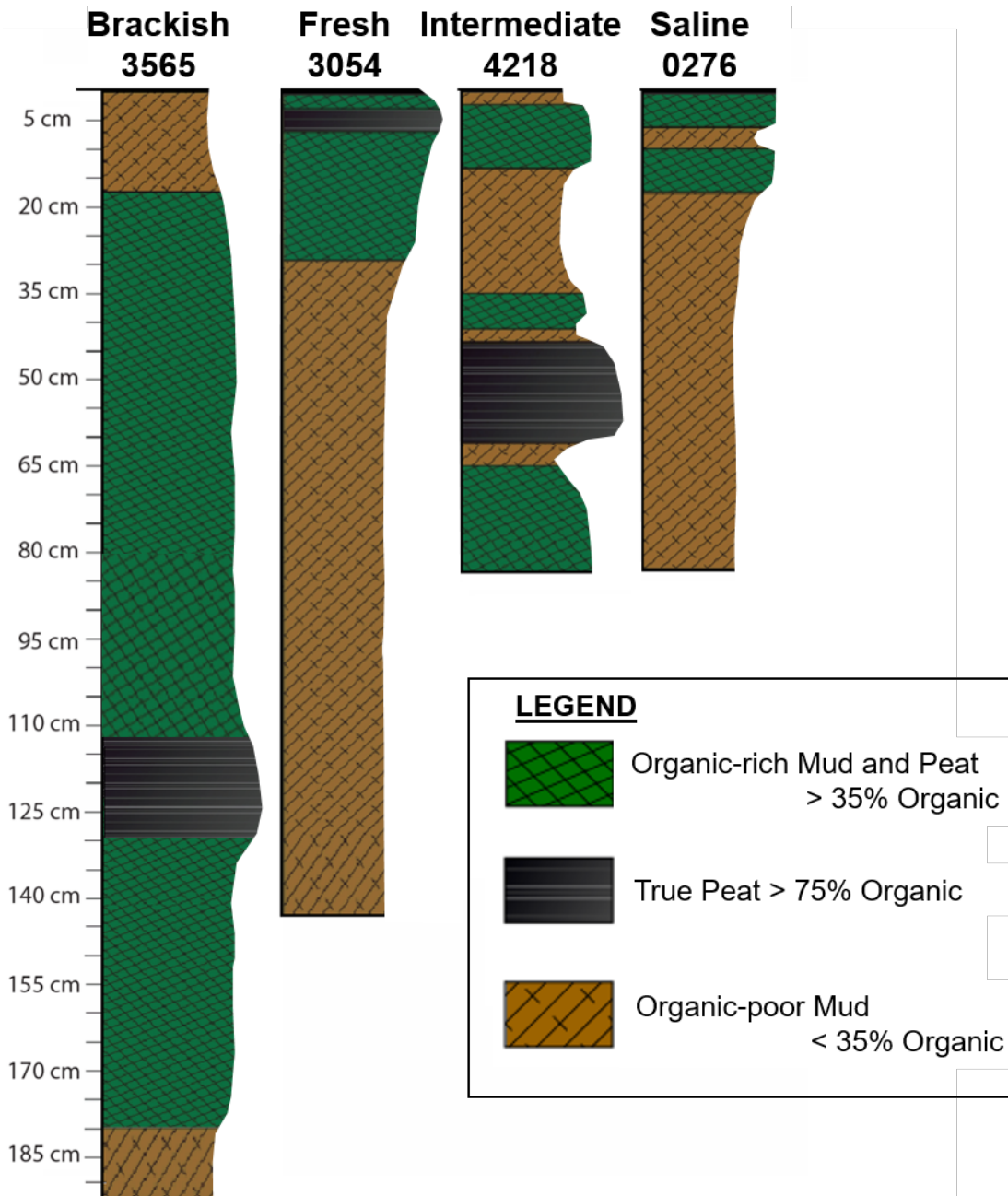


Figure 26. Stratigraphic columns of organic matter content for the cores from the four study sites. Organic matter content is derived from LOI analysis and divided into three categories: Organic-rich Mud and Peat, True Peat, and Organic-poor Mud (Table 4) based on the categorization of Kusters et al. (1989). Core descriptions are available in Appendix E.

5.2.2 Soil Properties

Auger cores were also examined for soil properties including porosity (ratio of the volume of void spaces to particles (organic and mineral)). Organic matter density was also calculated using a density of 1.24 g/cm^3 . The down core results of this analysis from the four study sites are shown in Figure 27. The porosity profiles show that the Fresh and Saline sites contain high porosities at the top of the core ($> 90\%$) but decline steadily to the base of the core (87 cm) (see Figure 27) to about 65%. The Intermediate site shows a relatively high porosity throughout the 87 cm core length (85-90%), while the Brackish site has relatively low porosity at the core top (0-10 cm) and then has a high porosity (85%-90%) to a depth of 190 cm (Figure 27).

The total organic matter content is shown in Figure 28 and Table 6 for the four study sites. The allochthonous versus autochthonous origin of the organic matter and its relative importance in the overall organic (LOI) content, the proportion of roots and detrital organic matter was determined (Figure 28) as explained in the methods section. Each of the four study site auger cores shows a concentration in root mass at various depths within the subsurface depending on marsh type. At the Fresh site, roots and root fragments make up majority of the upper 20 cm. The Intermediate and Brackish sites contain the most root mass overall in the organic-rich marsh layer that comprises the cored interval. The Intermediate site has the largest organic matter content of the four sites, with rooting concentrated in the 20-30 cm depth interval. The Brackish site contains rooting to a depth of 140 cm although detrital organic matter comprises most of the overall organic content. The Saline site is similar to the Fresh site with organic content decreasing down core.

Table 6. Organic matter content (%) for the four study sites in Barataria Basin derived by Loss On Ignition (LOI).

| CRMS Sites | Organic Matter Content (%) 0-87 cm | Organic Matter Content (%) Total Core Length |
|--------------------------|---------------------------------------|---|
| Fresh 3054 | 42.2 ± 26.0 | 32.5 ± 26.3 |
| Intermediate 4218 | 47.3 ± 17.8 | 47.3 ± 17.8 |
| Brackish 3565 | 40.6 ± 21.2 | 49.1 ± 21.7 |
| Saline 0276 | 23.2 ± 16.3 | 23.2 ± 16.3 |

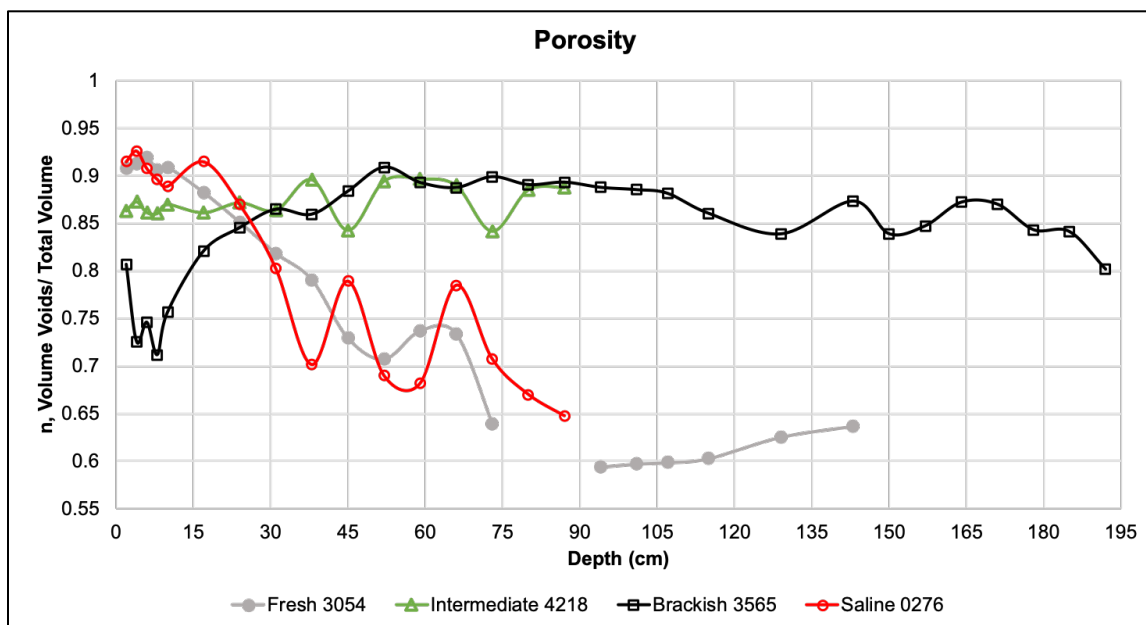


Figure 27. Downcore porosity at each four study sites in Barataria Basin from auger core samples.

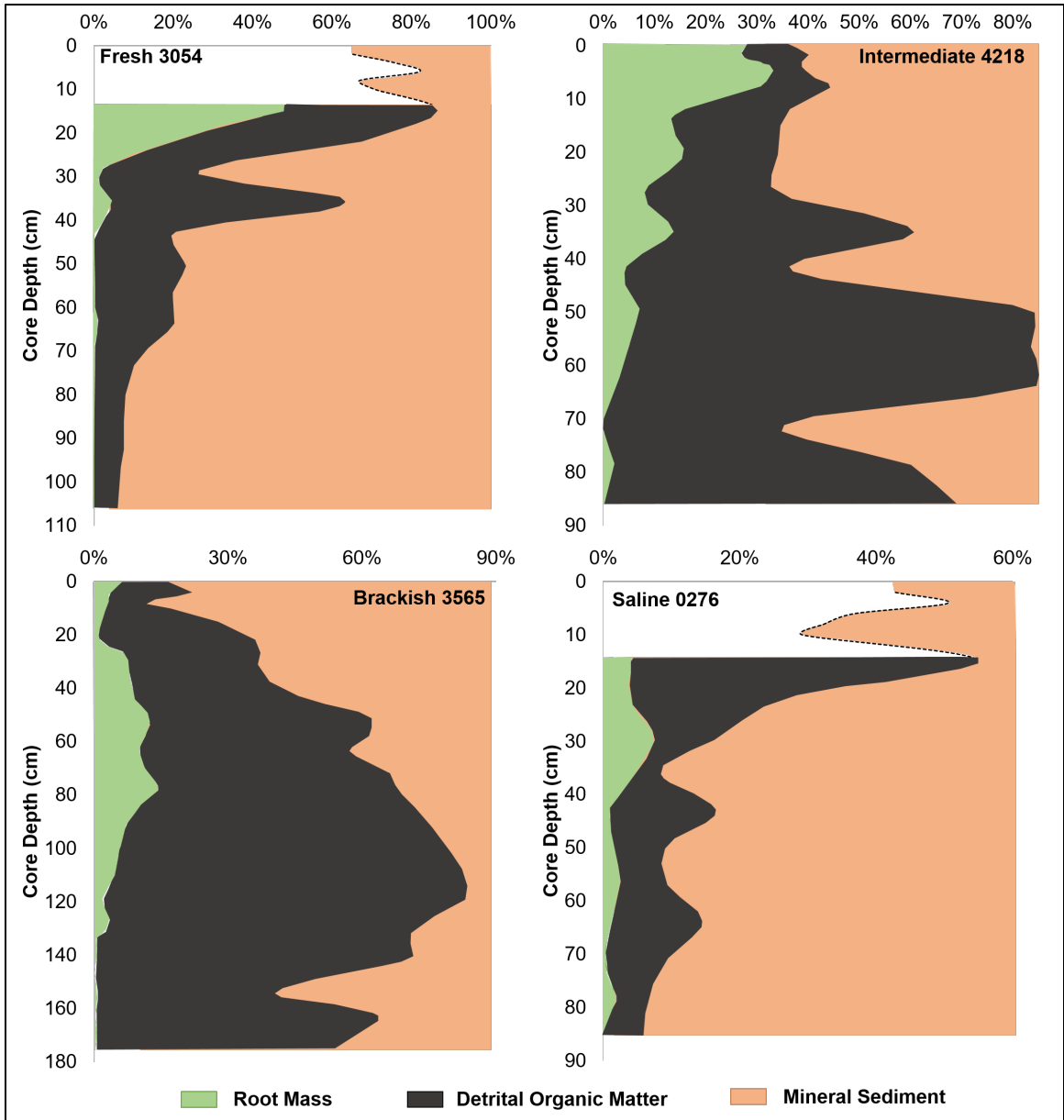


Figure 28. Total organic matter and mineral content with depth for the cores from the four study sites as determined by Loss On Ignition (LOI). The overall organic matter content was divided into large root fragments and detrital organic material. The dotted lines in the Fresh and Saline sites are intervals where only LOI analysis was conducted and the organic matter differentiation could not be made.

5.2.3 Radionuclide-derived Sediment Accumulation Rates

Excess ^{210}Pb activities ($^{210}\text{Pb}_{\text{xs}}$) with depth are shown in Figure 29 and 30 for the four study sites. Each of the four sites showed a distinct logarithmic decrease with depth that can be utilized to calculate a ~ 100 y average sediment accumulation rate for the site since ^{210}Pb has a half-life of 22.3 y and excess activity is measurable to 4-5 half-lives. This $^{210}\text{Pb}_{\text{xs}}$ down core decay is used to derive average accumulation rates that range from 7.1 +/- 3.0 mm/yr at the Saline site to 9.0 +/- 1.2 mm/yr at the Brackish site (Table 7).

The same core samples and gamma spectrometer analyses yielded activities of the anthropogenic radiotracer ^{137}Cs . Down core ^{137}Cs activities show a clear depth peak in activity (Figures 29 and 30) resulting in calculated ^{137}Cs accumulation rates of between 2.9 (Fresh and Saline sites) and 9.3 mm/y (Brackish site) (Table 7). While there is correlation between the site of highest ^{210}Pb and ^{137}Cs accumulation rate (Brackish), the timespans of integration from the two radiotracers are different: up to ~ 100 y for the ^{210}Pb and 2018-1963 = 55 y for ^{137}Cs . For further comparison of sediment accumulation rates at the four study sites, Table 1 also shows for comparison the calculated vertical accretion rate measured by R-SET tables at the adjacent CRMS station by Jankowski et al. (2017). These rates are averaged over a shorter timescale, ranging from the last 8-11 years (Table 7).

Table 7. Lead-210, Cesium-137, and CRMS VA rates compared linearly, consolidated to 75% porosity assuming 25% mineral at 2.65 g/cm³, and 75% consolidation of porosity assuming 25% is organic (1.24 g/cm³) and mineral sediment. The breakdown of organic matter and mineral sediment is determined by LOI analysis. Rates are reported in mm/yr.

| | Fresh 3054 | Intermediate 4218 | Brackish 3565 | Saline 0276 |
|--|---------------------|--------------------------|----------------------|---------------------|
| Lead- 210 | | | | |
| Linear Sediment Accumulation Rate | 4.5 ± 1.0 | 8.0 ± 0.7 | 9.0 ± 1.2 | 7.1 ± 3.0 |
| Consolidated Linear Accumulation Rate (Mineral) | 4.2 ± 1.4 | 2.4 ± 0.21 | 2.2 ± 0.49 | 6.3 ± 3.4 |
| Consolidated Linear Accumulation Rate (Organic) | 2.9 ± 1.0 | 1.5 ± 0.13 | 1.5 ± 0.32 | 4.0 ± 2.2 |
| Consolidated Linear Accumulation Rate (Mineral+Organic) | 4.8 ± 1.5 | 3.3 ± 0.3 | 3.4 ± 0.65 | 6.8 ± 3.6 |
| Cesium- 137 | | | | |
| Linear Sediment Accumulation Rate | 2.9 + 0.91/- 1.3 | 5.5 +0.91/-1.6 | 9.3 +1.3/-1.3 | 2.9 +0.91/-1.3 |
| Consolidated Linear Accumulation Rate (Mineral) | 0.36 +0.42/-0.19 | 1.7 +0.35/-0.59 | 3.7 +0.26/-0.28 | 0.53 +0.24/-0.29 |
| Consolidated Linear Accumulation Rate (Organic) | 0.24 +0.27/-0.12 | 1.1 +0.23/-0.38 | 2.4 +0.17/-0.18 | 0.34 +0.16/-0.29 |
| Consolidated Linear Accumulation Rate (Mineral+Organic) | 0.60 +0.56/-0.30 | 2.1 +0.48/-0.73 | 4.6 +0.41/-0.41 | 0.70 +0.31/-0.39 |
| CRMS | | | | |
| Sediment Accumulation Rate | 8.9 ± 21.1 | 21.0 ± 6.0 | 15.4 ± 10.8 | 14.4 ± 13.3 |
| Time Range | 2009 - 2015 | 2008 - 2015 | 2006 - 2015 | 2008 - 2015 |
| Consolidated Linear Accumulation Rate (Mineral) | 0.88 ± 0.53 | 1.7 ± 1.2 | 2.9 ± 2.6 | 0.91 ± 0.64 |
| Consolidated Linear Accumulation Rate (Organic) | 0.57 ± 0.34 | 1.1 ± 0.78 | 1.8 ± 1.6 | 0.59 ± 0.41 |
| Consolidated Linear Accumulation Rate (Mineral+Organic) | 1.6 ± 0.96 | 2.2 ± 1.5 | 3.6 ± 2.9 | 1.3 ± 0.93 |

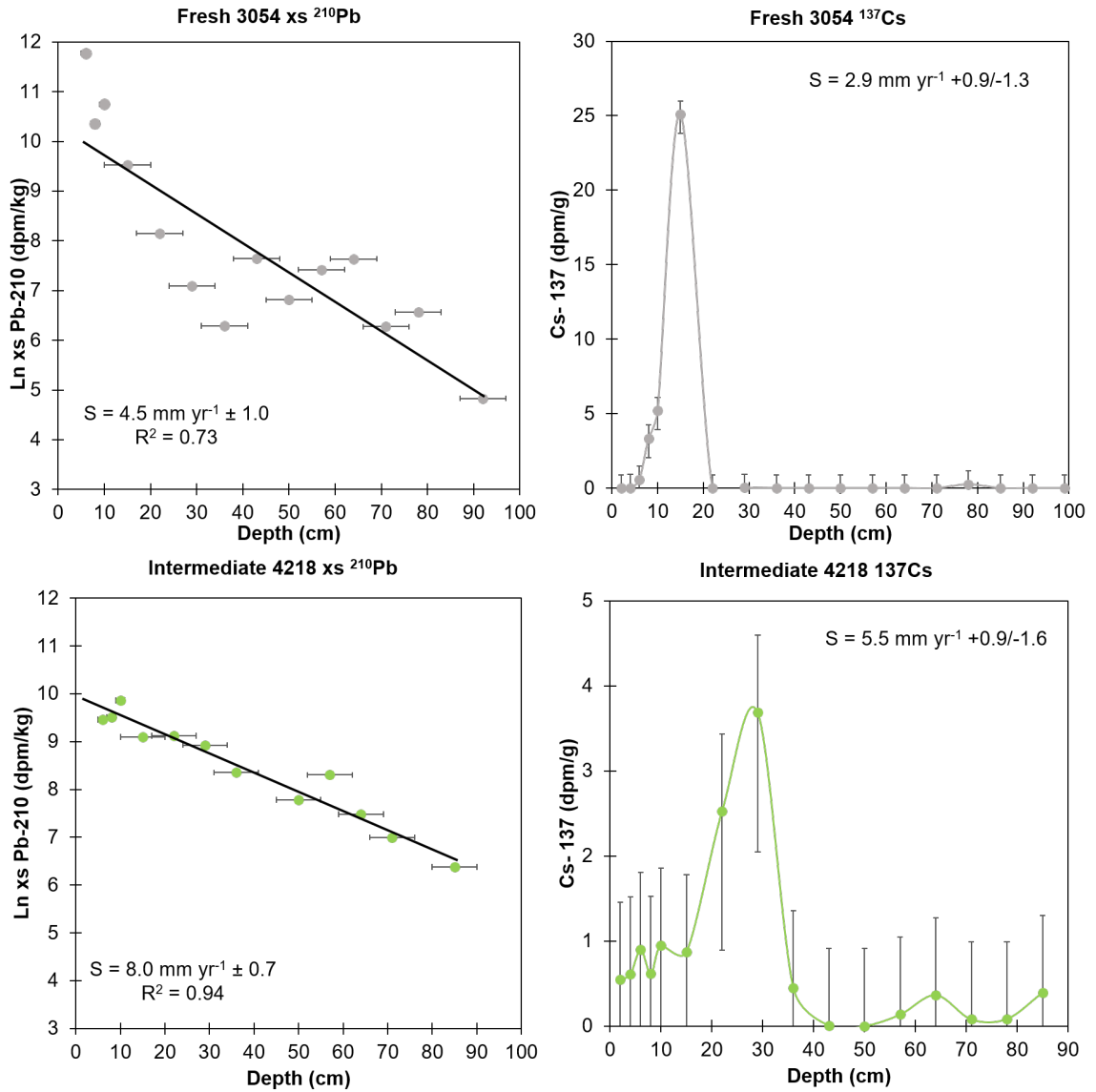


Figure 29. Downcore activities and accumulation rates derived from radionuclide dating of ^{210}Pb and ^{137}Cs for the Fresh and Intermediate sites. The peak in the Cesium records corresponds to the year 1963.

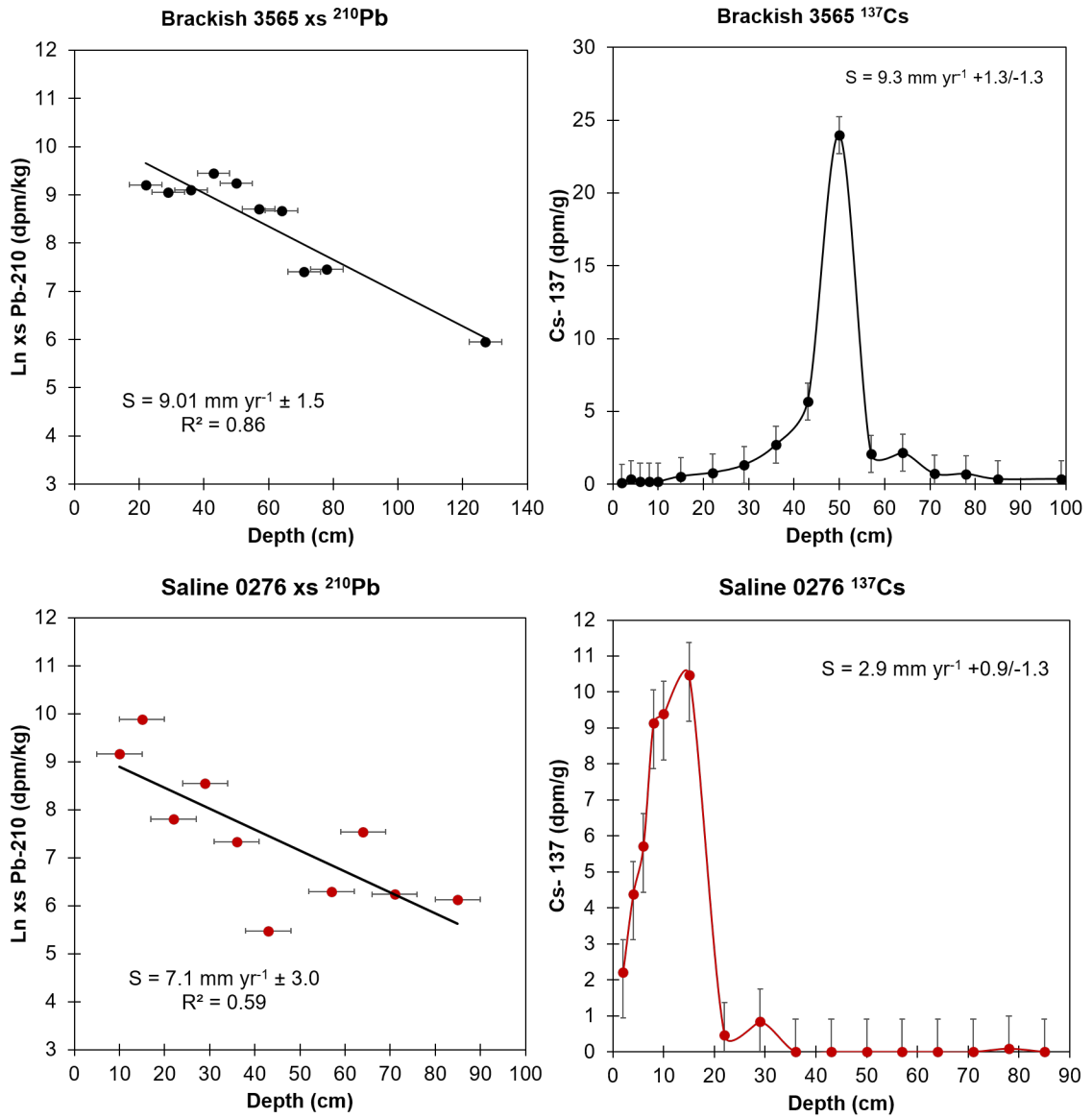


Figure 30. Downcore activities and accumulation rates derived from radionuclide dating of ^{210}Pb and ^{137}Cs for the Brackish and Saline sites. The peak in the Cesium records corresponds to the year 1963.

6. DISCUSSION

6.1 Marsh Expansion and Contraction: Mechanisms and Controls

The results of the present, high-resolution surface elevation monitoring study suggest that Barataria Basin coastal marshes of a variety of ecotypes from fresh to saline expand and contract in elevation on short-time scales (hours to days) in response to local water level fluctuations in adjacent water bodies (e.g., canals, bayous, and lakes). Previous studies that used high-resolution elevation measurements (Cahoon et al., 2011 and references therein) demonstrate that subsurface hydrologic interactions influence this marsh elevation change. The Cahoon. (2011) study focuses on the magnitude of perturbations to the marsh surface due to short-term hydrologic and groundwater interactions at two different wetland sites including a saline marsh wetland at Old Oyster Bayou, LA east of Atchafalaya Bay. At this site, R-SET's were installed at depths of 0.35 m, ~4 m, and 17 m and monitored at 1-3-month intervals over an 18-month period. An ultrasonic CR-SET similar to that applied in the present study was installed to a depth of 2 m with a target 15 cm into the subsurface (integrating the depth window from 15 cm to 2 m while the present study integrates 15 cm to 1.5 m) collecting data every 30 minutes (every one-minute in the present study). The Cahoon study also uses feldspar marker horizons to quantify vertical accretion and use that to calculate shallow subsidence (VA-SEC) from multiple depth intervals (0-0.35 m, 0-2 m, 0-4 m, and 0-17 m). Marsh porewater levels were also recorded using a pressure transducer installed in a PVC well to about 50 cm sediment depth collecting data at 30-minute intervals. Several phenomena identified by the Cahoon et al. (2011) study corroborate the results of the present experiment's results from multiple marsh types. Marsh surface elevation changes,

continuously measured by their CR-SET, and less frequently by their R-SETs, were directly correlated to wind direction (meteorological tide) and regional drought (drawdowns) patterns. When groundwater elevation falls this results in dewatering and contraction of the marsh surface, while in the present study, water levels in the adjacent water bodies (CRMS gauges) serve as a proxy for groundwater level. Cahoon et al. (2011) note that *the change in marsh surface elevation quickly decline[s] with decreases in water level but it also shows a rapid, albeit slower, response to subsequent flooding events*. The rapid equilibration (61% of the variation in marsh surface elevation were attributed to this) between the two suggest that canal water level in the present study is a valuable proxy for groundwater level in the marsh substrate. Water infiltration and drainage causing shrink-swell of marsh substrates has been observed by other studies as well, typically using R-SET measurements widely spaced in time (Nuttle and Hemond, 1988; Smith and Cahoon, 2003; Whelan et al., 2005) and has been attributed to evapotranspiration by marsh plants and changes in hydrology. The Cahoon et al. (2011) study concludes that changes in marsh surface elevation are a result of hydrologic conditions mediated by meteorological conditions that force water in and out of the estuary, and evapotranspiration by plants. They hypothesize that during extended low porewater levels, marsh surface contraction leads to increases in overburden load, causing consolidation of mineral and organic-rich substrate from degassing/dewatering.

The direct coupling of canal, and by hydrologic connectivity, Bay and Gulf water levels, with marsh groundwater level and marsh surface elevation has several possible controls not examined in previous studies. Importantly, no sedimentological or stratigraphic evidence was presented by Cahoon et al. (2011). The present study also

examined different marsh ecotypes, each with distinct flooding regimes, marsh species specific aboveground and belowground characteristics, mineral sourcing and trapping efficiency, and underlying stratigraphy.

The pathway of subsurface water exchange between the marsh and the nearest water body (hereafter just standardized as “canal”) is clearly lateral (Figures 31 - 33), and hence coupled to the substrate characteristics between the CR-SET and the canal. There is no evidence of decoupling from the underlying substrate (e.g., floatant formation; Swarzenski et al., 1991) in the ultrasonic data measuring the elevation change in the 15 cm to 1.5 m depth interval at the four sites. It is the alternating filling and draining of this marsh vadose (unsaturated zone) layer that is the primary control on the observed marsh elevation changes of up to a cm over hours to a few days. In the four study sites, where marsh organic-rich surficial layer varied from 30 to 100 cm thick, (30 cm at the Saline site, and 100 cm at the Brackish site), at no time during the entire experimental period did water levels fall low enough to reach the subsurface NAVD88 elevation of the base of the marsh layer (ranging from -73.8 cm NAVD88 (Saline) to -58 cm NAVD88 at the four sites (Brackish)). Hence, a two-zone system is envisioned, with the deeper portion of the marsh organic-rich layer serving as a phreatic (always saturated) zone.

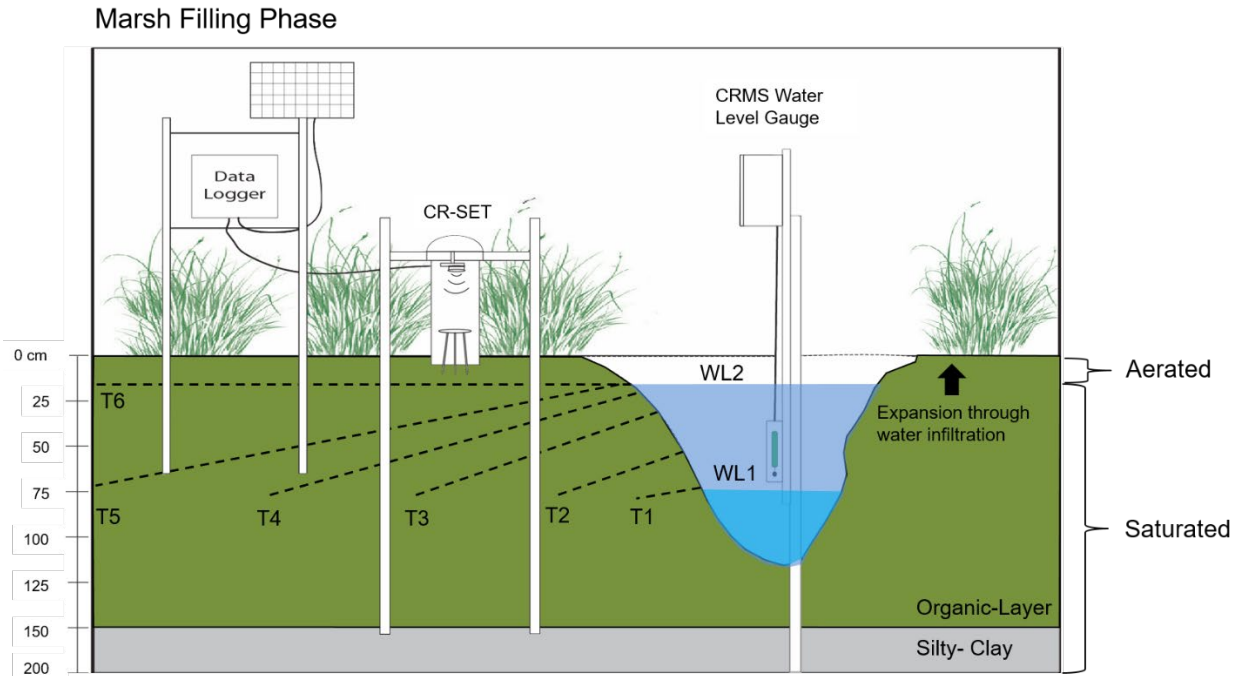


Figure 31. Schematic representation of internal water exchange (time markers from T1 – T6) when expansion of the marsh surface results from lateral filling of the marsh substrate when water levels rises in the adjacent canal.

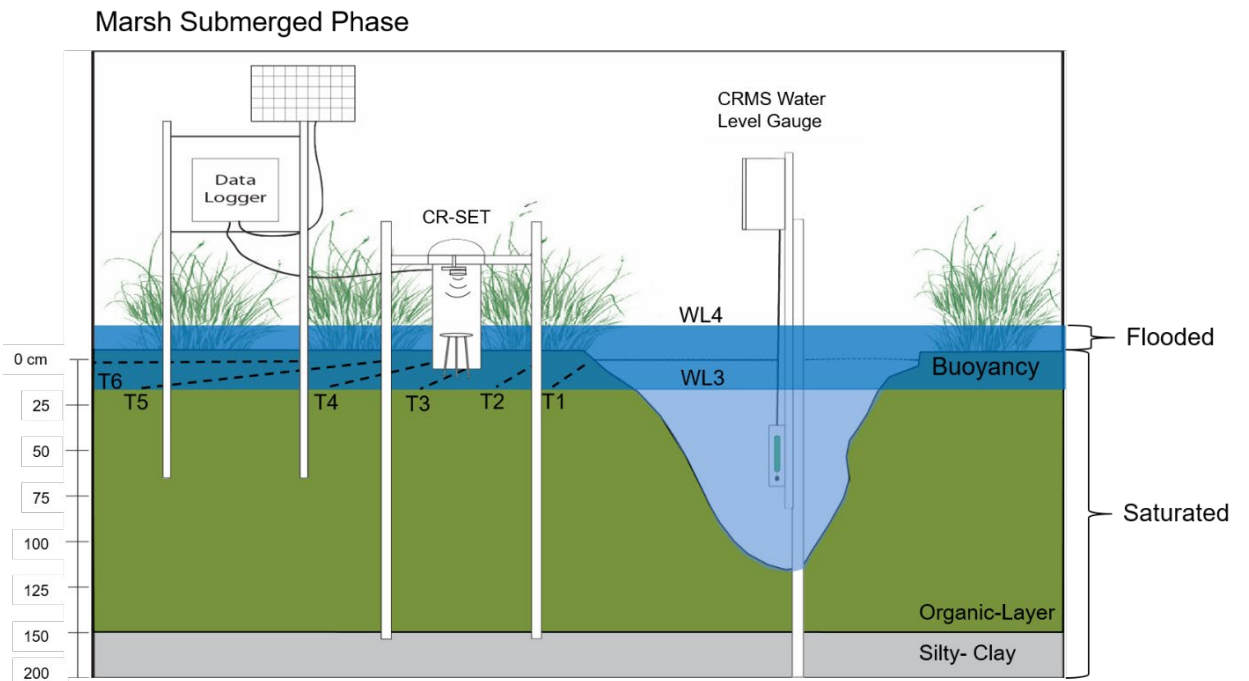


Figure 32. Schematic representation of internal water exchange (time markers from T1 – T6) when continued water level rise in the adjacent canal results in submergence of the marsh surface, resulting in buoyancy an occasional partial liftoff of the surficial sediment (0-10 cm sediment interval).

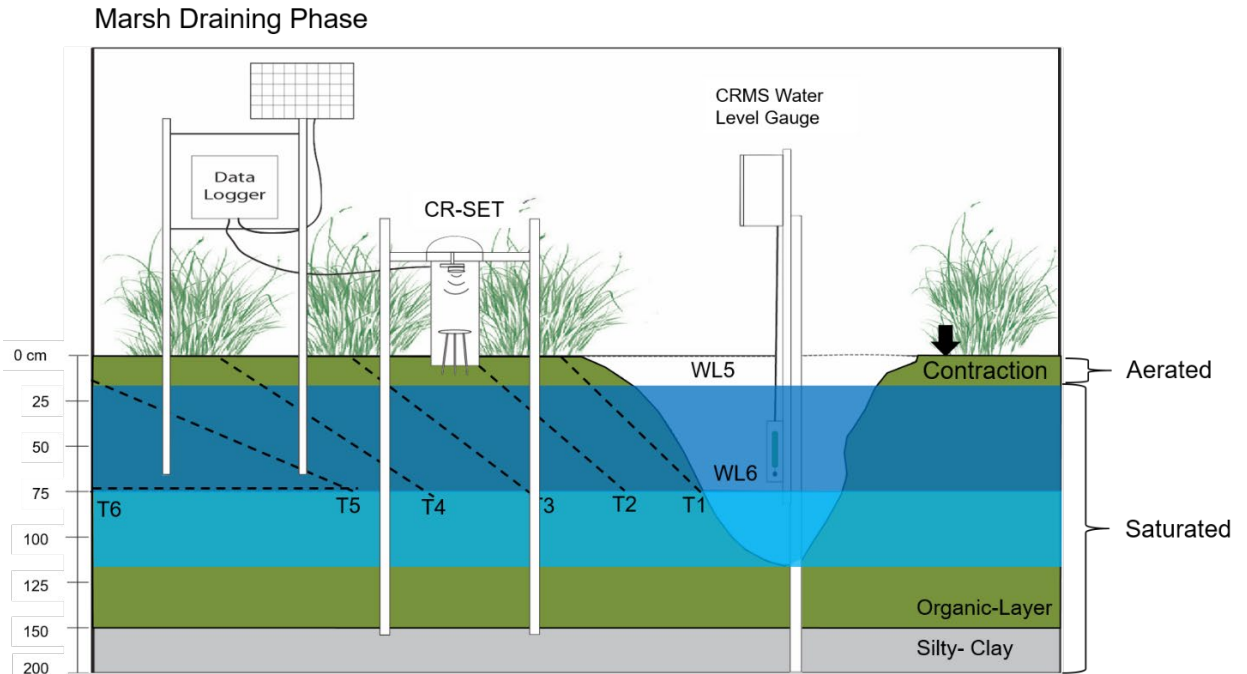


Figure 33. Schematic representation of internal water exchange (time markers from T1 – T6) when a water level fall in the adjacent canal results in contraction of the marsh surface resulting from the progressive draining of the marsh substrate back into the canal.

The concept of lateral filling is supported by observed lag times between the onset of canal rise and the onset of marsh elevation increase being linked to distance between the CR-SET and the nearest canal (Figures 16-18). The most distant from the canal (Fresh site, 67 m from marsh edge) does not respond to all water level fluctuations, suggesting that permeability controls the lateral subsurface migration of water into the vadose zone of the marsh layer (Figure 31). The shortest lag times are observed at the Intermediate and Saline sites that are 11.8 m and 5.7 m from the nearest canal, respectively.

In the marsh elevation versus water elevation plots (Figure 14), the variability in measured elevation at a given water level ($\approx \pm 11$ cm) is far more than the measurement precision of the ultrasonic sensors (± 0.5 mm). At lower water levels (Figures 31 and

34), the variability of the surface elevation increases up to the point where the marsh surface is flooded. At the marsh surface, the trend reverses and the variability at a given water elevation decreases as the marsh is flooded. The main source of elevation variability at a given water level is interpreted to be caused by (1) the rate at which water level rises and falls in the canal, and (2) whether sufficient time passed since the previous water level change for the vadose: phreatic boundary to reach equilibrium. Given the lag time induced by soil permeability and distance from the canal, slow versus rapid changes will result in a different marsh elevation (internal filling rate). There is a maximum variability point in marsh elevation (Figure 34) that corresponds to a maximum fluctuation point in water levels during the study period. This maximum variability occurs at the lowest water levels because there is a much thicker vadose zone to fill in a given time, although these extreme low water events are less frequent. For example, water levels at the brackish site reach a minimum of -22 cm NAVD88 less than one day out of the water year (Figure 34). As canal water levels approach the marsh surface there is less water required (thinner vadose zone) to fill to equilibrium with the canal (even though these levels are less frequent than the maximum fluctuation point), until there is virtually no observed variability in marsh surface elevation in multiple events that reach a canal elevation corresponding to the marsh surface elevation (Figure 34). The permeability of the vadose zone in the wetland is also clearly a factor influencing this relationship as is described in a later section.

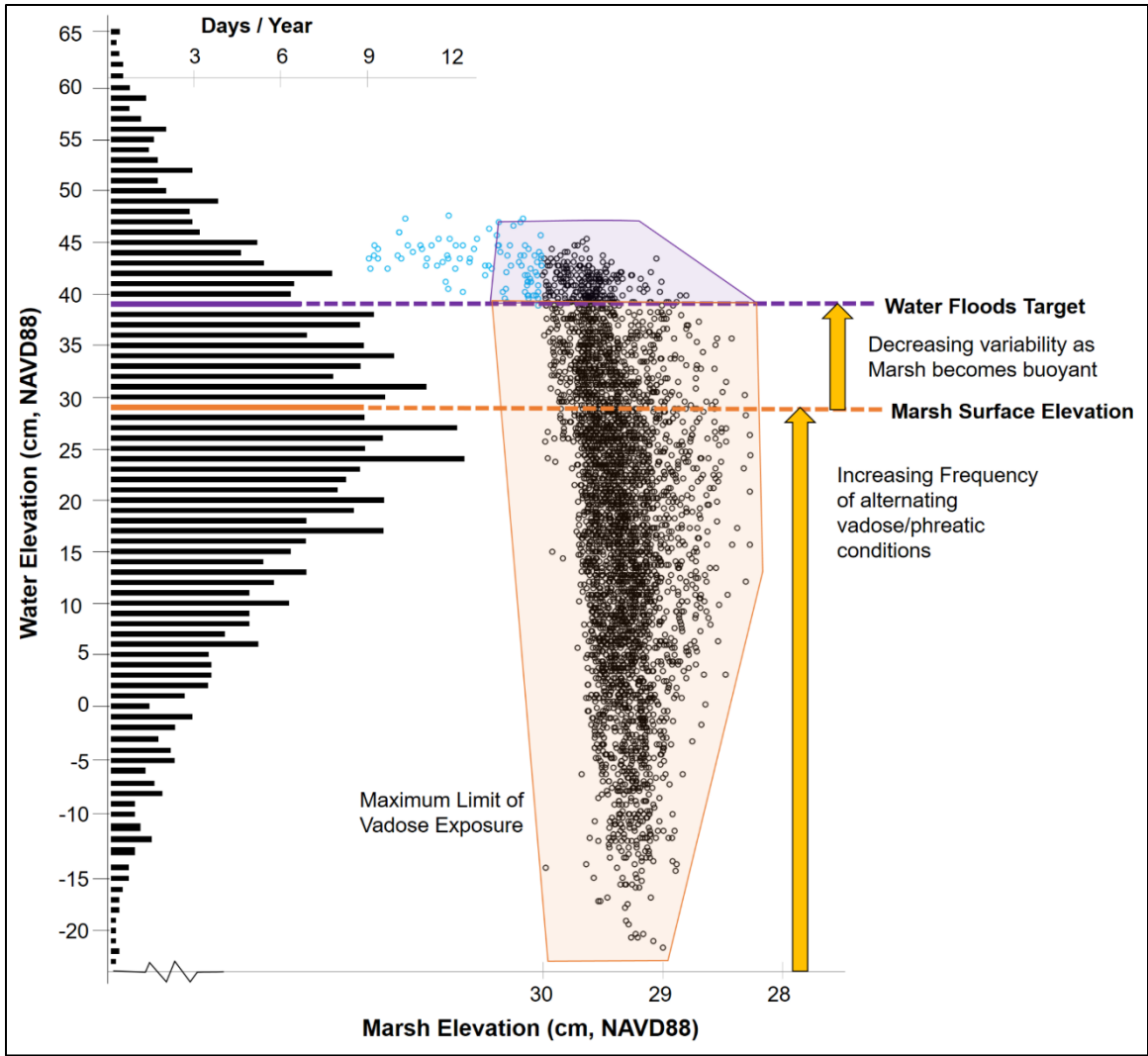


Figure 34. Variability in marsh surface elevation (ultrasonic sensor) at a given water elevation attributed to the event-based individuality of changes in water level that result in marsh soil column filling and draining with water from adjacent canals. This plot represents the period of record for the water level statistics (histogram) is from October 2012 – September 2019 at the Brackish site (CRMS 3565). The period of record for the marsh elevation (black dots) is from 1 December 2018 to 29 May 2019. The black dots represent the marsh elevation when it is not flooded. The blue dots represent periods when water levels exceed 10 cm over the marsh surface, flooding the target, and resulting in tracking of the water surface. Water elevations above this point (local elevation > 70 cm NAVD88) occur at a frequency of less than 0.5 days/year.

Another important implication of this vadose zone linkage with canal water level is that the marsh edges experience more frequent and more extreme draining and filling cycles than the marsh interior. For example, in a pre-frontal period of strong onshore

winds, water levels rise in the canal, and at T1 the marsh edge vadose zone fills quickly and the vadose: phreatic boundary stays in close equilibrium with the canal water level (Figure 31). As water levels continue to rise, water infiltrates further laterally into the marsh (permeability lag), and, depending on how prolonged (hours to days) the period of rising-to-high water level high is depicted by T2 through T5, will control how far lateral water flow extends inland and the magnitude of the vadose: phreatic rise at any one site. If the period of high and stable water is sufficiently long, the vadose: phreatic boundary will equilibrate with canal water level (T6). The lag time is different for each individual event where the surface elevation fluctuates closely with slow rises and falls in water levels. Inversely, the surface elevation has longer lag times to fast rises and falls in water levels.

As more flooding occurs the marsh floods unevenly in and around the site due to the microtopography of the marsh, therefore taking more than 10 cm of water to completely flood the marsh. This may account for the decreasing variability in recorded marsh elevation associated with individual flooding events (Figure 34). During time intervals where canal water level reaches an elevation that inundates the marsh surface (Figure 32), the CR-SET data collected in this study are limited to ultrasonic sensor data at water elevations 0-10 cm above the marsh (elevations above the 10 cm target was inundated): there is also data from zero to maximum observed marsh surface flooding from the linear position sensor at the Saline site (Figure 35). When the marsh is inundated, and the entire vadose zone is flooded, marsh elevations continue to rise throughout water loading events of <10 cm (Figure 32). CRMS sites, where all the CR-SET platforms were located, are purposefully not established in floating marsh sites that

rise and fall seasonally with water levels in the floodbasin (CRMS-Factsheet, 2010). The absence of any decoupling signal in the ultrasonic records during limited flooding, is also likely a function of them recording a target with a foundation depth of 15 cm, rather than the sediment surface itself.

Evidence of possible marsh surface decoupling is observed from the linear position sensor at the Saline site which is measuring the marsh surface itself during periods of inundation (Figures 15 and 35). This dataset, and the absence of event-to-event elevation offsets in the ultrasonic data at the same site, suggests that these decoupling events occur in the uppermost, highest porosity surficial layer (0 to 15 cm) that is not recorded in the ultrasonic data because of the target foundation depth (15 cm). Each linear position sensor event recorded in Figure 15 has a different signature, i.e., base elevations can be up to several millimeters different, but all show a trend of increased marsh surface elevation or no elevation change with increasing water level. As water levels recede and the marsh surface resettles, the linear position sensor at the Saline site records different baseline elevations, which explains the multiple linear regressions. This is interpreted as a possible partial decoupling of the highly porous surficial marsh layer (0-15 cm depth) due to buoyancy and carrying the linear sensor positioned on the surface upward with it. This liftoff and return cycle is plotted in detail for a single event where water inundation reached 60 cm on 27-30 December 2018 at the Saline site in Figure 35. The highest water level recorded at the Saline site during the study period was 80.2 cm NAVD88 which is about 67 cm of flooding above the Saline site marsh surface (13.2 cm NAVD88), which equates to a water loading of 6.8 kPa. The absence of depression of the marsh surface observed during this most extreme event suggests this magnitude of water

loading is probably insufficient to depress the marsh surface and offset the buoyancy effect, causing the data to deviate from the regression line.

This decoupling phenomenon observed in the Saline site linear position data, is a replication, in smaller vertical scale and over shorter intervals of time (e.g., hours to several days), of the floatant marshes that are found further inland throughout Terrebonne and Barataria Basins (O'Neil, 1949; Swarzenski et al., 1991; Sasser et al., 1995).

Swarzenski et al., (1991) find that floatant marshes within Barataria Basin that contain almost no mineral sediment respond display floatant response to water level fluctuations, while marshes high in mineral content that do not. Similarly, Sasser et al., (1995), find that marshes in Terrebonne Basin with the largest abundance of biomass (live and dead organic material) have the largest marsh mat vertical movement with water level fluctuations. This surficial layer floatant behavior observed at the Saline site has not been previously observed in the Cahoon et al. (2011) and earlier studies of more mineral rich and more saline Louisiana wetlands further down basin from floatant sites.

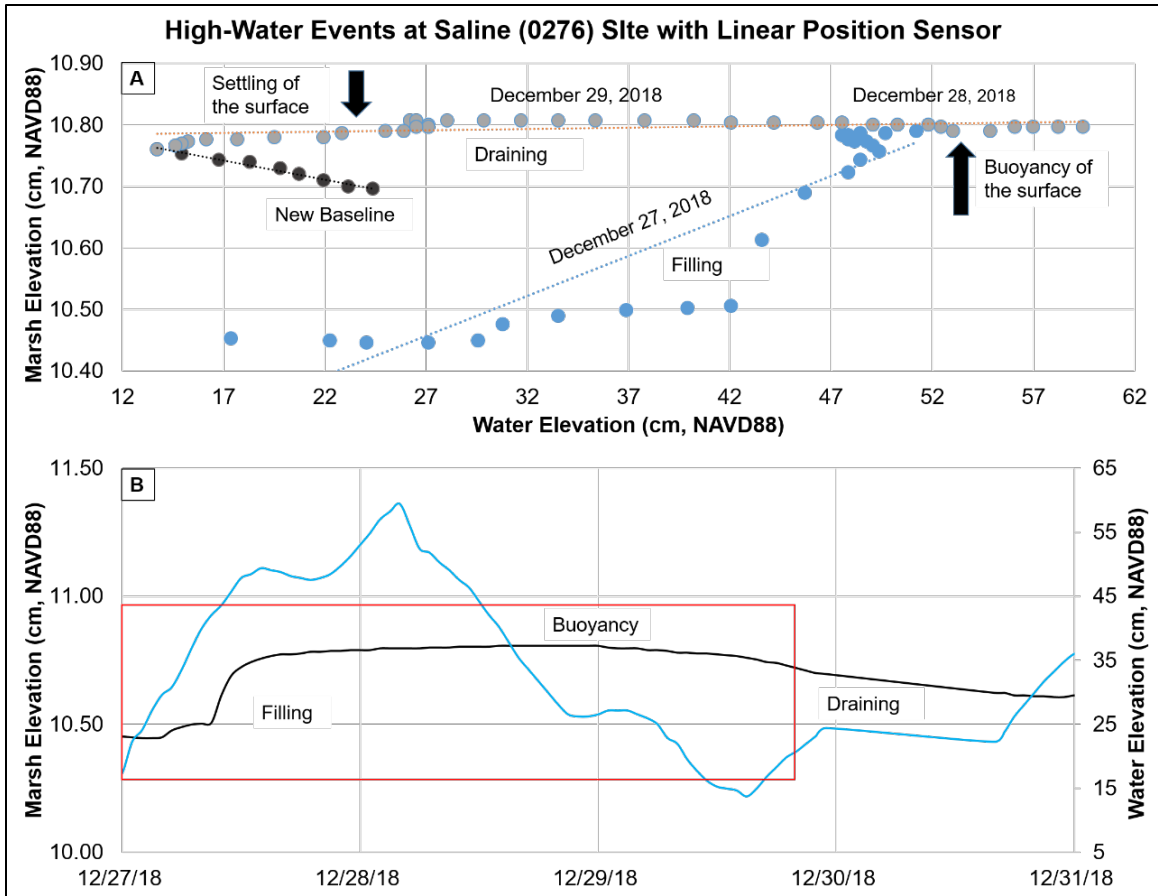


Figure 35. A) The interpreted filling, buoyancy, and draining phases of the marsh as recorded during a flooding and subsequent draining event at the Saline site (CRMS 0276) in December 2018 as recorded by the Linear Position Sensor (dots with lines fitted). B) Time series of water level (blue line) and mean marsh elevation (black line) represented in the upper plot (red box).

When water levels flow off the marsh, water is also drained from the marsh subsurface, which causes contraction of pore spaces and a falling marsh surface elevation (Figure 33), a factor that has been identified as contributing to marsh sediment consolidation by previous studies (Cahoon et al. 2011 and references therein). The marsh edges (T1) near the canals will drain much quicker than the marsh interior (T6). The overall effect of this rise and fall of the vadose-phreatic boundary (e.g., water table) in the marsh substrate is two-fold. First, if we assume local marsh elevation is in near equilibrium with mean sea level at the site due to a balancing of elevation loss drivers

(rising Gulf sea level and local subsidence) and elevation gain (mineral and organic accumulation) (Hatton et al., 1983; Cahoon and Reed 1995), then the marsh in a vertical sense would experience a decreasing frequency of phreatic exposure with depth, to a point of always being fully saturated (phreatic zone), coinciding with the maximum low water levels experienced annually due to meteorological and astronomical tidal episodically. Second, because draining and filling events are primarily lateral in nature, there would be a decreasing frequency of phreatic exposure at a given subsurface marsh elevation with increasing distance from the nearest tidally connected water body.

As the lateral filling and draining of the upper portion of the organic-rich marsh layer proceeds sequentially from marsh edge to interior, the distance of penetration is based, firstly, on the time period that the water level perturbation (rising or falling event) persists, but, likely as well, on the permeability of the substrate. A number of factors affect the permeability of soils, from particle size, soil stratification, void ratio (porosity) and interconnectivity of pores, the degree of saturation, and absorbed water, to entrapped air and organic material (South National Technical Center, 1989; Wilson and Gardner, 2006; Mitsch and Gosselink, 2015). Organic soils also have a wide range of hydraulic conductivities due to the plant fiber content and bulk density of peat (Mitsch and Gosselink, 2015). The permeability range of organic-rich soils containing homogenous clays are practically impervious ranging from 10^{-9} to 10^{-7} cm/sec. Very fine sands, organic and inorganic silts, and stratified clay deposits range from 10^{-7} to 10^{-3} cm/sec (South National Technical Center, 1989; Mitsch and Gosselink, 2015). In the present study, although in situ permeability testing was not conducted, some of the key parameters that control permeability for subsurface exchange of water with the adjacent

canal were measured in the organic-rich marsh layer site cores. This included porosity, organic matter content (LOI) and composition (live rooting: total organics), organic: mineral ratio, and granulometry of the mineral fraction (Table 8). Porosities measured directly from the site cores likely only provide a “snapshot” in the down core porosity profile—the draining and filling phenomenon means the timing of coring relative to canal water level will be a controlling factor. A more realistic proxy for the permeability of each of the sites will be the degree that the marsh surface rises and falls over the measured canal water interval (Figures 16-20), which indicates the greatest magnitude of water exchange. The Intermediate and Saline sites have the largest average surface elevation range (2.72 ± 0.40 cm intermediate, 2.11 ± 0.56 cm saline) over the observed range of water levels below that of the marsh surface (Table 8). Water exchange in the Fresh (1.72 ± 0.23 cm) and Brackish (1.75 ± 0.26 cm) sites are relatively low.

Permeability and observed water exchange are likely partly controlled by a combination of organic content, with large organic detritus characteristic of marshes favoring high porosity and high-water absorbance capacity. Averaged over the cored 0-87 cm marsh layer, organic content is relatively high (41-47%) in all but the Saline site (23%) (Table 8). However, the content and character of the mineral fraction in these organic: mineral mixtures also play a role in overall permeability and water retention capacity, and is relatively consistent between sites; fine silt at the Fresh, Intermediate, and Saline sites, with predominantly medium silt at the Brackish site (Table 8). Although the grain size is similar between the Fresh, Intermediate, and Saline sites, the Intermediate site has the highest organic matter content and core porosity compared to the other three sites. The Intermediate site also has the highest VA rates (21.0 mm/yr),

accretes the most organic matter (9.9 mm/yr), and has the highest calculated shallow subsidence (VA-SEC from CRMS data) rate (13.8 mm/yr), and also contains a 25 cm thick True Peat (>75% organic matter) interval within the upper 87 cm of the core (Figure 26). Organic soils are very porous, especially when flooded, therefore are correlated with the magnitude of surface elevation fluctuations. Holm et al. (2000) examined vertical movement of oligohaline (brackish and intermediate) marshes within Terrebonne Basin and found that high organic matter contents and low soil bulk density areas experience larger vertical movement. This is true for the organic-rich Intermediate site in this study. The Intermediate site also shows a strong correlation to evapotranspiration cycles as observed by Cahoon et al. (2011).

The Saline site also showed large marsh surface elevation fluctuations (with the ultrasonic sensor) but a smaller range (± 0.45 cm) with the linear position sensor, despite containing the lowest organic matter content of the four study sites. However, the marsh surface is submerged over 85% of the water year, compared with 35-65% at the other three sites. The frequency of draining and filling events and their impact on sediment consolidation would be reduced relative to the other sites. It is also possible that there are preferred hydrologic exchange pathways through the soil column depending on grain size, that allow for water infiltration and drainage through certain depths of the soil column, further affecting surface elevation response (Xin et al., 2012).

Table 8. Bulk properties potentially affecting the permeability of marsh soils. All sedimentological statistics are averaged over the 0-87 cm core interval at each site.

| Sites | Fresh | Intermediate | Brackish | Saline |
|--|-------------------------|-------------------------|---------------------------|-------------------------|
| Organic Matter (%) ± SD | 42.2 ± 26.0 | 47.3 ± 17.8 | 40.6 ± 21.2 | 23.2 ± 16.3 |
| CRMS VA Rates (mm/yr) | 8.9 | 21.0 | 15.4 | 14.4 |
| Organic VA Mineral VA (mm/yr) | 3.8 5.1 | 9.9 11.1 | 6.3 9.1 | 3.3 11.1 |
| Core Porosity (%) ± SD | 82 ± 9.4 | 87 ± 1.8 | 84 ± 6.7 | 80 ± 1.0 |
| Average D50 Grain Size ± SD | 11.9 ± 7.9 Fine Silt | 13.3 ± 4.7 Fine Silt | 21.1 ± 8.3 Medium Silt | 13.1 ± 9.1 Fine Silt |
| Vadose Zone Thickness (cm) | 38 | 23 | 28 | 6 |
| Live Rooting Thickness (cm) | 40 | 45 | 87 | 30 |

6.2 Implications for Subsidence in Louisiana Coastal Wetlands

Barataria Basin is no exception to the complexity of multiparameter subsidence mechanisms experienced coast wide (Dokka, 2006; Yuill et al., 2000; Yu et al., 2012). The mechanism thought to be responsible for vast land loss which occurs in the shallow subsurface is the compaction of young, thick Holocene sediments as well as the compaction of the surficial marsh (1-2 meters); the latter has the most potential for compaction with adequate sediment deposition (Törnqvist et al., 2008). Studies such as Jankowski et al., (2017) and Nienhuis et al., (2017) show the spatial complexity in shallow subsidence rates (interval from sediment surface to CRMS R-SET foundation depths) for Barataria Basin with no clear pattern of thicker Holocene packages causing

increased subsidence. Other Barataria Basin studies like Byrnes et al., (2019) suggest that subsidence rates are much lower than previous studies and are linked to Holocene sediment thickness, although the Byrnes et al., (2019) study measures a much deeper interval than above mentioned studies and omit the shallow subsidence component. If the Jankowski and Nienhuis studies provide the best evidence to date of shallow subsidence rates in Barataria Basin, are these rates compromised by the fact they are derived in part from R-SET measurements that are likely affected by short-term marsh surface elevation fluctuations as recognized in the present study: elevation changes that can be on the order of +/- 20 mm (Intermediate site) over hours/days?

CRMS measures both the vertical accretion and total elevation change for over 390 sites throughout coastal Louisiana. CRMS R-SET foundation depths vary from site to site, and therefore the interval in which they measure surface elevation change (SEC) are different between sites but in the present study area is generally 10-30 m and thus in the Holocene sediment interval. This is much thicker than the interval measured in the present study (0.15-1.5 m depth). To examine the effect of observed marsh surface fluctuation, a correction to previously calculated SECs (Jankowski et al., 2017) was made using a mean marsh elevation normalized to a mean water level (equivalent to local marsh surface elevation) by using the regressions displayed in Figure 18. The SECs for each data point collected at the CRMS R-SET was then corrected for the offset of the water level recorded at that R-SET measurements date and time and a new SEC-VA calculation done to derive a corrected shallow subsidence rate: results are shown in Figure 36 and Table 9. While the results show slight differences in the overall shallow subsidence rates at the four study sites after the correction was applied, it can be

concluded that this adjustment falls within the errors of the original curve fits, and therefore the Jankowski et al., (2017) methodology remains a valid method for measuring shallow subsidence rates over the period of record at CRMS sites.

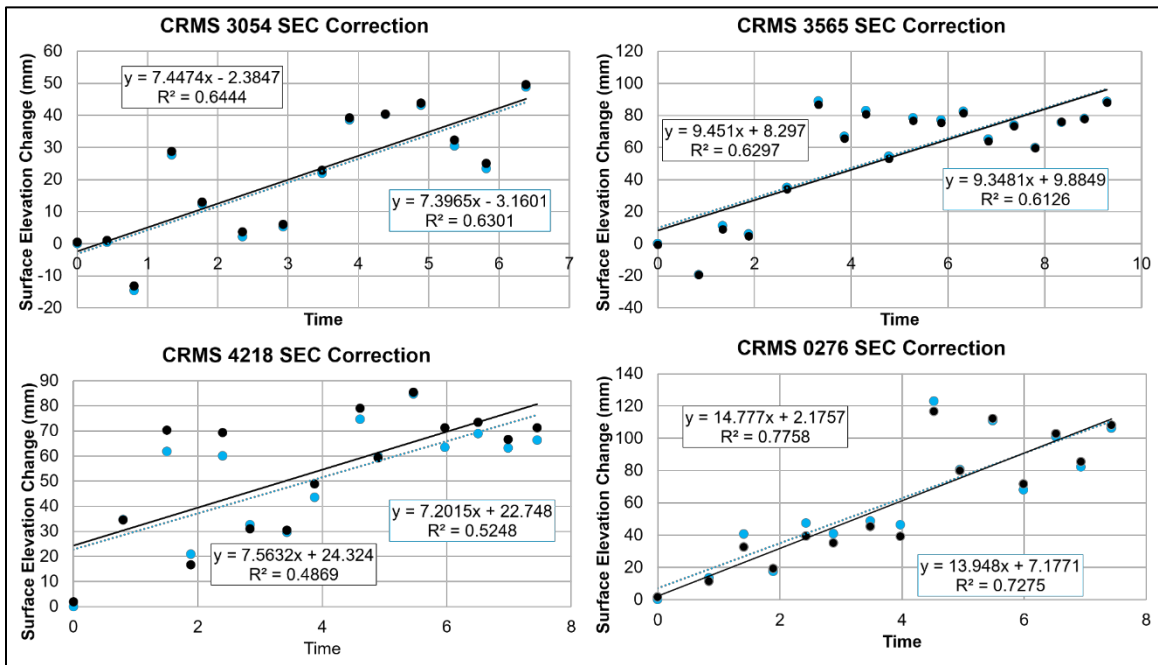


Figure 36. Corrected Surface Elevation Change (SEC) rates for the four study sites from CRMS R-SET data collected at the sites. Correction was applied by using a baseline marsh level elevation after correction to a median canal water level elevation derived from the CR-SET data from the four study sites. Original SEC rates are in blue. Corrected SEC rates are in black.

Table 9. Corrected SEC rates from Figure 35 utilized to derive corrected Shallow Subsidence (SS) rates from those calculated by Jankowski et al. (2017). All values in mm.

| Sites | VA | Original SEC | Original SS | Corrected SEC | Corrected SS |
|-------------------|------|--------------|-------------|---------------|--------------|
| Fresh 3054 | 8.9 | 7.3 | 1.6 | 7.4 | 1.5 |
| Intermediate 4218 | 21.0 | 7.2 | 13.8 | 7.6 | 13.4 |
| Brackish 3565 | 15.4 | 9.3 | 6.1 | 9.5 | 5.9 |
| Saline 0276 | 14.4 | 14.0 | 0.4 | 14.8 | -0.4 |

Given the rates of observed SEC, VA and SS at the CRMS study sites (e.g., mm to a few 10's of mm/y), if the fluctuation of CR-SET marsh surface elevations can be

removed from the signal, the period of record (6-11 months) should be sufficient to measure short-term SS at the four sites for the 15 cm to 150 cm depth interval. This analysis was performed in Figures 37 and 38. All data points were normalized to a mean water surface/marsh surface elevation using the same method presented for Figure 36. Weekly average elevations were then derived using only the points where the marsh surface was not flooded. The results from two of the sites (Fresh and Brackish) show little mean surface elevation change over the period of record (Figures 37 and 38). Surprisingly, the Intermediate and Saline sites exhibit marsh elevation (SEC) increases despite these sites showing the highest and lowest SEC from the CRMS R-SET data (Table 9). Several reasons may be responsible for the observed trends in the weekly SEC averages. SEC in the ultrasonic CR-SET data represents a combination of short-term (weeks to months) deposition (or erosion) and shallow subsidence. The former can be significant during periods such as the Winter-Spring frontal season when the marshes are periodically inundated with turbid water resuspended from adjacent water bottoms (Reed, 1989). The seasonal signal is not removed from the water level normalized and weekly averaged SEC signal in Figures 37 and 38.

Seasonal differences in water level and thus marsh elevation, particularly in the Spring-Summer, can also be due to increased organic productivity increasing the role of evapotranspiration, and high Gulf-driven site water levels (Figure 23 and 24). Increased seasonal water level can also be expected to increase deposition (VA) through trapping of mineral and detrital organic matter. CRMS R-SET values of SEC from the sites (Figure 36) also show periods at all the sites of no SEC change or even net elevation increase that can last up to several years. Comparison of WY 2019 water statistics at the sites (Figure

23) with a longer-term (WY 2012-2019; Figure 24) shows that averaged over the year, WY 2019 was 14.1% (Fresh), 3.1% (Intermediate), 5.9% (Brackish) and 14.5% (Saline) higher at the four sites. VA rates for 2018 at the CRMS sites are also higher than previous rates calculated, with the exception of the Brackish site (CRMS 3565) (Appendix C).

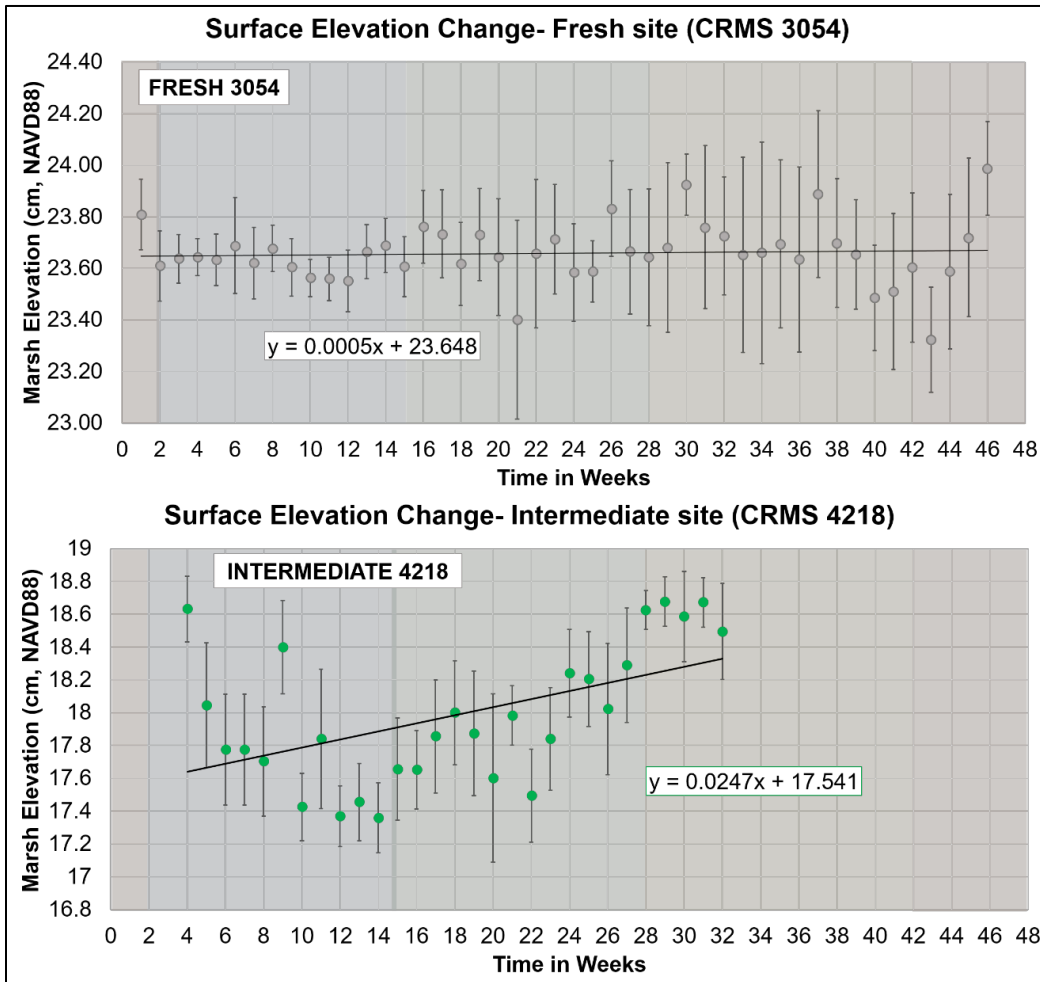


Figure 37. Weekly averaged and normalized surface elevation change CR-SET measurements throughout the study period for the Fresh and Intermediate sites. Weekly averages were normalized to a mean canal water dept (CRMS gauge) to remove the observed seasonal and diel effect on marsh elevation as described in the text. CR-SET data only involves the period when the marsh surface was not submerged. Meteorological seasons are illustrated by the different colors through time. Orange corresponds to Fall (September 1 – November 30), blue is Winter (December 1 – February 28), Green is spring (March 1 – May 31), and yellow is Summer (June 1 – August 31). The period of record plotted begins on 7 November 2018 and ends on 25 Septemeber 2019.

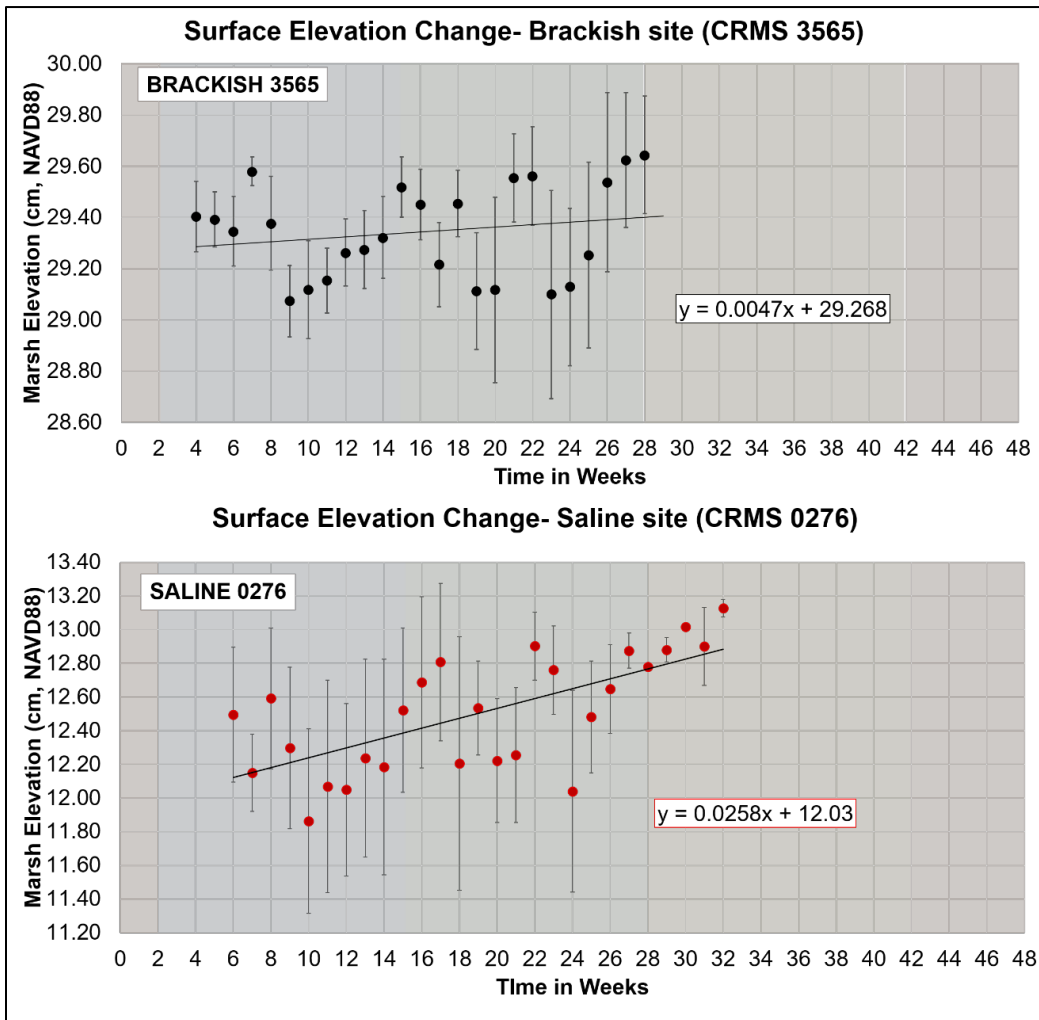


Figure 38. Weekly averaged and normalized surface elevation change CR-SET measurements throughout the study period for the Brackish and Saline sites. Weekly averages were normalized to a mean canal water dept (CRMS gauge) to remove the observed seasonal and diel effect on marsh elevation as described in the text. CR-SET data only involves the period when the marsh surface was not submerged. Meteorological seasons are illustrated by the different colors through time. Orange corresponds to Fall (September 1 – November 30), blue is Winter (December 1 – February 28), Green is spring (March 1 – May 31), and yellow is Summer (June 1 – August 31). The period of record plotted begins on 7 November 2018 and ends on 25 Septmeber 2019.

As outlined above, the lateral groundwater exchange between canal and marsh substrate has a demonstrated (1) time lag that increases with distance of the sensor from the canal indicating progressive draining from the marsh edge inland, and (2) a vadose

zone in the marsh substrate that decreases in frequency of exposure with depth as well as the distance from the marsh edge. This suggests the possibility of another impact of marsh groundwater exchange on subsidence rates in Barataria Basin — peat oxidation. Accelerated peat oxidation in the New Orleans vicinity from anthropogenic drainage of organic-rich marsh substrates in former marsh/swamp environments for construction after World War II has been noted as a primary cause of land subsidence (Snowden et al., 1977; Dixon et al., 2006). To cause an acceleration in marsh organic material decomposition, an increase in oxygen exposure would have to be demonstrable in Barataria wetlands for the period of accelerated wetland loss since the 1930's.

The frequency subsurface exposed to oxygen (vadose conditions) can be determined by water level histograms: these statistics are examined in two ways in Figures 39 and 40. Figures 39 and 40 are a presentation of the water level statistics at the four sites relative to the local elevation of the marsh surface. These data demonstrate that there is significant interannual variability in the depth of the vadose zone and overall percentage of the year that the marsh is submerged from year to year. WY2019, because of higher Gulf water levels, was significantly lower in exposure to vadose conditions than the WY2012-2019 average as mentioned previously. While variable from year-to-year, previous examination of longer-term Gulf levels associated with atmospheric and long-term tidal components (Kolker et al., 2011) show no evidence supporting decreased Gulf levels and increased marsh vadose conditions at the sites. Further, rising global ocean sea levels would favor more frequent submergence if VA of organic and mineral matter accretion at the sites could not keep pace. Interestingly, the elevation of the Saline site (Figure 40) shows that the site may not be keeping pace as the longer-term average water

level statistic show it is submerged about 85% of the time, suggesting possible incipient marsh drowning (Hatton et al., 1983; Reed, 1995; Couvillion et al., 2013).

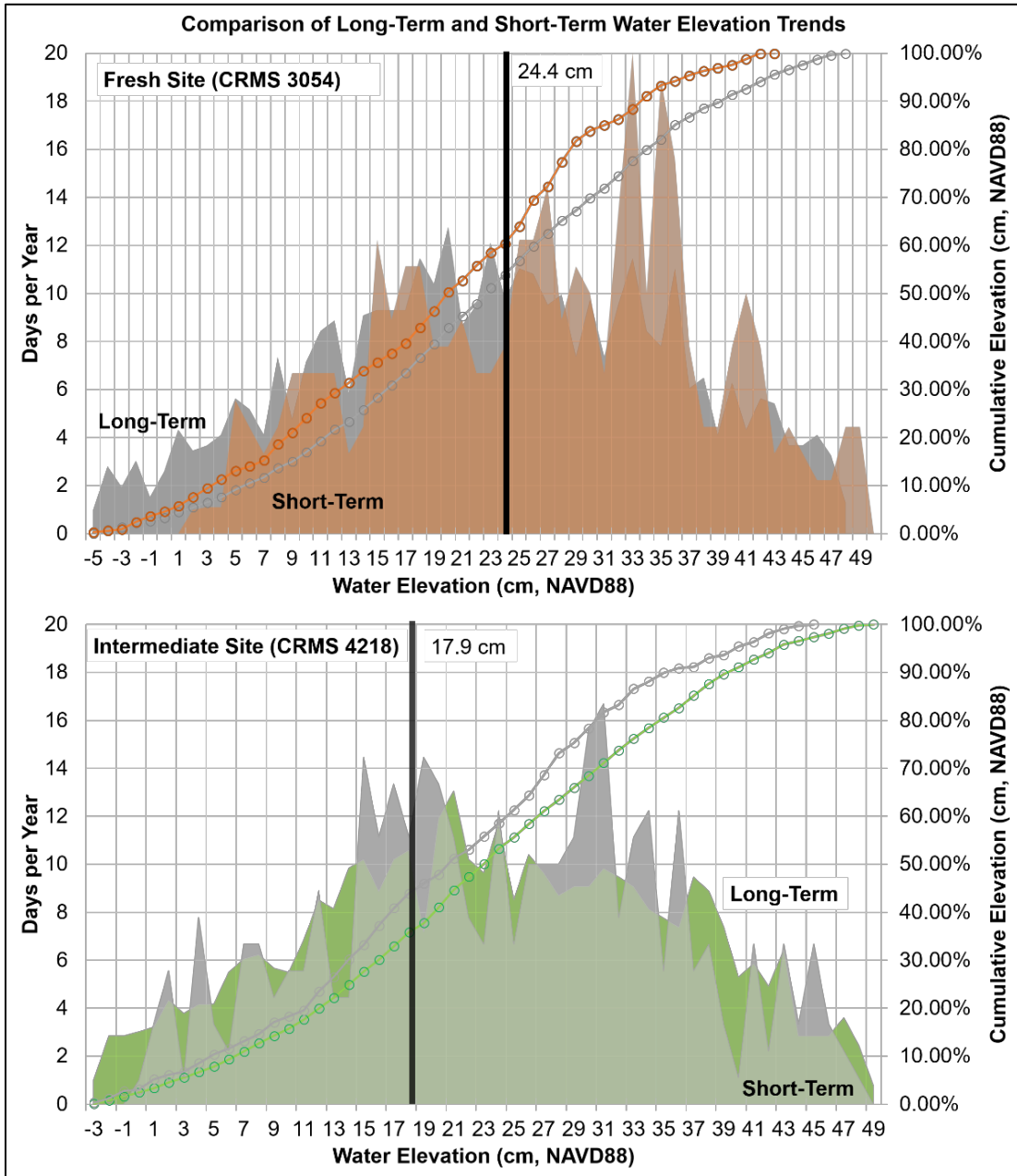


Figure 39. Long-term (WY 2012-2019) and short-term (WY 2019) site-specific water elevation statistics for the Fresh and Intermediate sites from CRMS water gauges at the sites. Water elevations have had the 5th and 95th percentiles removed. The black vertical bars represent the median marsh elevation at the site.

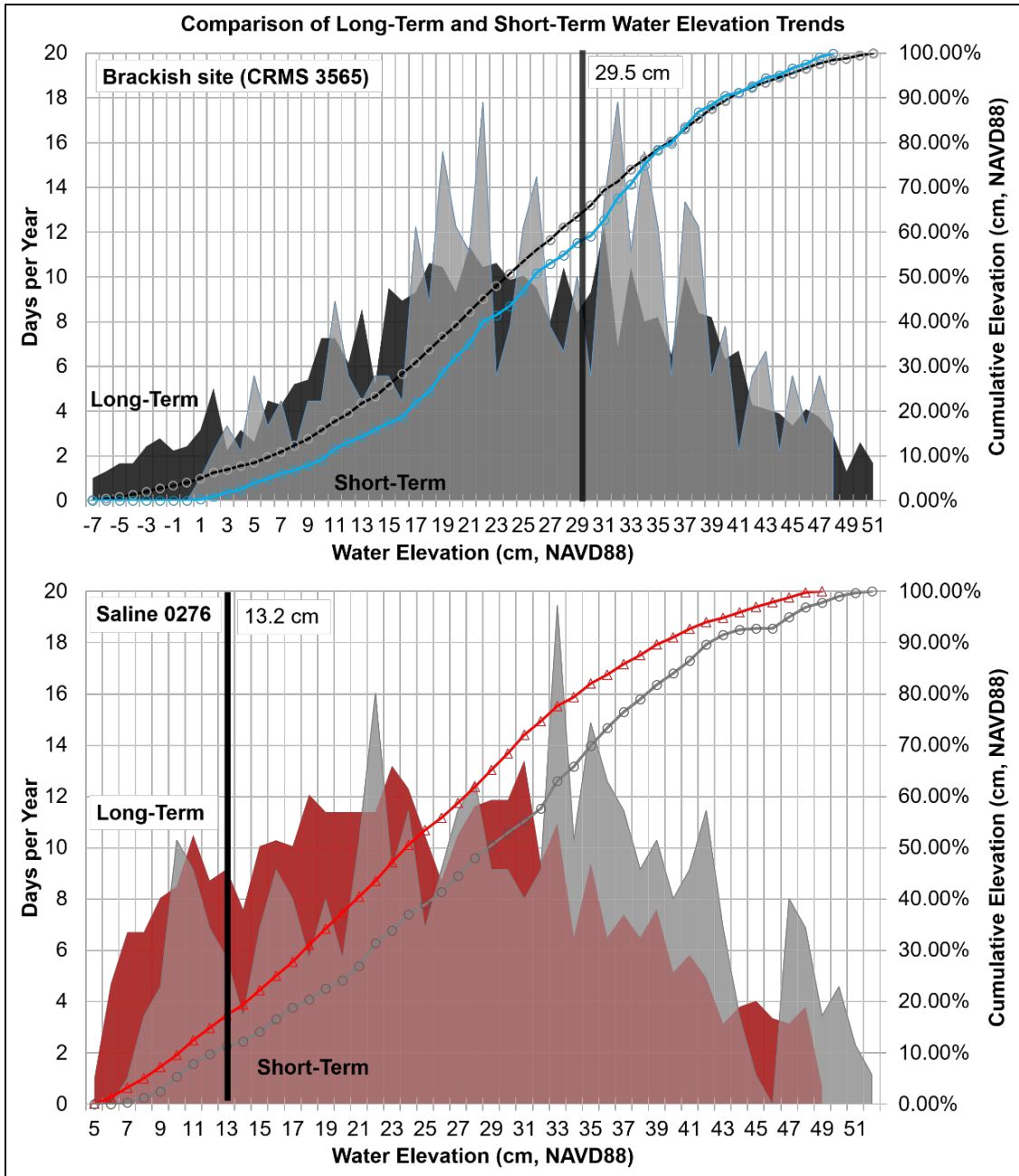


Figure 40. Long-term (WY 2012-2019) and short-term (WY 2019) site-specific water elevation statistics for the Brackish and Saline sites from CRMS water gauges at the sites. Water elevations have had the 5th and 95th percentiles removed. The black vertical bars represent the median marsh elevation at the site.

Another way to examine if there is an impact of peat oxidation at these sites due to vadose conditions that have increased through time is through utilizing stratigraphic evidence of the reduction in organic matter preservation (Figures 41 and 42). A cursory

comparison of the stratigraphic organic matter percentages against the vadose zone for WY 2012-2019 shows no clear pattern—only the Brackish site shows a correlation between the vadose zone limits and lower organic matter contents in the associated stratigraphic layer. However, organic matter content is a complex combination of local aboveground and belowground productivity (Hopkinson et al., 1978), mineral sediment supply that is linked to trapping and the turbidity of water flooding the marsh surface, as well as the organic matter decomposition rate (Stumpf et al., 1983; Nyman et al., 1995). To examine this interplay more quantitatively, the core stratigraphy has been divided into three separate zones. The uppermost is the 0-6 cm interval which is interpreted as reflecting the “pristine” organic matter flux rate ($\text{g}/\text{cm}^2/\text{yr}$) prior to any subsurface decomposition. This is determined using CRMS VA rates for each and organic matter LOI's from the 0-6 cm interval. The second interval is from 6 cm to the base of the vadose zone at each site. This depth is determined using the 95th percentile from the long-term water statistics (-5 cm at the Fresh site, -4 cm at the Intermediate, -7 cm at the Brackish, and 5 cm at the Saline). ^{137}Cs accumulation rates and OM:mineral ratios for this zone are used to estimate organic matter storage rates ($\text{g}/\text{cm}^2/\text{yr}$) for this interval. The linear Cs results suggest the base of this interval is 24 ± 41 yBP at the Fresh site, 55 ± 26 yBP for the Intermediate, 44 ± 15 yBP for the Brackish, and 25 ± 15 yBP for the Saline site. The third interval is from the base of the vadose zone to the bottom of the 87 cm long core, a zone that is always below the water table (phreatic) according to the WY2012-2019 water statistics. The ^{210}Pb accumulation rates and OM:mineral ratios are used for the this deeper (older) interval where the age of the Fresh site at 87 cm depth is

138 ± 45 yBP, 103 ± 9 yBP at the Intermediate, 108 ± 16 yBP at the Brackish, and 99 ± 63 yBP at the Saline site.

The results of this analysis (Table 10) show the organic matter storage rate of the fresh and saline sites decreases within the vadose zone relative to the OM storage rate within the Pristine and Phreatic zones. The intermediate and brackish sites show the opposite trend where the organic storage rate is largest within the vadose zone. Storage of both organic and mineral sediments are highest within the phreatic zone at all sites suggesting more mineral deposition before MR&T levees. The organic matter storage rates are a combination of deposition and decomposition rates. The OM storage rates are highest in the deeper phreatic zone than the vadose zone at all four sites suggesting either peat oxidation within the vadose zone and/or the effect of more mineral deposition in the past, causing higher productivity.

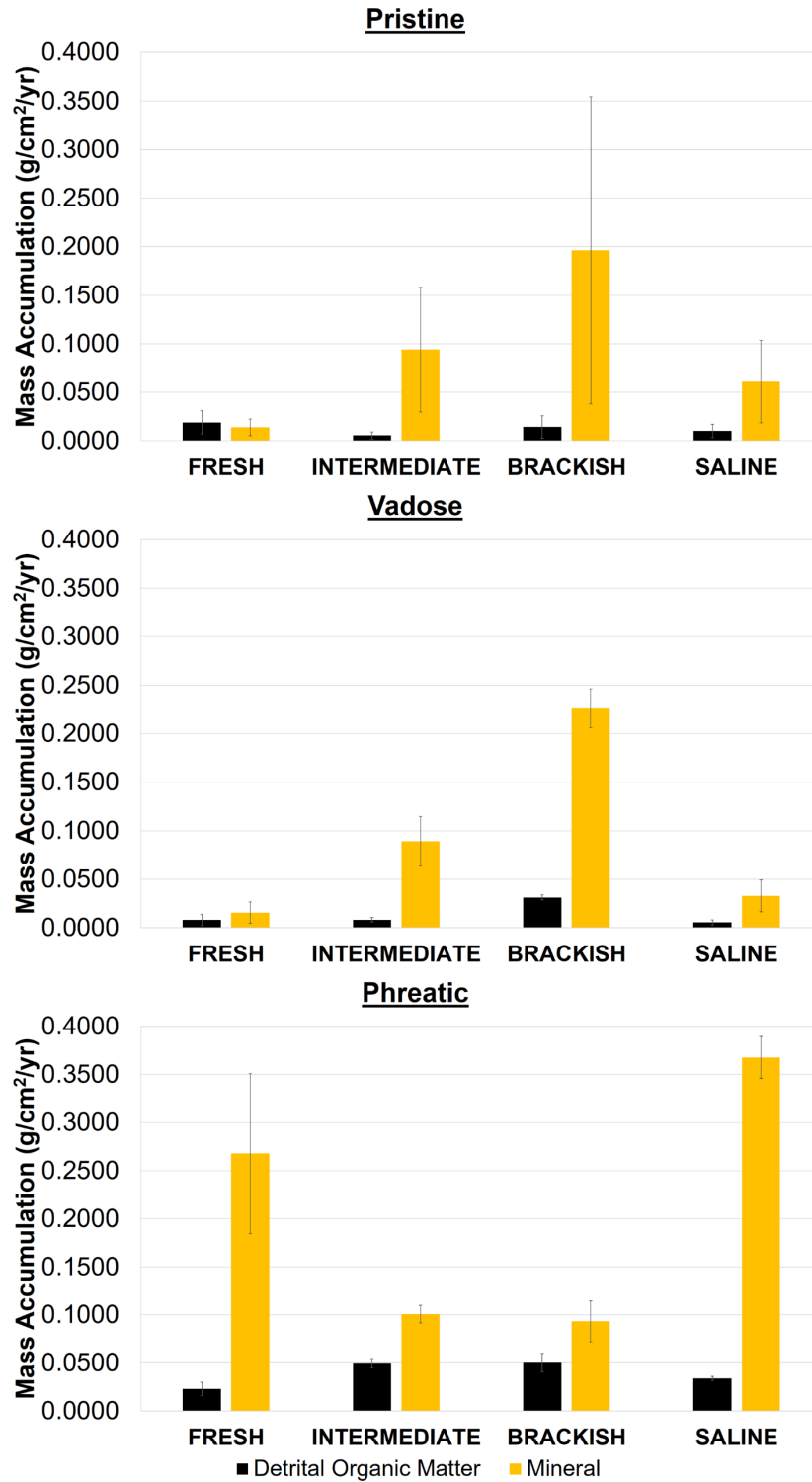


Figure 31. Detrital Organic Matter Storage Rates (determined from LOI and Root Analyses) compared with Mineral flux at the four study-sites.

Table 10. Core stratigraphy sectioned into; the surficial VA (0-6 cm), the Vadose Zone (6 cm to 5th percentile water elevations from 2012-2019), and the Phreatic Zone (base of Vadose zone to end of 87 cm core) at each site. All rates have been consolidated to a porosity of 75%. Vertical Accretion and Sediment Accumulation rates (Pb, Cs) were calculated based on the new consolidated depth. Organic and mineral fluxes were calculated by averaging the % organic matter content within the previously described zones using a mineral density of 2.65 g/cm³ and an organic density of 1.24 g/cm³.

| Pristine Zone | Sites | CRMS VA Rate (cm/yr) | %OM | Organic Storage Rate (g/cm²/yr) | Mineral Flux (g/cm²/yr) |
|----------------------|--------------|--|------------|---|---|
| | Fresh | 0.16 | 74.4 | 0.037 ± 0.02 | 0.027 ± 0.02 |
| | Intermediate | 0.22 | 35.6 | 0.024 ± 0.02 | 0.094 ± 0.06 |
| | Brackish | 0.36 | 17.7 | 0.019 ± 0.02 | 0.196 ± 0.16 |
| | Saline | 0.13 | 43.4 | 0.017 ± 0.01 | 0.049 ± 0.03 |
| Vadose Zone | Sites | Cs-137 Sediment Accumulation Rate (cm/yr) | %OM | Organic Storage Rate (g/cm²/yr) | Mineral Flux (g/cm²/yr) |
| | Fresh | 0.06 | 51.3 | 0.010 ± 0.006 | 0.020 ± 0.014 |
| | Intermediate | 0.21 | 35.9 | 0.023 ± 0.007 | 0.050 ± 0.025 |
| | Brackish | 0.46 | 27.6 | 0.039 ± 0.003 | 0.084 ± 0.003 |
| | Saline | 0.07 | 34.5 | 0.007 ± 0.004 | 0.016 ± 0.004 |
| Phreatic Zone | Sites | Pb-210 Sediment Accumulation Rate (cm/yr) | %OM | Organic Storage Rate (g/cm²/yr) | Mineral Flux (g/cm²/yr) |
| | Fresh | 0.48 | 19.5 | 0.029 ± 0.009 | 0.062 ± 0.079 |
| | Intermediate | 0.33 | 53.9 | 0.055 ± 0.005 | 0.118 ± 0.009 |
| | Brackish | 0.34 | 58.6 | 0.062 ± 0.013 | 0.132 ± 0.019 |
| | Saline | 0.68 | 18.5 | 0.039 ± 0.002 | 0.083 ± 0.022 |

Due to the decreased OM storage within the vadose zone of the fresh and saline sites, and the abundance of mineral sediment in the vadose zone of the intermediate and brackish sites (with a greater OM percentage), there is a reduction in the storage of organic material within the vadose zone. A process that further explains mostly mineral sediment within the vadose zone is porewater drainage into adjacent water ways during low tides (Howes and Goehring, 1994). Once the marsh soil drains, the low bulk

density peat is exported through the subsurface pore pathways. The link between stratigraphy and possible peat oxidation are not clear because there are multiple factors at play. This includes (1) over the past century mineral deposition and organic accretion rates are non-steady state due to flood control measures and modifications to the Mississippi River (Kesel et al., 1989), (2) as marshes face accelerating sea level rise rates, the marsh organic production rates can increase (event though stressed from higher water levels and salinities) due to increased waterborne nutrient fluxes (DeLaune et al., 1983; Mitsch and Gosselink, 2015). Marsh collapse can occur once stress on marsh vegetation associated with rising water levels outpaces increased organic accretion rates (Couvillion et al., 2013). It is possible that the saline site in this study is accreting organic material to keep up with sea level rise considering the top of the core contains the highest percentage of organic matter, and is flooded over 85% of the year(Figure 42). Also, (3) the stratigraphic signal could be difficult to see as new accretion at the sediment surface and compaction shifts the limits of the particular depth zones (e.g., pristine, vadose, and phreatic) through time and progressively moves an individual interval to greater depth..

selected area of Barataria Basin near the study sites to examine how the land:water ratio and linear extent of shoreline has changed through time. The results show that fragmentation of these coastal marshes from 1932 until 1995 resulted in a reduction in land area from 70% to 45% before stabilizing through the 2016 survey (Figure 43). Marsh edge perimeter doubled from 1932 to about 1977, followed by a three-fold increase between 1977 and 1987. The increase of marsh edge perimeter during this time is likely due to an overall reduction in remaining land area. While this trend of marsh fragmentation has been observed coast-wide and ascribed to multiple mechanisms (e.g., regional subsidence, storm erosion, canal cutting, etc.), a closer examination of the time-series shows the period of canal cutting was concentrated between 1932 and 1977. In later images, where solid marsh was canalized in 1956 raster images, little to no change in wetland area occurred in the 1970's; this was followed by widespread regional marsh collapse in 1985 into the 1990's (Figure 43). This trend is also found within the Lafourche delta where 90% of solid marsh was present in 1945 and decreased to only 9% of solid marsh by 1985 (Evers et al., 1992). The direct impacts of canals are readily measurable where from 1955 to 1978, canal surface area accounted for 10% of direct wetland loss in Barataria Basin (Conner and Day, 1987). Thus, there is evidence of a possible peat oxidation effect in the time series of an accelerated phase of wetland loss in the 1980's and 90's following the rapid phase of perimeter increase in the 1970's and early 80's.

Several factors complicate this hypothesis that increasing marsh edge effect led to a secondary phase of wetland loss through marsh collapse by increasing subsidence rates through peat oxidation. Hatton et al. (1983) found that marsh edges contain more mineral

sediment, and marsh interiors contain more organic material, reflecting a trapping of the majority mineral sediment by marsh leaves and stems along a berm. This would alter the permeability of the substrate controlling drain-fill cycles along with water level statistics. More mineral proportion would tend to increase permeability by decreasing the “sponge”-like effect of the marsh soils (Andriessse, 1988), favoring further penetration inland of vadose-phreatic cycling in the marsh edge. However, increased expansion and contraction of the organic-rich marsh layer is known to drive rapid peat subsidence (Rieley et al. 2007) and compaction which reduces permeability (Cahoon et al., 2011). A final source of co-variance may be the 19th and 20th century reduction in mineral sources for the wetlands to support VA from the construction of river levees and the decline in suspended sediment delivered from the basin (Delaune et al., 1983; Kesel, 1988).

The hypothesis that anthropogenic wetland loss through canal cutting and other mechanisms led to (1) an increase in peat oxidation-induced relative sea level rise because it was so widespread and concentrated over a period of only a few decades, and (2) that this resulted in widespread marsh collapse in Barataria Basin and other areas of coastal Louisiana that were widely dissected by canals, remains unproven and will require further study. Kolker et al. (2011) link the timing of wetland loss rate peaks in the 1930’s-1970’s to subsidence resulting from the peak in hydrocarbon extraction from under the coastal wetlands. This extraction also was the period of peak canal cutting to access the rig sites, but it remains unclear whether both factors were subsidence drivers.

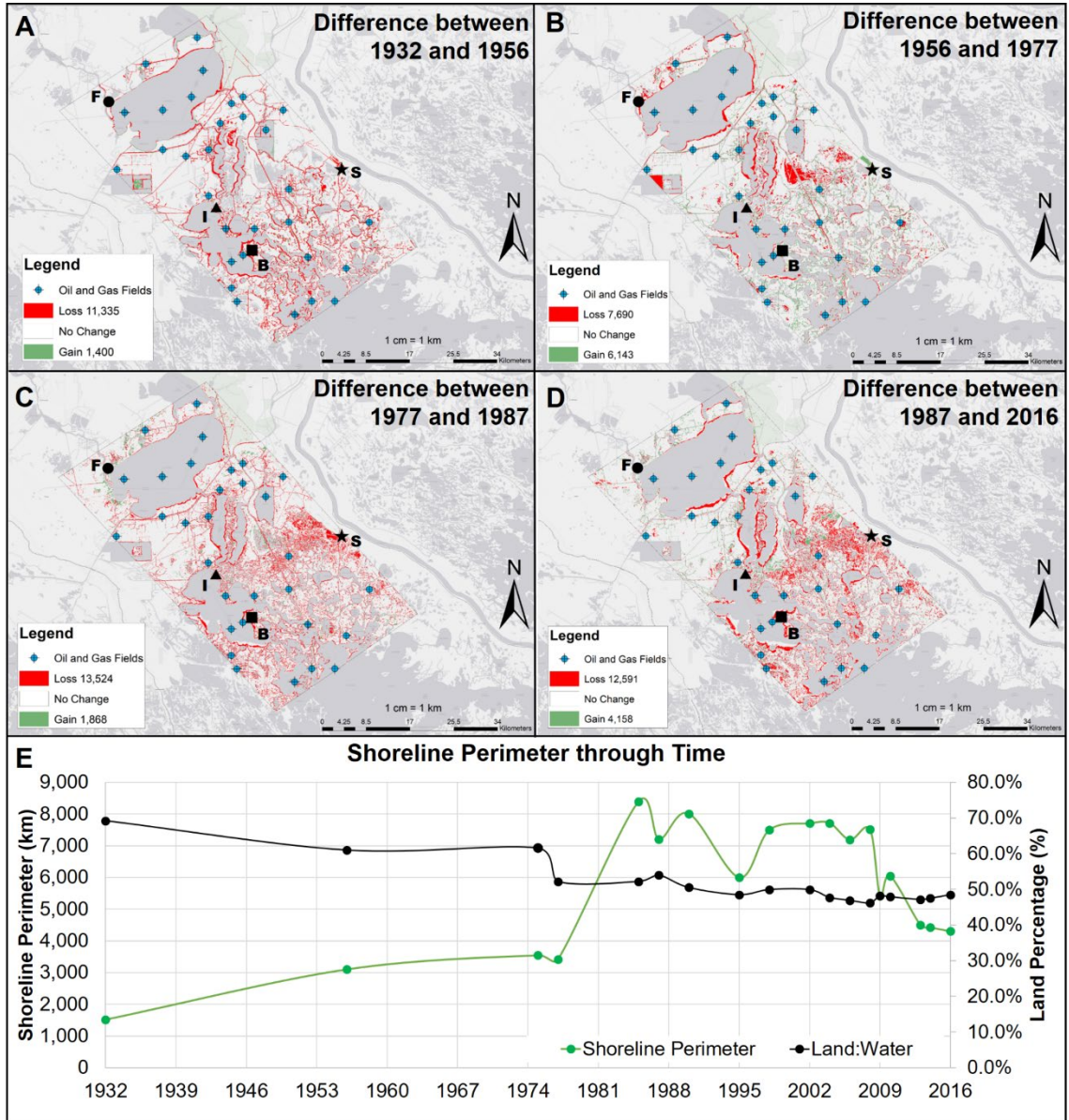


Figure 43. Land-Water Area Difference maps from 1932- 1956, 1956-1977, 1977-1987, and 1987-2016 from USGS data (Couvillion et al., 2018) for the area near the proposed Mid- Barataria Sediment Diversion that is also in the region of the four study sites (Fresh, Intermediate, Brackish, and Saline). E) Plot of changing land:water ratio (black line) and total length of shoreline perimeter (green line) for these and four other (intermediate) time slices from the USGS wetland area maps.

7. CONCLUSIONS

The results of the present study suggest the following about the impact of the surficial, organic-rich marsh deposits in Barataria Basin on water exchange and subsidence:

- 1.) Lateral exchange of groundwater through the marsh subsurface is shown to cause (hours to days) short- term perturbations to the marsh surface elevation. This results in expansion and contraction of the marsh surface up to 3 cm.
- 2.) Groundwater exchange frequency, extent, and interior penetration is driven by water levels in adjacent water bodies which are controlled by meteorological and astronomical tides, and ultimately, by Gulf water level.
- 3.) The use of CR-SET's in multiple ecotypes shows that groundwater exchange rates are also controlled by substrate type which controlled permeability.
- 4.) Marsh expansion and contraction has a minimal impact on the shallow subsidence rates calculated by other investigators from CRMS VA and SEC data.
- 5.) Analysis of vertical accretion and accumulation rates on different time scales show evidence of declining mineral supply rates overall through time in the marsh layer but also exhibit site-to-site variability in the response of organic matter loading and preservation.
- 6.) A new hypothesis is outlined suggesting that canal cutting increased organic matter oxidation and subsidence rates for a period in the 1980's and 1990's in Barataria Basin wetlands by increasing groundwater exchange and the spatial extent, exposure frequency and thickness of the marsh vadose zone.

APPENDICES

Appendix A: Ultrasonic Sensor Experiment to Examine Behavior when Sediment Surface is Flooded

The purpose of this experiment is to test if the ultrasonic sensor can penetrate through the water column to measure the marsh surface or if the sensor immediately measures the water surface. There are four sets of measurements made during the ultrasonic experiment in the laboratory on a test core:

- 1) At the sediment surface with no water in the core tube.
- 2) At the sediment surface with water sitting -1 cm below the surface.
- 3) Water at the sediment surface.
- 4) +1 cm of water above the surface.

Each measurement set includes ~10 distance readings. After each set of measurements and before the next set, the ultrasonic sensor was stopped from recording to prevent contamination from water being injected into the core tube. The experiment shows that the sediment surface increases as water fills the core column (Figure A1). When water levels are at 1 cm above the sediment surface the ultrasonic sensor recorded the water elevation and not the sediment surface elevation (Figure A1).

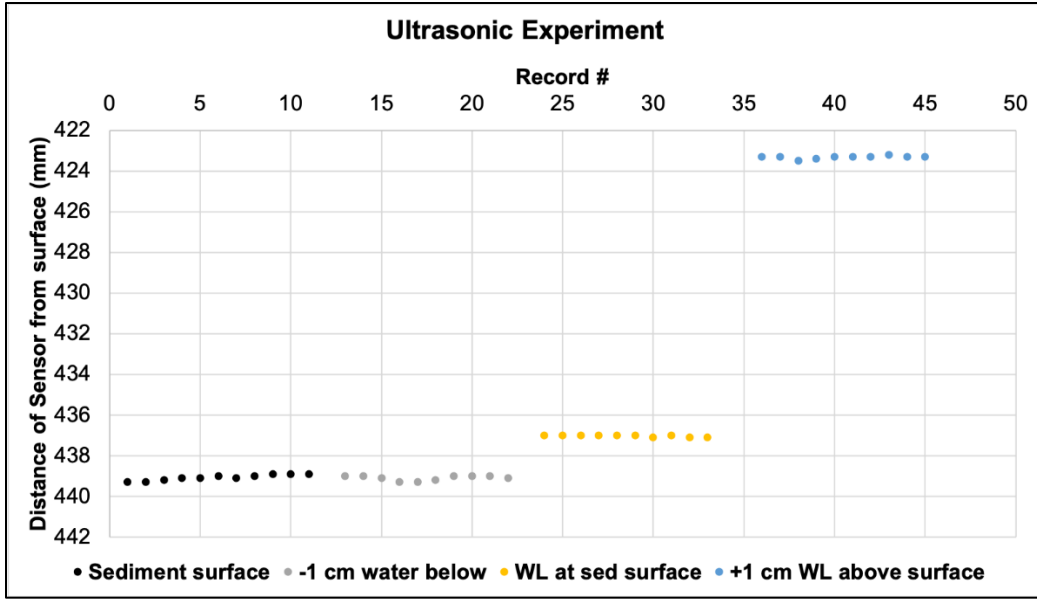


Figure A1. A column of marsh sediment was taken from the Fresh site (CRMS 3054). Water is drained from the core tube to the point below the sediment surface. The ultrasonic sensor is positioned above the sediment surface for approximately 11 measurements (black). Water is slowly injected into the core tube until 1 cm from the sediment surface (gray) for approximately 10 measurements. Water is again, slowly injected into the core until it is level with the sediment surface (yellow) for approximately 10 measurements. Lastly, water is injected into the core tube approximately 1 cm above the sediment surface (blue) and the ultrasonic sensor tracks the water elevation and not the marsh surface.

Table A1. The average distance and standard error of the four sets of measurements made during the ultrasonic sensor experiment

| Measurement Sets | Average Distance (mm) | Difference (mm) | Standard Error |
|---------------------------|-----------------------|-----------------|----------------|
| Sediment Surface | 439.07 | - | 0.04 |
| -1 cm water below | 439.10 | 0.003 | 0.04 |
| WL at sediment surface | 437.03 | 0.2 | 0.08 |
| +1 cm water above surface | 423.32 | -1.39 | 0.02 |

Appendix B: Additional Marsh Surface Elevation Figures

These figures are additional to Figure 13 in the main text showing the behavior of the marsh surface elevation records at the CR-SET sites with changing water elevation from the nearby CRMS gauge.

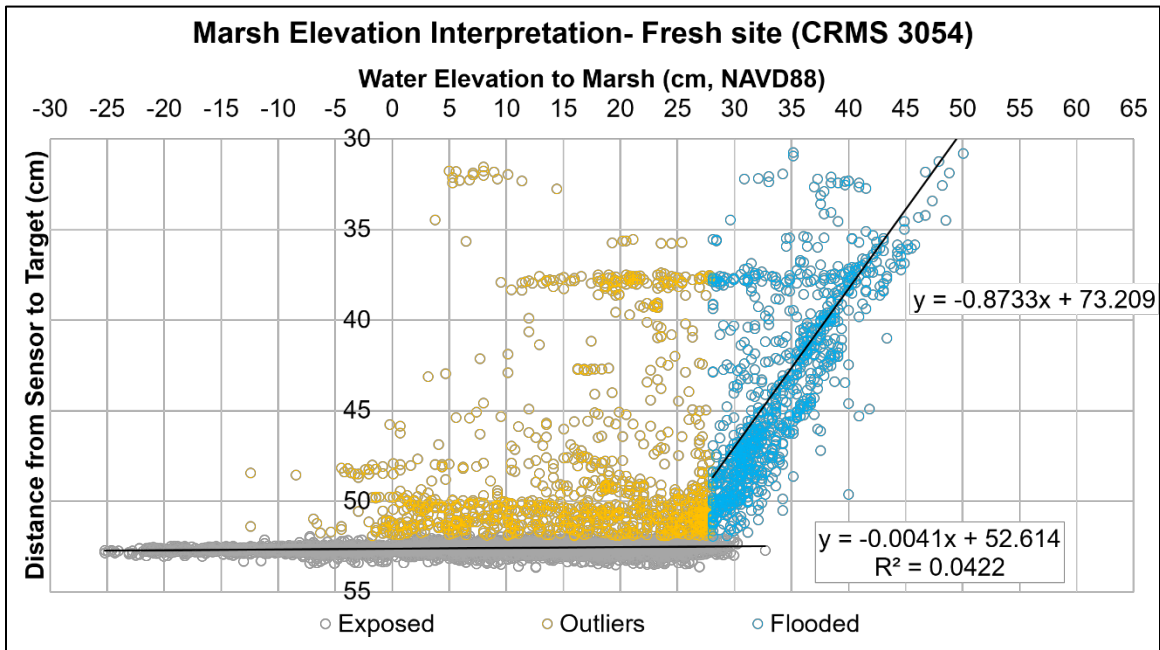


Figure B4. Marsh surface versus water surface elevation at the Fresh site over the period of record

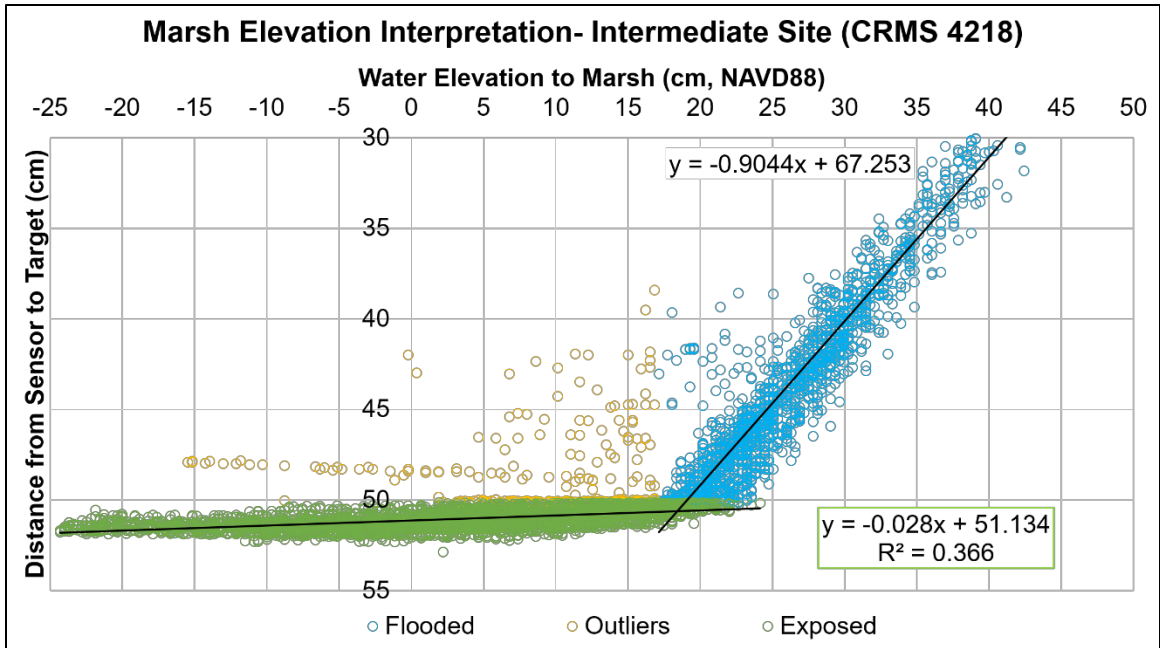


Figure 5B. Marsh surface versus water surface elevation at the Intermediate site over the period of record.

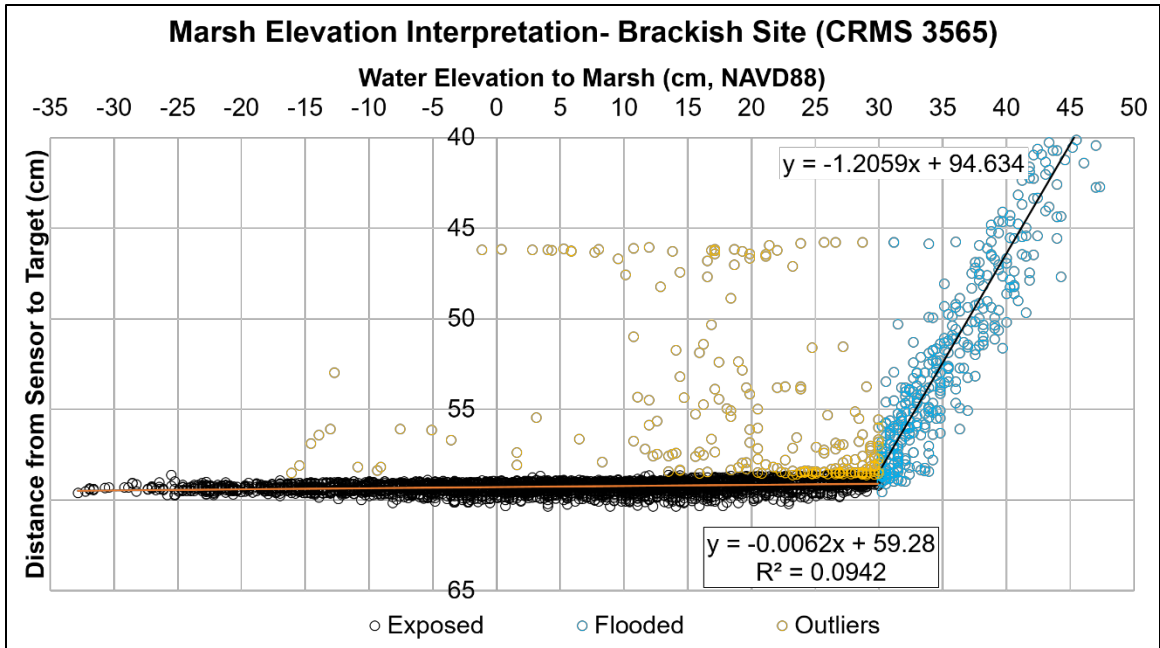


Figure 6B. Marsh surface versus water surface elevation at the Brackish site over the period of record.

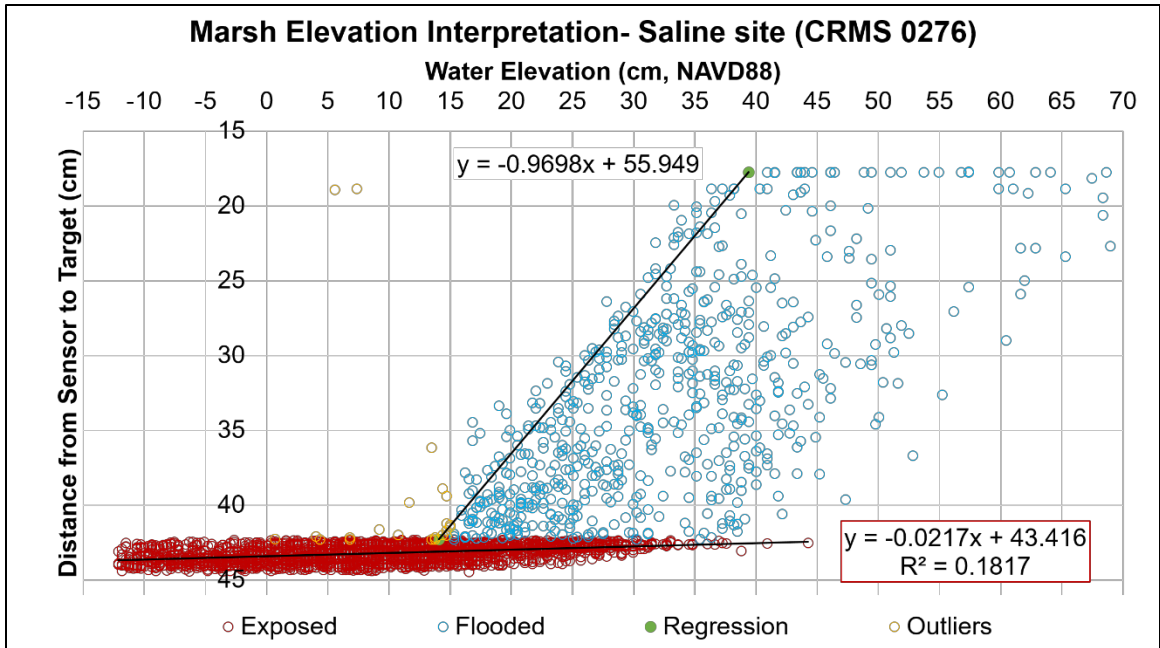


Figure 7B. Marsh surface versus water surface elevation at the Saline site over the period of record.

Appendix C: Vertical Accretion Measurements at the Four CRMS Study sites 2009-2018

The table below is a compilation of the average vertical accretion rates through time at each of the CRMS sites used within this study. This study was conducted during the 2019 water year (October 2018 – September 2019), which was a higher water year, on average, than previous years (discussed within the Results). The table below shows that vertical accretion during the 2018 sampling year was higher than previous years at all four sites.

Table C1. Average Vertical Accretion (mm) of Plot Set 1 (9 measurements) through time.

| CRMS Sites | 2018 | 2017 | 2016 | 2015 | 2014 | 2013 | 2012 | 2011 | 2010 | 2009 |
|---------------------|-------------|-------------|-------------|-------------|-------------|-------------|-------------|-------------|-------------|-------------|
| Fresh | 121.8 | 99.1 | N/A | 73.3 | 51.3 | N/A | 37.6 | 42.8 | 19.5 | 14.3 |
| Intermediate | 168.7 | 42.3 | N/A | 140.7 | 95.5 | N/A | 93.6 | 28.8 | 13.0 | 23.9 |
| Brackish | 149.3 | 151.7 | N/A | 139.5 | 126.8 | N/A | 106.1 | 113.3 | 94.6 | 115.2 |
| Saline | 121.8 | 114.4 | N/A | 87.4 | 126.4 | N/A | 116.1 | 51.2 | 31.1 | 41.1 |

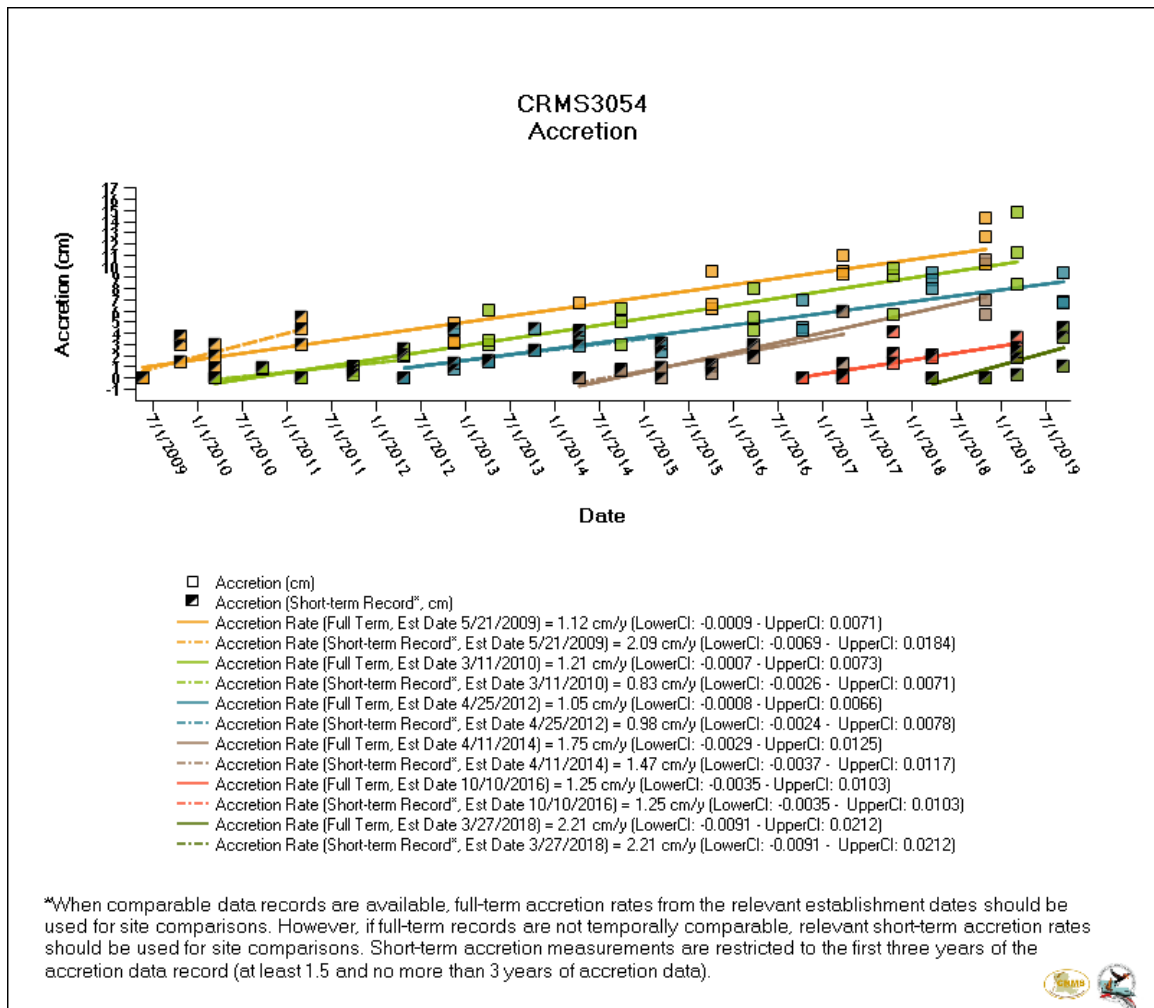


Figure C1. Vertical accretion rates at the Fresh site through time reported by CPRA. Table found at <https://lacoast.gov/chart/Charting.aspx?laf=crms&tab=2>

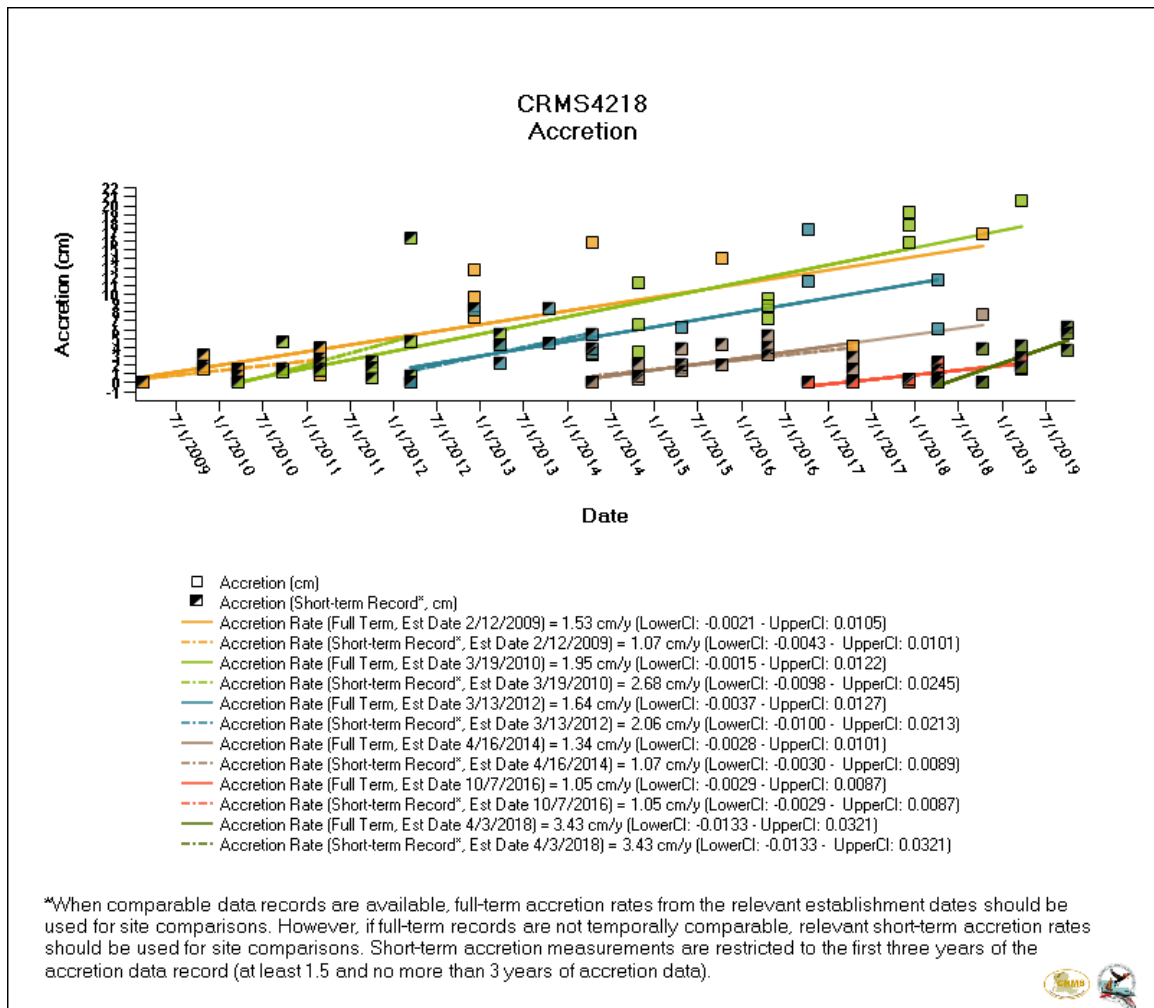


Figure C2. Vertical accretion rates at the Intermediate site through time reported by CPRA. Table found at <https://lacoast.gov/chart/Charting.aspx?laf=crms&tab=2>

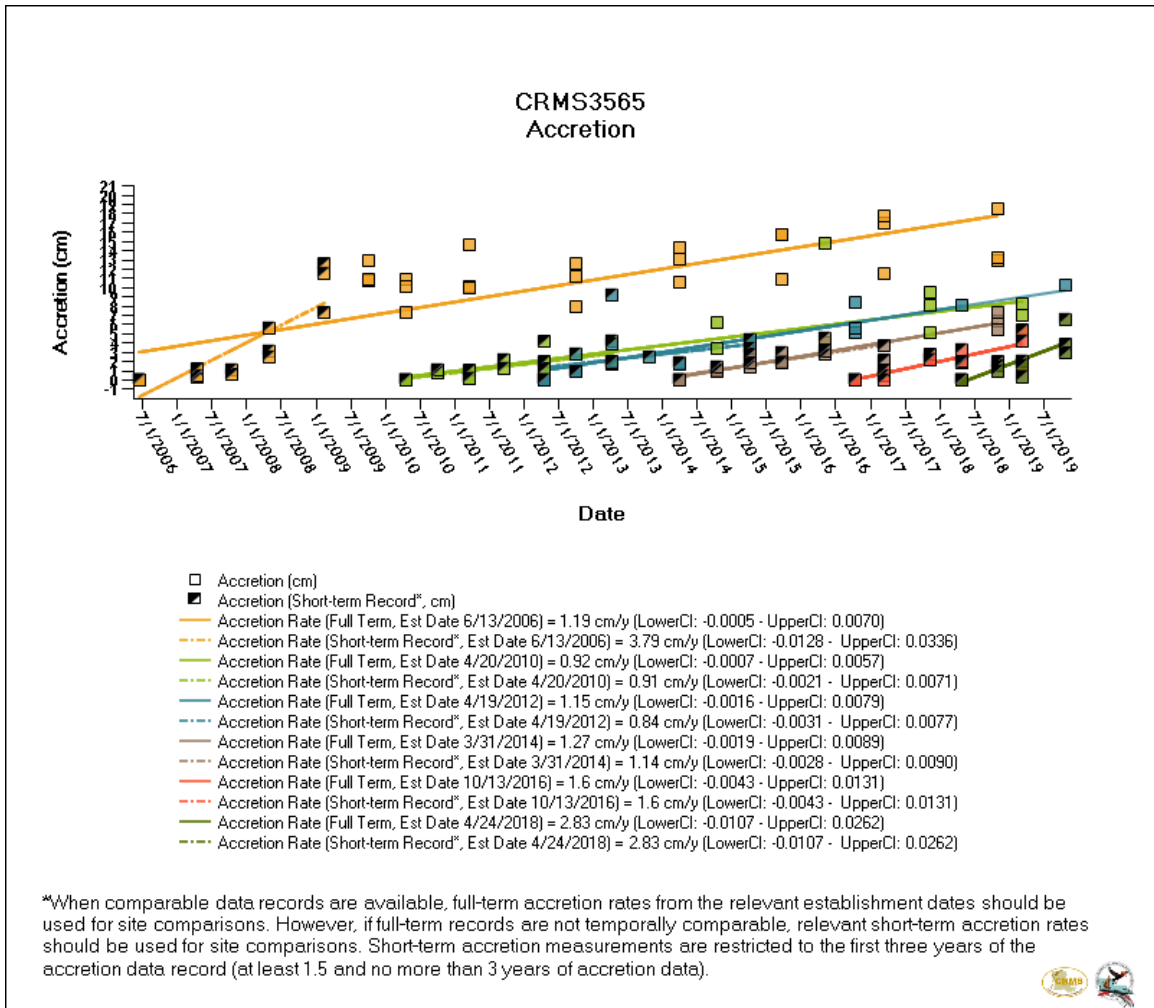


Figure C3. Vertical accretion rates at the Brackish site through time reported by CPRA. Table found at <https://lacoast.gov/chart/Charting.aspx?laf=crms&tab=2>

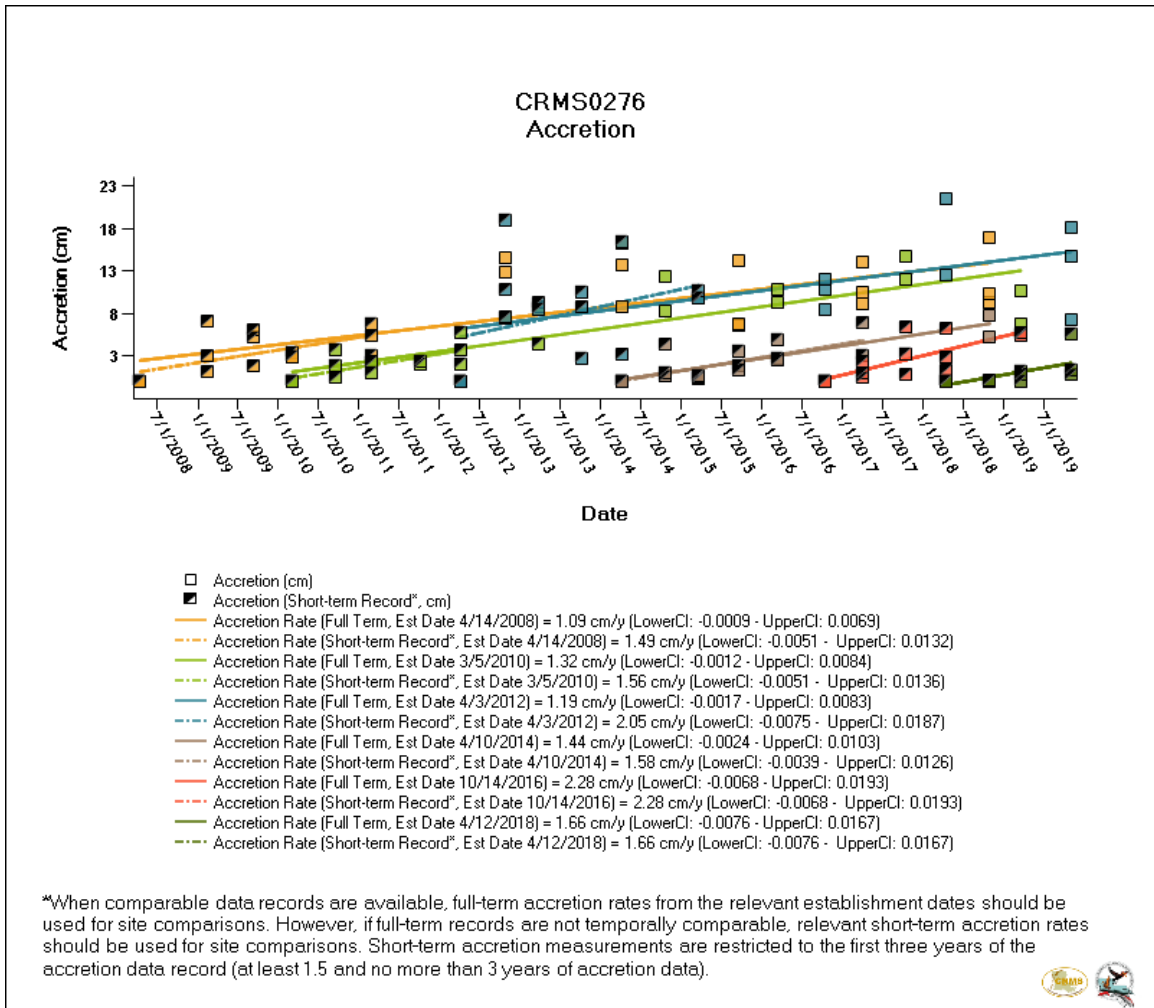


Figure C4. Vertical accretion rates at the Saline site through time reported by CPRA. Table found at <https://lacoast.gov/chart/Charting.aspx?laf=crms&tab=2>

Appendix D: Platform Orientations at the Study Sites

The maps below show the distance of the CR-SET's (used in this study) from the corresponding CRMS water level gauge.

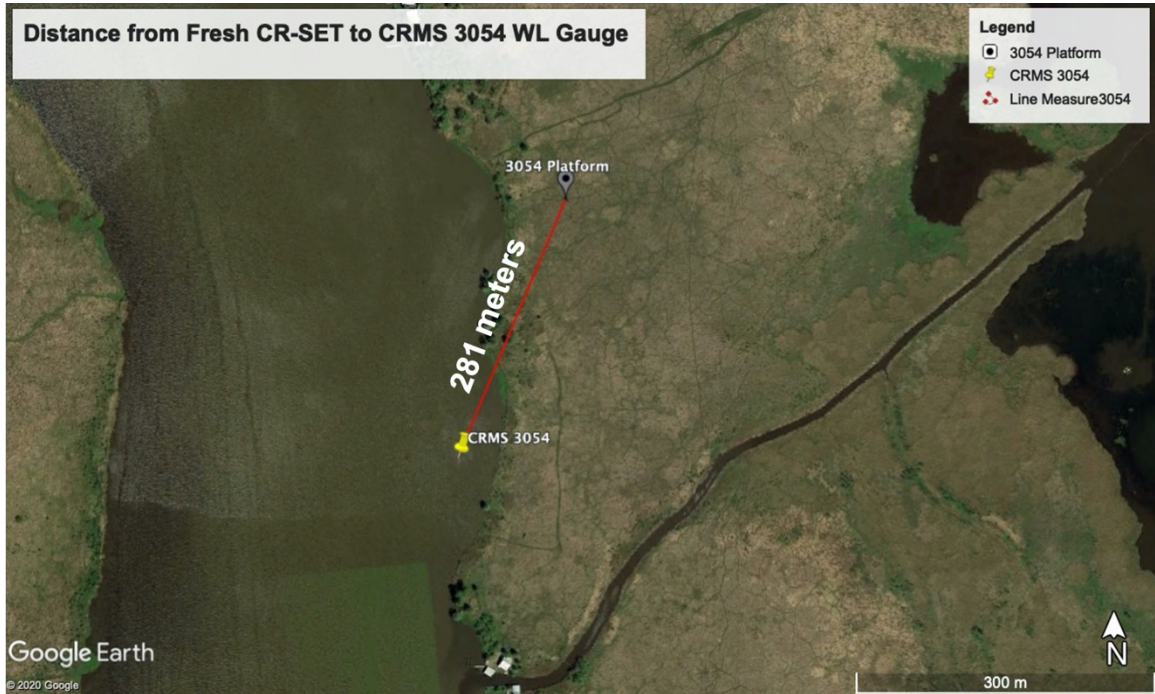


Figure D1. Distance from Fresh CR-SET to CRMS water level gauge.

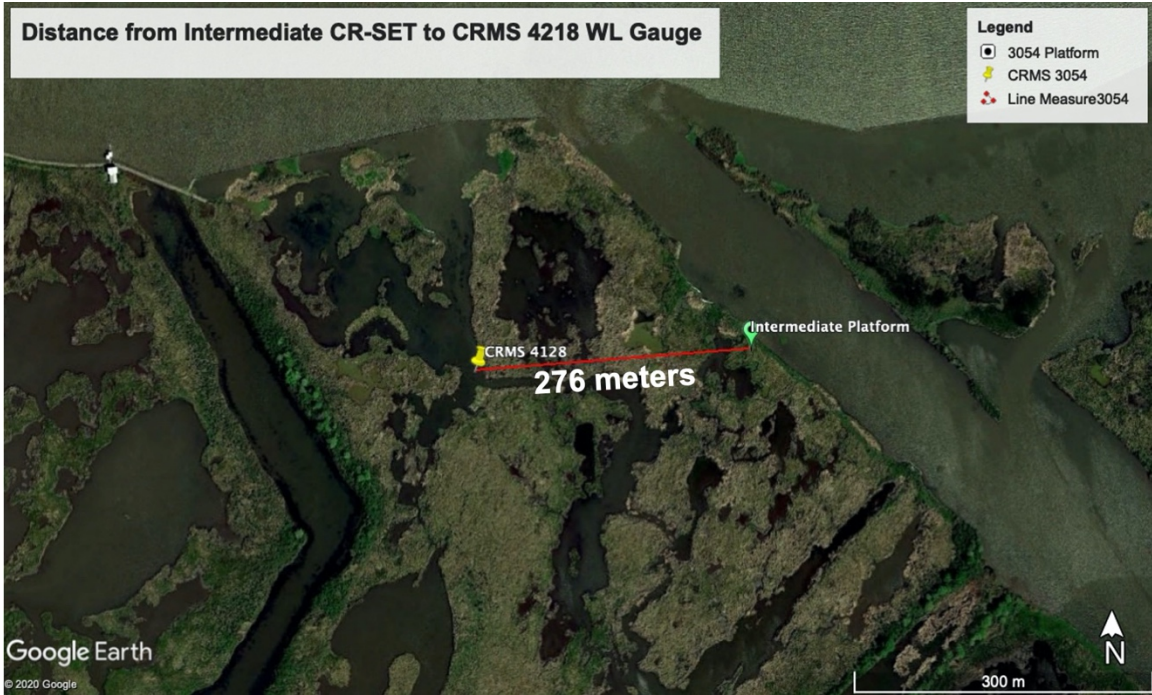


Figure D2. Distance from Intermediate CR-SET to CRMS water level gauge.



Figure D3. Distance from Brackish CR-SET to CRMS water level gauge.

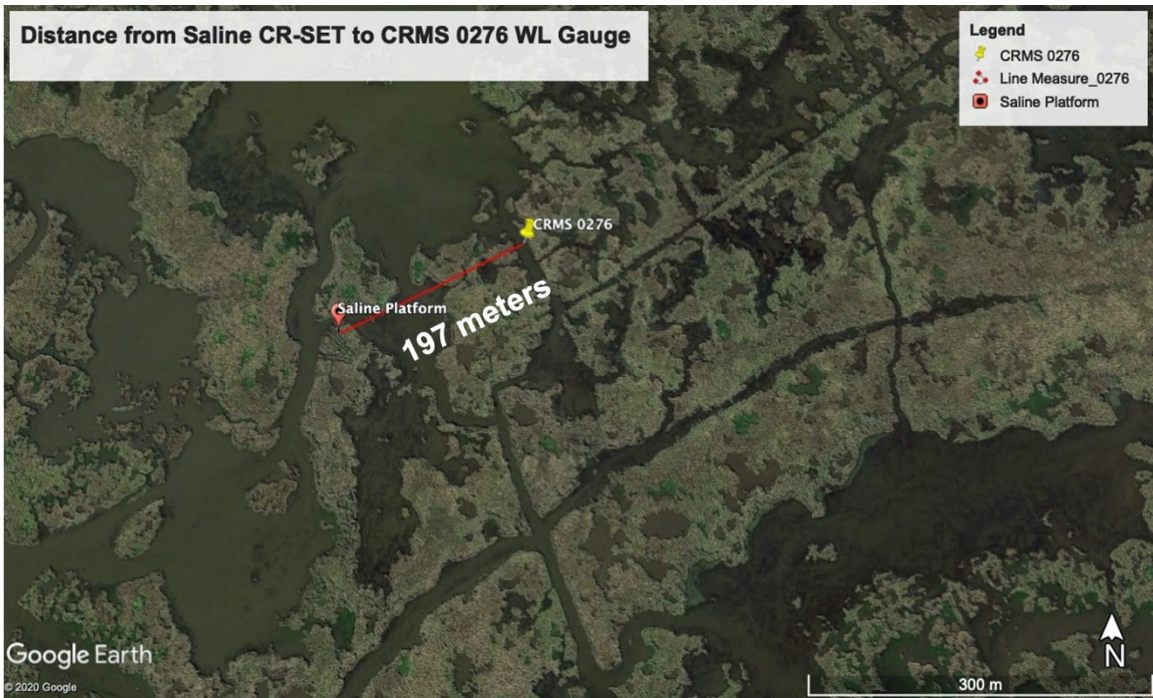


Figure D4. Distance from Saline CR-SET to CRMS water level gauge.

Appendix E. Core Descriptions

Descriptions of the texture, color, and grain size is provided below for each of the four study sites. The descriptions were used in combination with both the LOI and the D50 grain size to construct stratigraphic columns- noting the thickness of the root mat, and changes in organic-rich vs. mineral-rich intervals.

Table E2. Down core descriptions of grain size, texture, and color at the Fresh site.

| Interval (cm) | Description |
|---------------|--|
| 0-17 | Organic-rich, brown Smooth to the touch Contains roots and stems |
| 17-23 | Less organics, brown Silty |
| 23-42 | Gray and Brown clay Very smooth No live organics |
| 42-52 | Light brown silty clay interbedded with black peat |
| 52-57 | Black soil, small roots Clayey silt |
| 57-71 | Dark brown and black Clay, smooth to touch |
| 71-73 | Orange streaks (oxidation) interbedded with gray and brown clay |
| 73-92 | Dominantly clay, some fine silt Mostly gray with orange streaks |
| 92-101 | Brown clay |
| 108-115 | Dark brown clay Contains very small roots |
| 115-148 | Dark brown clay, becoming black in color. |

Table E3. Down core descriptions of grain size, texture, and color at the Intermediate site.

| Interval (cm) | Description |
|----------------------|--|
| 0-29 | Roots and stems, dark brown in color Silty to touch Very watery |
| 38-43 | Dark brown and smooth, contains silt Organic-rich |
| 45-64 | Black soil- peat, very smooth clay Small roots and stems |
| 64-87 | Increasing in silt content Still black in color and contains organics |

Table E4. Down core descriptions of grain size, texture, and color at the Brackish site.

| Interval (cm) | Description |
|----------------------|---|
| 0-17 | Brown and gritty to touch, silty Very watery Marsh mat is about 115 cm long |
| 17-45 | Organic-rich, smooth dark brown soil Contains roots and stems |
| 52-87 | Very organic-rich, dark brown in color Silty to touch |
| 92-115 | Grading from silty dark brown to clayey black soil Very smooth peat |
| 143-150 | Silty with clay. Still black in color. Contains no roots or stems |
| 150-171 | Silty but black in color. Organic-rich |
| 171-178 | Gray Clay with dark brown streaks |

Table E5. Down core descriptions of grain size, texture, and color at the Saline site.

| Interval (cm) | Description |
|----------------------|---|
| 0-10 | Dark Brown soil, very silty Contains organic materials- roots and stems Very watery |
| 17-30 | Increasing in clay content- gray streaks |
| 30-50 | Smooth to touch, mostly clay Still contains organics- small roots |
| 52-59 | Gray clay and transitions into dark brown clayey silt |
| 59-64 | Very watery Brown in color and smooth clay |
| 64-73 | Watery brown clay with small roots visible Mostly clayey silt |
| 78-87 | Smooth but silty, no visible organics Grades from brown to gray silty clays. |

Appendix F: D50 Grain Size

Ancillary to the D50 grain size stratigraphic columns provided in Figure 25, below are the D10, D50, and D90 grain sizes for each of the four study sites.

Table F1. Fresh site grain size statistics.

| Depth Intervals (cm) | D10 | D50 | D90 |
|----------------------|------|------|------------|
| 0-2 | 0.66 | 7.54 | 201 |
| 2-4 | 0.95 | 10.8 | 44.3 |
| 4-6 | 1.55 | 14.2 | 921 |
| 6-8 | 1.11 | 13.9 | 316 |
| 8-10 | 0.58 | 8.02 | 1370 |
| 15-17 | 1.44 | 24.7 | 1450 |
| 22-24 | 3.78 | 25.7 | 1450 |
| 29-31 | 0.58 | 9.92 | 1220 |
| 36-38 | 0.61 | 9.99 | 614.975 |
| 43-45 | 0.52 | 6 | 75.6 |
| 50-52 | 0.49 | 26.1 | 1215.83333 |
| 57-59 | 0.88 | 18 | 428 |
| 64-66 | 0.42 | 3.35 | 801 |
| 71-73 | 0.35 | 1.39 | 20.85 |
| 78-80 | 0.45 | 6.27 | 1220 |
| 85-87 | 0.51 | 4.72 | 57.6909091 |
| 92-94 | 0.54 | 5.46 | 31.8 |
| 99-101 | 0.57 | 8.82 | 1380 |
| 106-108 | 0.51 | 4.24 | 223.117647 |
| 113-115 | 0.42 | 2.39 | 14.8 |
| 120-122 | 0.51 | 5.58 | 305 |
| 127-129 | 0.4 | 1.79 | 37.5 |
| 134-136 | - | - | - |
| 141-143 | 0.68 | 8.85 | 41 |

Table F2. Intermediate site grain size statistics.

| Depth Intervals (cm) | D10 | D50 | D90 |
|---------------------------------|------------|------------|------------|
| 0-2 | 0.76 | 12.1 | 42.9 |
| 2-4 | 1 | 16 | 57.4 |
| 4-6 | 0.76 | 10.5 | 50.5 |
| 6-8 | 0.80 | 12.5 | 60.7 |
| 8-10 | 1.14 | 15.6 | 55.5 |
| 15-17 | 0.72 | 8.3 | 36.6 |
| 22-24 | 0.74 | 12.2 | 68.1 |
| 29-31 | 1.11 | 18.7 | 74.6 |
| 36-38 | 0.88 | 17.9 | 81.4 |
| 43-45 | 0.94 | 16.6 | 55.6 |
| 50-52 | 0.57 | 11 | 1160 |
| 57-59 | 0.31 | 6.19 | 39.6 |
| 64-66 | 0.28 | 4.95 | 30.7 |
| 71-73 | 1.22 | 22.3 | 59.3 |
| 78-80 | 0.93 | 16 | 52.3 |
| 85-87 | 0.67 | 12.3 | 65 |

Table F3. *Brackish site grain size statistics.*

| Depth Intervals (cm) | D10 | D50 | D90 |
|---------------------------------|------------|------------|------------|
| 0-2 | 1.49 | 22.1 | 59.9 |
| 2-4 | 1.06 | 21.6 | 67.4 |
| 4-6 | 1.68 | 26.1 | 69.9 |
| 6-8 | 1.09 | 22.5 | 57.6 |
| 8-10 | 1.67 | 30.7 | 81.5 |
| 15-17 | 2.3 | 35.7 | 127 |
| 22-24 | 1.27 | 36.3 | 130 |
| 29-31 | 0.96 | 21.4 | 96.5 |
| 36-38 | 1.28 | 22.1 | 67.3 |
| 43-45 | 0.96 | 18.9 | 65.7 |
| 50-52 | 0.79 | 17.6 | 76 |
| 57-59 | 1.16 | 18.1 | 58.8 |
| 64-66 | 0.94 | 15.8 | 55.2 |
| 71-73 | 0.58 | 9.53 | 49.1 |
| 78-80 | 0.65 | 11.3 | 55.7 |
| 85-87 | 0.46 | 7.11 | 34.4 |
| 92-94 | - | - | - |
| 99-101 | 0.62 | 9.79 | 55.1 |
| 106-108 | - | - | - |
| 113-115 | 0.28 | 1.53 | 13.5 |
| 120-122 | 0.35 | 1.58 | 16.1 |
| 127-129 | 0.56 | 7.35 | 39.6 |
| 134-136 | - | - | - |
| 141-143 | - | - | - |
| 148-150 | 0.64 | 11.3 | 67.9 |
| 155-157 | 0.60 | 11.8 | 84.7 |
| 162-164 | 0.66 | 12.9 | 1370 |
| 169-171 | 0.70 | 12.7 | 61.3 |
| 176-178 | 1.98 | 21.3 | 69.6 |
| 183-185 | 0.49 | 6.44 | 63.7 |
| 190-192 | 0.46 | 5.39 | 62.4 |

Table F4. Saline site grain size statistics

| Depth Intervals (cm) | D10 | D50 | D90 |
|---------------------------------|------------|------------|------------|
| 0-2 | 1.45 | 37.4 | 1800 |
| 2-4 | 1.11 | 16.5 | 603 |
| 4-6 | 0.79 | 15.8 | 888 |
| 6-8 | 0.77 | 12.6 | 506 |
| 8-10 | 0.56 | 5.22 | 19.5 |
| 15-17 | 0.69 | 9.51 | 35.8 |
| 22-24 | 1.03 | 19.3 | 974 |
| 29-31 | 1.04 | 11.5 | 161 |
| 36-38 | 0.66 | 6.08 | 80.8 |
| 43-45 | 0.44 | 3.14 | 437 |
| 50-52 | 0.42 | 2 | 345 |
| 57-59 | 0.48 | 8.14 | 615.08 |
| 64-66 | 0.58 | 14.3 | 933 |
| 71-73 | 0.51 | 5.36 | 63.6 |
| 78-80 | 0.90 | 24.9 | 1270 |
| 85-87 | 0.78 | 18.5 | 60.9 |

Appendix G: Total Organic Matter, Detrital, Root Mass, Mineral Sediment

Breakdown

Provided below are the percentages of detrital organic matter, live rooting, and mineral percentage used to construct Figure 28.

Table G1. The total organic matter determined by LOI analysis and the breakdown between detrital organic matter, live rooting, mineral sediment, and corresponding porosity within the total organics at the Fresh site. Sample depths at this site are used from the same core that both LOI and grain size are measured from. The sample depths at this site are the intervals between the original sampling procedures used in this study.

| Depth (cm) | Total Organic Matter % | Detrital % | Live Rooting % | Mineral % | Porosity % |
|------------|------------------------|------------|----------------|-----------|------------|
| 15 | 86.86 | 38.59 | 48.26 | 13.14 | 86.67 |
| 22 | 66.96 | 48.90 | 18.06 | 33.04 | 83.49 |
| 29 | 26.23 | 24.63 | 1.60 | 73.77 | 80.46 |
| 36 | 63.75 | 59.47 | 4.29 | 36.25 | 76.01 |
| 43 | 20.26 | 19.48 | 0.78 | 79.74 | 71.85 |
| 50 | 23.31 | 23.12 | 0.19 | 76.69 | 72.23 |
| 57 | 19.62 | 19.44 | 0.18 | 80.38 | 73.55 |
| 64 | 19.79 | 19.14 | 0.65 | 80.21 | 68.67 |
| 71 | 11.88 | 11.71 | 0.17 | 88.12 | 63.93 |
| 78 | 8.23 | 8.21 | 0.01 | 91.77 | - |
| 85 | 7.39 | 7.37 | 0.02 | 92.61 | 59.42 |
| 92 | 7.21 | 7.19 | 0.02 | 92.79 | 59.58 |
| 99 | 6.32 | 6.29 | 0.03 | 93.68 | 59.81 |
| 106 | 5.89 | 5.88 | 0.00 | 94.11 | 60.10 |

Table G2. The total organic matter determined by LOI analysis and the breakdown between detrital organic matter, live rooting, mineral sediment, and corresponding porosity within the total organics at the Intermediate site. An additional core within 1 meter of the original core was taken for this analysis.

| Depth (cm) | Total Organic Matter % | Detrital % | Live Rooting % | Mineral % | Porosity % |
|------------|------------------------|------------|----------------|-----------|------------|
| 2 | 33.45 | 7.48 | 25.97 | 66.55 | 86.32 |
| 4 | 37.39 | 12.18 | 25.21 | 62.61 | 87.27 |
| 6 | 35.85 | 5.05 | 30.80 | 64.15 | 86.15 |
| 8 | 37.91 | 7.18 | 30.74 | 62.09 | 86.04 |
| 10 | 40.92 | 13.29 | 27.63 | 59.08 | 86.99 |
| 15 | 33.12 | 20.17 | 12.95 | 66.88 | 86.13 |
| 22 | 31.67 | 16.79 | 14.88 | 68.33 | 87.18 |
| 29 | 31.94 | 24.19 | 7.75 | 68.06 | 86.39 |
| 36 | 56.30 | 43.63 | 12.67 | 43.70 | 89.61 |
| 43 | 34.26 | 30.25 | 4.01 | 65.74 | 84.28 |
| 50 | 76.99 | 70.08 | 6.91 | 23.01 | 89.45 |
| 57 | 77.64 | 73.09 | 4.55 | 22.36 | 89.70 |
| 64 | 77.68 | 74.95 | 2.72 | 22.32 | 89.00 |
| 71 | 33.14 | 32.93 | 0.21 | 66.86 | 84.18 |
| 78 | 55.01 | 52.99 | 2.02 | 44.99 | 88.52 |
| 85 | 63.97 | 63.40 | 0.56 | 36.03 | 88.76 |

Table G3. The total organic matter determined by LOI analysis and the breakdown between detrital organic matter, live rooting, mineral sediment, and corresponding porosity within the total organics at the Brackish site. An additional core within 1 meter of the original core was taken for this analysis.

| Depth (cm) | Total Organic Matter % | Detrital % | Live Rooting % | Mineral % | Porosity % |
|------------|------------------------|------------|----------------|-----------|------------|
| 2 | 15.70 | 9.32 | 6.38 | 84.30 | 80.69 |
| 4 | 22.03 | 17.30 | 4.73 | 77.97 | 72.59 |
| 6 | 15.23 | 12.02 | 3.21 | 84.77 | 74.60 |
| 8 | 11.52 | 8.22 | 3.30 | 88.48 | 71.19 |
| 10 | 16.93 | 13.90 | 3.03 | 83.07 | 75.65 |
| 15 | 27.12 | 25.39 | 1.73 | 72.88 | 82.09 |
| 22 | 35.39 | 33.96 | 1.44 | 64.61 | 84.55 |
| 27 | 37.08 | 30.31 | 6.77 | 62.92 | 86.48 |
| 34 | 37.46 | 29.67 | 7.79 | 62.54 | 85.96 |
| 43 | 45.78 | 36.45 | 9.33 | 54.22 | 88.38 |
| 50 | 61.07 | 48.84 | 12.23 | 38.93 | 90.91 |
| 57 | 61.61 | 49.99 | 11.62 | 38.39 | 89.30 |
| 64 | 57.20 | 47.07 | 10.13 | 42.80 | 88.77 |
| 71 | 65.34 | 53.29 | 12.05 | 34.66 | 89.90 |
| 78 | 67.71 | 53.27 | 14.45 | 32.29 | 89.07 |
| 85 | 72.36 | 63.11 | 9.24 | 27.64 | 89.32 |
| 92 | - | - | - | - | - |
| 99 | 62.91 | 59.86 | 3.05 | 37.09 | 88.54 |
| 106 | - | - | - | - | - |
| 113 | 83.46 | 79.96 | 3.50 | 16.54 | 86.05 |
| 120 | 81.99 | 80.14 | 1.84 | 18.01 | 83.89 |
| 127 | 74.53 | 70.84 | 3.69 | 25.47 | 87.34 |
| 134 | 70.68 | 69.92 | 0.75 | 29.32 | 83.91 |
| 141 | 70.51 | 69.94 | 0.57 | 29.49 | 84.74 |
| 148 | 52.54 | 52.35 | 0.19 | 47.46 | 87.22 |
| 155 | 40.52 | 39.89 | 0.63 | 59.48 | 87.02 |
| 162 | 63.34 | 62.92 | 0.42 | 36.66 | 84.34 |
| 169 | 59.65 | 59.08 | 0.57 | 40.35 | 84.13 |
| 176 | 53.88 | 53.51 | 0.37 | 46.12 | 80.19 |

Table G4. *The total organic matter determined by LOI analysis and the breakdown between detrital organic matter, live rooting, mineral sediment, and corresponding porosity within the total organics at the Saline site. Sample depths at this site are used from the same core that both LOI and grain size are measured from. The sample depths at this site are the intervals between the original sampling procedures used in this study.*

| Depth (cm) | Total Organic Matter % | Detrital % | Live Rooting % | Mineral % | Porosity % |
|-------------------|-------------------------------|-------------------|-----------------------|------------------|-------------------|
| 15 | 29.23 | 25.23 | 3.99 | 70.77 | 89.25 |
| 22 | 55.02 | 47.54 | 7.48 | 44.98 | 83.64 |
| 29 | 26.57 | 21.64 | 4.93 | 73.43 | 75.21 |
| 36 | 17.16 | 15.89 | 1.27 | 82.84 | 74.54 |
| 43 | 8.51 | 6.76 | 1.75 | 91.49 | 73.96 |
| 50 | 16.51 | 14.08 | 2.42 | 83.49 | 68.58 |
| 57 | 9.15 | 8.13 | 1.02 | 90.85 | 73.33 |
| 64 | 9.62 | 9.32 | 0.29 | 90.38 | 74.63 |
| 71 | 14.41 | 12.72 | 1.69 | 85.59 | 68.89 |
| 78 | 9.44 | 9.13 | 0.30 | 90.56 | 65.89 |
| 85 | 6.63 | 6.27 | 0.35 | 93.37 | 64.77 |

Appendix H. Total Lead-210 and Cs-137 Activity

The downcore Lead-210 and Cs-137 activities (dpm/g) and errors are provided in the tables below. These activities are used to create Figures 29 and 30 and are used to calculate sediment accumulation rates linearly and compare consolidated rates to a specific porosity.

Table H6. Down core Pb-210 and Cs-137 activities and errors at the Fresh site.

| Depth Interval (cm) | xs Pb-210 Activity (dpm/g) | xs Pb-210 error | Cs-137 Activity (dpm/g) | Cs-137 error |
|---------------------|----------------------------|-----------------|-------------------------|--------------|
| 0 to 2 | 5.13 | 0.72 | 0.00 | 0.00 |
| 2 to 4 | 118.78 | 14.61 | 0.02 | 0.76 |
| 4 to 6 | 130.29 | 16.15 | 0.57 | 0.88 |
| 6 to 8 | 31.43 | 5.44 | 3.33 | 0.52 |
| 8 to 10 | 46.55 | 6.17 | 5.20 | 0.46 |
| 15 to 17 | 13.76 | 2.47 | 25.09 | 0.60 |
| 22 to 24 | 3.47 | 1.09 | 0.00 | 0.00 |
| 29 to 31 | 1.20 | 1.25 | 0.03 | 0.13 |
| 36 to 38 | 0.54 | 0.96 | 0.00 | 0.00 |
| 43 to 45 | 2.08 | 1.20 | 0.00 | 0.00 |
| 50 to 52 | 0.91 | 1.02 | 0.00 | 0.00 |
| 57 to 59 | 1.67 | 1.26 | 0.00 | 0.00 |
| 64 to 66 | 2.08 | 0.87 | 0.00 | 0.00 |
| 71 to 73 | 0.53 | 0.86 | 0.00 | 0.00 |
| 78 to 80 | 0.71 | 1.48 | 0.26 | 0.15 |
| 85 to 87 | -0.68 | 2.25 | 0.00 | 0.00 |
| 92 to 94 | 0.13 | 0.63 | 0.00 | 0.00 |
| 99 to 101 | -0.07 | 0.73 | 0.00 | 0.00 |
| 106 to 108 | 0.58 | 0.87 | 0.00 | 0.00 |
| 113 to 115 | 0.15 | 0.68 | 0.00 | 0.00 |
| 120 to 122 | | | | |
| 127 to 129 | -0.06 | 1.07 | 0.00 | 0.00 |
| 134 to 136 | | | | |
| 141 to 143 | -0.86 | 0.56 | 0.00 | 0.00 |

Table H2. Down core Pb-210 and Cs-137 activities and errors at the Intermediate site.

| Depth Interval (cm) | xs Pb-210 Activity (dpm/g) | xs Pb-210 error | Cs-137 Activity (dpm/g) | Cs-137 error |
|----------------------------|-----------------------------------|------------------------|--------------------------------|---------------------|
| 0 to 2 | 13.08 | 3.36 | 0.55 | 0.13 |
| 2 to 4 | 15.61 | 3.83 | 0.61 | 0.13 |
| 4 to 6 | 12.87 | 3.28 | 0.90 | 0.13 |
| 6 to 8 | 13.53 | 3.45 | 0.61 | 0.14 |
| 8 to 10 | 19.17 | 4.44 | 0.95 | 0.15 |
| 15 to 17 | 8.93 | 2.69 | 0.87 | 0.14 |
| 22 to 24 | 9.18 | 2.77 | 2.52 | 0.17 |
| 29 to 31 | 7.54 | 2.56 | 3.68 | 0.19 |
| 36 to 38 | 4.26 | 2.22 | 0.45 | 0.13 |
| 43 to 45 | -0.31 | 1.41 | 0.01 | 0.11 |
| 50 to 52 | 2.40 | 1.57 | 0.00 | 0.00 |
| 57 to 59 | 4.05 | 17.00 | 0.13 | 0.07 |
| 64 to 66 | 1.77 | 1.54 | 0.36 | 0.11 |
| 71 to 73 | 1.10 | 1.69 | 0.08 | 0.10 |
| 78 to 80 | -2.41 | 1.69 | 0.08 | 0.13 |
| 85 to 87 | 0.59 | 0.25 | 0.39 | 0.09 |

Table H3. Down core Pb-210 and Cs-137 activities and errors at the Brackish site.

| Depth Interval (cm) | xs Pb-210 Activity (dpm/g) | xs Pb-210 error | Cs-137 Activity (dpm/g) | Cs-137 error |
|----------------------------|-----------------------------------|------------------------|--------------------------------|---------------------|
| 0 to 2 | 4.73 | 1.61 | 0.10 | 0.10 |
| 2 to 4 | 8.69 | 2.38 | 0.35 | 0.12 |
| 4 to 6 | 5.75 | 1.77 | 0.19 | 0.10 |
| 6 to 8 | 3.06 | 0.89 | 0.18 | 0.08 |
| 8 to 10 | 4.32 | 0.96 | 0.17 | 0.10 |
| 15 to 17 | 7.84 | 1.55 | 0.53 | 0.13 |
| 22 to 24 | 10.00 | 1.61 | 0.79 | 0.15 |
| 29 to 31 | 8.57 | 1.52 | 1.32 | 0.16 |
| 36 to 38 | 8.95 | 1.45 | 2.71 | 0.16 |
| 43 to 45 | 12.66 | 2.19 | 5.68 | 0.24 |
| 50 to 52 | 10.31 | 1.76 | 23.97 | 0.51 |
| 57 to 59 | 6.05 | 1.06 | 2.07 | 0.11 |
| 64 to 66 | 5.85 | 1.24 | 2.16 | 0.16 |
| 71 to 73 | 1.64 | 1.40 | 0.71 | 0.15 |
| 78 to 80 | 1.73 | 1.04 | 0.69 | 0.15 |
| 85 to 87 | -0.16 | 0.81 | 0.34 | 0.11 |
| 92 to 94 | - | - | - | - |
| 99 to 101 | -0.16 | 0.81 | 0.34 | 0.11 |
| 106 to 108 | - | - | - | - |
| 113 to 115 | - | - | - | - |
| 120 to 122 | - | - | - | - |
| 127 to 129 | 0.38 | 0.95 | 0.26 | 0.12 |
| 134 to 136 | -5.23 | 2.99 | 0.04 | 0.31 |
| 141 to 143 | -2.04 | 2.34 | 0.00 | 0.00 |
| 148 to 150 | 2.31 | 1.54 | 0.00 | 0.00 |
| 155 to 157 | 0.57 | 1.00 | 0.00 | 0.00 |
| 162 to 164 | 0.46 | 1.43 | 0.20 | 0.14 |
| 169 to 171 | 1.63 | 1.25 | 0.00 | 0.00 |
| 176 to 178 | 1.52 | 1.21 | 0.00 | 0.00 |
| 183 to 185 | 0.09 | 1.12 | 0.00 | 0.00 |
| 190 to 192 | 0.19 | 0.93 | 0.00 | 0.00 |

Table H4. Down core Pb-210 and Cs-137 activities and errors at the Saline site.

| Depth Interval (cm) | xs Pb-210 Activity (dpm/g) | xs Pb-210 error | Cs-137 Activity (dpm/g) | Cs-137 error |
|----------------------------|-----------------------------------|------------------------|--------------------------------|---------------------|
| 0 to 2 | 17.81 | 3.27 | 2.21 | 0.30 |
| 2 to 4 | 22.37 | 4.00 | 4.38 | 0.47 |
| 4 to 6 | 16.98 | 2.56 | 5.71 | 0.27 |
| 6 to 8 | 13.52 | 2.69 | 9.14 | 0.40 |
| 8 to 10 | 9.52 | 2.11 | 9.39 | 0.34 |
| 15 to 17 | 19.71 | 3.51 | 10.47 | 0.45 |
| 22 to 24 | 2.45 | 1.19 | 0.46 | 0.19 |
| 29 to 31 | 5.16 | 9.50 | 0.84 | 1.03 |
| 36 to 38 | 1.53 | 0.88 | 0.00 | 0.00 |
| 43 to 45 | 0.24 | 0.95 | 0.00 | 0.00 |
| 50 to 52 | -0.04 | 0.59 | 0.00 | 0.00 |
| 57 to 59 | 0.54 | 0.90 | 0.00 | 0.00 |
| 64 to 66 | 1.88 | 1.19 | 0.00 | 0.00 |
| 71 to 73 | 0.51 | 0.71 | 0.00 | 0.00 |
| 78 to 80 | -0.04 | 0.84 | 0.09 | 0.09 |
| 85 to 87 | 0.46 | 0.70 | 0.00 | 0.00 |

LITERATURE CITED

Allison, M., Yuill, B., Törnqvist, T., Amelung, F., Dixon, T.H., Erkens, G., Stuurman, R., Jones, C., Milne, G., Steckler, M., Syvitski, J., and July, P.T., 2016, Global Risk and Research Priorities for Coastal Subsidence: *Eos, Transactions American Geophysical Union*, , no. 97, p. 22-27.

Andriessse, J. P. (1988). *Nature and management of tropical peat soils. Soil resources, Management and Conservation Service*. FAO, Rome. Land and Water Development Division. Bulletin 50.

Appleby, P., & Oldfield, F. (1978). The calculation of lead-210 dates assuming a constant rate of supply of unsupported ^{210}Pb to the sediment. *Catena*, 5(1), 1–8. doi: 10.1016/s0341-8162(78)80002-2

Bailey, E. C. K. A. (1983). Characteristics of peat deposits in Mississippi River Delta Plain: ABSTRACT. *AAPG Bulletin*, 67. doi: 10.1306/ad460751-16f7-11d7-8645000102c1865d

Barras, J. A. (2005). Land area changes in coastal Louisiana after Hurricanes Katrina and Rita. *Circular, Science and the Storms: The USGS Response to the Hurricanes of 2005*, 97-112. doi:10.3133/cir13065b

Baumann, R. H., (1980). Mechanisms of maintaining marsh elevation in a subsiding environment. MS thesis, Louisiana State University, Baton Rouge, Louisiana.

Blum, M. D., & Roberts, H. H. (2009). Drowning of the Mississippi Delta due to insufficient sediment supply and global sea-level rise. *Nature Geoscience*, 2(7), 488-491. doi:10.1038/ngeo553

Blum, M. D., & Roberts, H. H. (2012). The Mississippi Delta Region: Past, Present, and Future. *Annual Review of Earth and Planetary Sciences*, 40(1), 655–683. doi: 10.1146/annurev-earth-042711-105248

Bomer, E. J., Bentley, S. J., Hughes, J. E., Wilson, C. A., Crawford, F., & Xu, K. (2019). Deltaic morphodynamics and stratigraphic evolution of middle Barataria Bay and middle Breton Sound regions, Louisiana, USA: Implications for river-sediment diversions. *Estuarine, Coastal and Shelf Science*, 224, 20–33. doi: 10.1016/j.ecss.2019.03.017

Boumans, R. M., & Day, J. W. (1993). High precision measurements of sediment elevation in shallow coastal areas using a sedimentation-erosion table. *Estuaries*, 16(2), 375. doi:10.2307/1352509

Boyd, R., & Penland, S. (1981). Washover of deltaic barriers on Louisiana coast: ABSTRACT. *AAPG Bulletin*, 31, 243-248. doi:10.1306/03b5981e-16d1-11d7-8645000102c1865d

Bridgeman, J.G. 2018. Understanding Mississippi Delta subsidence through stratigraphic and geotechnical analysis of a continuous Holocene core at a subsidence Superstation. MS Thesis, Tulane University

Byrnes, M. R., Britsch, L. D., Berlinghoff, J. L., Johnson, R., & Khalil, S. (2019). Recent subsidence rates for Barataria Basin, Louisiana. *Geo-Marine Letters*, 39(4), 265-278. doi:10.1007/s00367-019-00573-3

Coastal Protection and Restoration Authority of Louisiana. (2012). Louisiana's Comprehensive Master Plan for a Sustainable Coast. *Coastal Protection and Restoration Authority of Louisiana. Baton Rouge, LA.*

Cahoon, D. R., & Turner, R. E. (1989). Accretion and canal impacts in a rapidly subsiding wetland II. Feldspar Marker Horizon Technique. *Estuaries*, 12(4), 260. doi:10.2307/1351905

Cahoon, D., & Reed, D. (1995). Relationships among marsh surface topography, hydroperiod, and soil accretion in a deteriorating Louisiana salt marsh. *Journal of Coastal Research*, 11(2), 357-369.

Cahoon, D. R., Marin, P. E., Black, B. K., & Lynch, J. C. (2000). A Method for measuring vertical accretion, elevation, and compaction of soft, shallow-water sediments. *Journal of Sedimentary Research*, 70(5), 1250-1253. doi:10.1306/020800701250

Cahoon, D. R., Lynch, J. C., Perez, B. C., Segura, B., Holland, R. D., Stelly, C., Stephenson, G., Hensel, P. (2002). High-precision measurements of wetland sediment elevation: II. The Rod Surface Elevation Table. *Journal of Sedimentary Research*, 72(5), 734-739. doi:10.1306/020702720734

Cahoon, D. R., Perez, B. C., Segura, B. D., & Lynch, J. C. (2011). Elevation trends and shrink–swell response of wetland soils to flooding and drying. *Estuarine, Coastal and Shelf Science*, 91(4), 463–474. doi: 10.1016/j.ecss.2010.03.022

Cahoon, D., Reed, D., Day, J., Lynch, J., Swales, A., & Lane, R. (2020). Applications and utility of the surface elevation table–marker horizon method for measuring wetland elevation and shallow soil subsidence-expansion. *Geo-Marine Letters*. doi:10.1007/s00367-020-00656-6

Chabreck, R H., "Vegetation, water and soil characteristics of the Louisiana coastal region" (1972). *LSU Agricultural Experiment Station Reports*. 147. <http://digitalcommons.lsu.edu/agexp/147>

- Chamberlain, E. L., Törnqvist, T. E., Shen, Z., Mauz, B., & Wallinga, J. (2018). Anatomy of Mississippi Delta growth and its implications for coastal restoration. *Science Advances*, 4(4). doi: 10.1126/sciadv.aar4740
- Chapman, V. J. (1960). *Salt marshes and salt deserts of the world*. London: Leonard Hill.
- Chmura, G. L., & Kesters, E. C. (1994). Storm deposition and ¹³⁷Cs accumulation in fine-grained marsh sediments of the Mississippi Delta Plain. *Estuarine, Coastal and Shelf Science*, 39(1), 33-44. doi:10.1006/ecss.1994.1047
- Coastal Protection and Restoration Authority of Louisiana, (2017). Louisiana's Comprehensive Master Plan for a Sustainable Coast. *Coastal Protection and Restoration Authority of Louisiana*. Baton Rouge, LA.
- Coastal Wetlands Planning, Protection, and Restoration Act (2010). Coastwide Reference Monitoring System (CRMS) Factsheet. Retrieved from https://www.lacoast.gov/crms/crms_public_data/publications/CRMS_FactSheet_Web.pdf
- Conner, W. H., Day, J. W., & Pendleton, E. C. (1987). The Ecology of Barataria Basin, Louisiana: An estuarine profile. *Washington, DC: National Wetlands Research Center, U.S. Fish and Wildlife Service, U.S. Dept. of the Interior*.

Conner, W. H., Day, J. W., Baumann, R. H., & Randall, J. M. (1989). Influence of hurricanes on coastal ecosystems along the northern Gulf of Mexico. *Wetlands Ecology and Management*, 1(1), 45-56. doi:10.1007/bf00177889

Couvillion, B.R.; Barras, J.A.; Steyer, G.D.; Sleavin, William; Fischer, Michelle; Beck, Holly; Trahan, Nadine; Griffin, Brad; and Heckman, David, (2011), Land area change in coastal Louisiana from 1932 to 2010: *U.S. Geological Survey Scientific Investigations Map 3164*, scale 1:265,000, 12 p. pamphlet.

Couvillion, B. R., & Beck, H. (2013). Marsh collapse thresholds for coastal Louisiana estimated using elevation and vegetation index data. *Journal of Coastal Research*, 63, 58-67. doi:10.2112/si63-006.1

Couvillion, B.R., Beck, Holly, Schoolmaster, Donald, and Fischer, Michelle, 2017, Land area change in coastal Louisiana 1932 to 2016: U.S. Geological Survey Scientific Investigations Map 3381, 16 p. pamphlet, <https://doi.org/10.3133/sim3381>.

Couvillion, B.R., (2018), Land area in coastal Louisiana (1932 to 2016) - land area spatial data - multi-date composites for specific years: *U.S. Geological Survey data release*, <https://doi.org/10.5066/P99LJJZZ>.

Craig, N. J., Turner, R. E., & Day Jr., J. W. (1979). Land loss in coastal Louisiana (U.S.A.). *Environmental Management*, 3(2), 133-144. doi:10.1007/BF01867025

Das, A., Justic, D., Inoue, M., Hoda, A., Huang, H., & Park, D. (2012). Impacts of Mississippi River diversions on salinity gradients in a deltaic Louisiana estuary: Ecological and management implications. *Estuarine, Coastal and Shelf Science*, *111*, 17-26. doi:10.1016/j.ecss.2012.06.005

Day, J. W., Britsch, L. D., Hawes, S. R., Shaffer, G. P., Reed, D. J., & Cahoon, D. (2000). Pattern and process of land loss in the Mississippi Delta: A spatial and temporal analysis of wetland habitat change. *Estuaries*, *23*(4), 425. doi: 10.2307/1353136

Deegan, L., Kennedy, H., & Costanza, R. (1983). Factors contributing to marsh land loss in Louisiana's Coastal zone. Developments in environmental modelling analysis of ecological systems. *State-of-the-Art in Ecological Modelling*, *5*, 915-919. doi:10.1016/b978-0-444-42179-1.50103-6

Deegan, L. A., Day, J. W., Gosselink, J. G., Yáñez-Arancibia, A., Chávez, G. S., & Sánchez-Gil, P. (1986). Relationships among physical characteristics, vegetation distribution and fisheries yield in Gulf of Mexico estuaries. *Estuarine Variability*, 83-100. doi:10.1016/b978-0-12-761890-6.50010-1

Delaune, R. D., Patrick, W. H., & Buresh, R. J. (1978). Sedimentation rates determined by ¹³⁷Cs dating in a rapidly accreting salt marsh. *Nature*, *275*(5680), 532–533. doi: 10.1038/275532a0

Delaune, R. D., Baumann, R. H., & Gosselink, J. G. (1983). Relationships among Vertical Accretion, Coastal Submergence, and Erosion in a Louisiana Gulf Coast Marsh. *SEPM Journal of Sedimentary Research*, Vol. 53. doi: 10.1306/212f8175-2b24-11d7-8648000102c1865d

Delaune, R. D., Nyman, J. A., & Patrick, W. H. (1994). Peat collapse, ponding and wetland loss in a rapidly submerging coastal marsh. *Journal of Coastal Research*, 10(4), 1021–1030.

Delaune, R. D., Jugsujinda, A., Peterson, G. W., & Patrick, W. H. (2003). Impact of Mississippi River freshwater reintroduction on enhancing marsh accretionary processes in a Louisiana estuary. *Estuarine, Coastal and Shelf Science*, 58(3), 653–662. doi: 10.1016/s0272-7714(03)00177-x

Dixon, T. H., Amelung, F., Ferretti, A., Novali, F., Rocca, F., Dokka, R., ... Whitman, D. (2006). Subsidence and flooding in New Orleans. *Nature*, 441(7093), 587–588. doi: 10.1038/441587a

Dokka, R. K., Sella, G. F., & Dixon, T. H. (2006). Tectonic control of subsidence and southward displacement of southeast Louisiana with respect to Stable North America. *Geophysical Research Letters*, 33(23). Doi: 10.1029/2006GL027250

Dokka, R. K. (2011). The role of deep processes in late 20th century subsidence of New Orleans and coastal areas of southern Louisiana and Mississippi. *Journal of Geophysical Research*, 116(B6). doi: 10.1029/2010jb008008

Evers, D. E., Gosselink, J. G., Sasser, C. E., & Hill, J. M. (1992). Wetland loss dynamics in southwestern Barataria basin, Louisiana (USA), 1945-1985. *Wetlands Ecology and Management*, 2(3), 103–118. doi: 10.1007/bf00215318

Fitzgerald, D. M., Kulp, M., Penland, S., Flocks, J., & Kindinger, J. (2004). Morphologic and stratigraphic evolution of muddy ebb-tidal deltas along a subsiding coast: Barataria Bay, Mississippi River delta. *Sedimentology*, 51(6), 1157–1178. doi: 10.1111/j.1365-3091.2004.00663.x

Fitzgerald, D., Kulp, M., Hughes, Z., Georgiou, I., Miner, M., Penland, S., & Howes, N. (2007). Impacts of rising sea level to backbarrier wetlands, tidal inlets, and barrier islands: Barataria coast, Louisiana. *Coastal Sediments*. doi: 10.1061/40926(239)91

Frazier, D. E. (1967). Recent deltaic deposits of the Mississippi River: their development and chronology: ABSTRACT. *Transactions- Gulf Coastal Association of Geological Societies*, 17.

Frazier, D. E., & Osanik, A. (1969). Recent peat deposits-Louisiana Coastal Plain. Geological Society of America Special Papers Environments of Coal Deposition: *Papers Presented at a Symposium by the Coal Geology Division of The Geological Society of America at the Annual Meeting Miami Beach, Florida, 1964*, 63–86. doi: 10.1130/spe114-p63

Gaglinao, S. M., Kemp, E. B., Wicker, K. M., Wiltenmuth, K. S., & Sabate, R. W. (2003). Neo-Tectonic Framework of Southeast Louisiana and Applications to Coastal Restoration. *GCAGS/GCSSEPM Transactions*, 53, 262–276.

Gleason, M. L., Elmer, D. A., Pien, N. C., & Fisher, J. S. (1979). Effects of Stem Density upon Sediment Retention by Salt Marsh Cord Grass, *Spartina alterniflora* Loisel. *Estuaries*, 2(4), 271. doi: 10.2307/1351574

González, J. L., & Tornqvist, T. E. (2006). Coastal Louisiana in crisis: Subsidence or sea level rise? *Eos, Transactions American Geophysical Union*, 87(45), 493. doi: 10.1029/2006eo450001

Hatton, R. S., Delaune, R. D., & Patrick, W. H. (1983). Sedimentation, accretion, and subsidence in marshes of Barataria Basin, Louisiana. *Limnology and Oceanography*, 28(3), 494–502. doi: 10.4319/lo.1983.28.3.0494

He, Q., & Walling, D. E. (1996). Use of Fallout Pb-210 Measurements to Investigate Longer-Term Rates and Patterns of Overbank Sediment Deposition on the Floodplains of Lowland Rivers. *Earth Surface Processes and Landforms*, 21(2), 141-154.

doi:10.1002/(sici)1096-9837(199602)21:23.0.co;2-9

Hijma, M. P., Shen, Z., Törnqvist, T. E., & Mauz, B. (2017). Late Holocene evolution of a coupled, mud-dominated delta plain–chenier plain system, coastal Louisiana, USA.

Earth Surface Dynamics, 5(4), 689-710. doi:10.5194/esurf-5-689-2017

Holm, G. O., Sasser, C. E., Peterson, G. W., & Swenson, E. M. (2000). Vertical Movement and Substrate Characteristics of Oligohaline Marshes Near a High-Sediment, Riverine System. *Journal of Coastal Research*, 16(1), 164–171.

Hopkinson, C. S., Gosselink, J. G., & Parrando, R. T. (1978). Aboveground Production of Seven Marsh Plant Species in Coastal Louisiana. *Ecology*, 59(4), 760-769.

doi:10.2307/1938780

Howes, B., & Goehringer, D. (1994). Porewater drainage and dissolved organic carbon and nutrient losses through the intertidal creek-banks of a New England salt

marsh. *Marine Ecology Progress Series*, 114, 289–301. doi: 10.3354/meps114289

Inoue, M., Park, D., Justic, D., & Wiseman, W. (2008). A high-resolution integrated hydrology-hydrodynamic model of the Barataria Basin system. *Elsevier: Environmental Modelling & Software*, 23, 1122–1132. doi: 10.1109/oceans.2002.1191857

Jankowski, K.L., Törnqvist, T.E., Fernandes, A.M., (2017). Vulnerability of Louisiana's coastal wetlands to present-day rates of relative sea-level rise. *Nature Communications*, 8, 14792. doi: 10.1038/ncomms14792

Jones, C. E., An, K., Blom, R. G., Kent, J. D., Ivins, E. R., & Bekaert, D. (2016). Anthropogenic and geologic influences on subsidence in the vicinity of New Orleans, Louisiana. *Journal of Geophysical Research: Solid Earth*, 121(5), 3867–3887. doi: 10.1002/2015jb012636

Keogh, M. E., & Törnqvist, T. E. (2019). Measuring rates of present-day relative sea-level rise in low-elevation coastal zones: a critical evaluation. *Ocean Science*, 15(1), 61–73. doi: 10.5194/os-15-61-2019

Koegh, M. E., Kolker, A. S., Snedden, G. A., & Renfro, A. A. (2019). Hydrodynamic controls on sediment retention in an emerging diversion-fed delta. *Geomorphology*, 332, 100–111. doi: 10.1016/j.geomorph.2019.02.008

Kennish, M. (2001). Coastal Salt Marsh Systems in the U.S.: A Review of Anthropogenic Impacts. *Journal of Coastal Research*, 17(3), 731-748.

Kesel, R. H., (1988). The decline in the suspended load of the Lower Mississippi River and its influence on adjacent wetlands. *Environmental Geology and Water Sciences*, 11(3), p 271-281. Doi: 10.1007/bf02574816

Kesel, R. H. (1989). The role of the Mississippi River in wetland loss in southeastern Louisiana, U.S.A. *Environmental Geology and Water Sciences*, 13(3), 183–193. doi: 10.1007/bf01665368

Kolker, A. S., Allison, M. A., & Hameed, S. (2011). An evaluation of subsidence rates and sea- Level variability in the Northern Gulf of Mexico. *Geophysical Research Letters*, 38. doi: 10.1029/2011GL049458

Kosters, E. C. (1989). Organic-clastic facies relationships and chronostratigraphy of the Barataria Interlobe Basin, Mississippi Delta Plain. *Journal of Sedimentary Research*, 59. doi: 10.1306/212f8f2b-2b24-11d7-8648000102c1865d

Kosters, E. C., & Suter, J. R. (1993). Facies relationships and systems tracts in the Late Holocene Mississippi Delta Plain. *Journal of Sedimentary Research*, 63(4), 727–733. doi: 10.1306/d4267bcc-2b26-11d7-8648000102c1865d

Ken W. Krauss, Chambers, J., Allen, J., David M. Soileau Jr., & Antoinette S. DeBosiert. (2000). Growth and Nutrition of Baldcypress Families Planted under Varying Salinity

Regimes in Louisiana, USA. *Journal of Coastal Research*, 16(1), 153-163. Retrieved July 31, 2020, from www.jstor.org/stable/4300020

Louisiana Comprehensive Wildlife Conservation Strategy (LA CWCS) (2005). Conservation Habitats & Species Assessments. Retrieved from <https://www.archive.wlf.louisiana.gov>

Li, C., White, J. R., Chen, C., Lin, H., Weeks, E., Galvan, K., & Bargu, S. (2011). Summertime tidal flushing of Barataria Bay: Transports of water and suspended sediments. *Journal of Geophysical Research*, 116(C4). doi: 10.1029/2010jc006566

Lynch, J. C., Meriwether, J. R., Mckee, B. A., Vera-Herrera, F., & Twilley, R. R. (1989). Recent Accretion in Mangrove Ecosystems Based on 137 Cs and 210 Pb. *Estuaries*, 12(4), 284-299. doi: 10.2307/1351907

Marmer, H. A. (1948), The currents in Barataria Bay, report, 30 pp., *Tex. A&M Res. Found., College Station, Tex.*

Meckel, T. (2008). An attempt to reconcile subsidence rates determined from various techniques in southern Louisiana. *Quaternary Science Reviews*, 27(15-16), 1517–1522. doi: 10.1016/j.quascirev.2008.04.013

McCook, D. 1991. Measurement and estimation of permeability of soils for animal waste storage facility design. (No. 717) *USDA*, SCS. http://www.nrcs.usda.gov/Internet/FSE_DOCUMENTS/nrcs141p2_024050.pdf

Mitsch, W. J., & Gosselink, J. G. (2015). *Wetlands* (5th ed.). Hoboken, NJ: John Wiley and Sons, Inc.

Morris, J. T., Sundareshwar, P. V., Nietch, C. T., Kjerfve, B., & Cahoon, D. R. (2002). Responses of Coastal Wetlands to Rising Sea Level. *Ecology*, 83(10), 2869–2877.

Morton, R. A., Buster, N. A., & Krohn, M. D. (2002). Subsurface Controls on Historical Subsidence Rates and Associated Wetland Loss in Southcentral Louisiana. Southcentral Louisiana: *Transactions Gulf Coast Association of Geological Societies*, 52, 767–778.

Morton, R. A., & Bernier, J. C. (2010). Recent subsidence-rate reductions in the Mississippi Delta and their geological implications. *Journal of Coastal Research*, 263, 555–561. doi: 10.2112/jcoastres-d-09-00014r1.1

Morton, R. A., & Barras, J. A. (2011). Hurricane Impacts on Coastal Wetlands: A Half-Century Record of Storm-Generated Features from Southern Louisiana. *Journal of Coastal Research*, 27(6A), 27–43. doi: 10.2112/JCOASTRES-D-10-00185.1

Nelson, S. A. C., Soranno, P. A., & Qi, J. (2002). Land-cover change in upper Barataria Basin estuary, Louisiana, 1972-1992: Increases in wetland area. *Environmental Management*, 29(5), 716–727. doi: 10.1007/s00267-001-0060-9

Nienhuis, J. H. (2017). A new subsidence map for coastal Louisiana. *GSA Today*. doi: 10.1130/gsatg337gw

Nittrouer, C., Sternberg, R., Carpenter, R., & Bennett, J. (1979). The use of Pb-210 geochronology as a sedimentological tool: application to the Washington continental shelf. *Marine Geology*, 31(3-4), 297–316. doi: 10.1016/0025-3227(79)90039-2

Nuttle, W. K., Hemond, H. F., (1988). Salt marsh hydrology: implications for biogeochemical fluxes to the atmosphere and estuaries. *Global Biogeochemical Cycles* 2, p. 91-114

Nyman, J. A., DeLaune, R. D., & Patrick, W. H. (1990). Wetland soil formation in the rapidly subsiding Mississippi River Deltaic Plain: mineral and organic Matter Relationships. *Estuarine, Coastal and Shelf Science*, 31, 57–69.

Nyman, J., Delaune, R., Roberts, H., & Patrick, W. (1993). Relationship between vegetation and soil formation in a rapidly submerging coastal marsh. *Marine Ecology Progress Series*, 96, 269–279. doi: 10.3354/meps096269

Nyman, J. A., Delaune, R. D., Pezeshki, S. R., Patrick Jr, W. H. (1995). Organic matter fluxes and marsh stability in a rapidly submerging estuarine marsh. *Estuaries* 18, 207-218

Nyman, J. A., Walters, R. J., Delaune, R. D., & Patrick, W. H. (2006). Marsh vertical accretion via vegetative growth. *Estuarine, Coastal and Shelf Science*, 69(3-4), 370–380.
doi: 10.1016/j.ecss.2006.05.041

O'Neil, T. (1949). *The muskrat in the Louisiana coastal marshes: A study of the ecological, geological, biological, tidal, and climatic factors governing the production and management of the muskrat industry in Louisiana*. New Orleans: Federal Aid Section, Fish and Game Division, Louisiana Dept. of Wildlife and Fisheries.

Ortiz, A. C., Roy, S., & Edmonds, D. A. (2017). Land loss by pond expansion on the Mississippi River Delta Plain. *Geophysical Research Letters*, 44(8), 3635-3642.
doi:10.1002/2017gl073079

Payandeh, A., Justic, D., Mariotti, G., Huang, H., & Sorourian, S. (2019). Subtidal Water Level and Current Variability in a Bar-Built Estuary During Cold Front Season: Barataria Bay, Gulf of Mexico. *Journal of Geophysical Research: Oceans*, 124(10), 7226–7246.
doi: 10.1029/2019jc015081

Pennington, W., Tutin, T. G., Cambray, R. S., & Fisher, E. M. (1973). Observations on Lake Sediments using Fallout ¹³⁷Cs as a tracer. *Nature*, *242*(5396), 324-326. Doi: 10.1038/242324a0

Penland, S., & Ramsey, K. (1990) Relative sea-level rise in Louisiana and the Gulf of Mexico: 1908-1988. *Journal of Coastal Research*, *6*(2), 323–342.

Penland, S., Wayne, L., Britsch, L., Williams, S. J., Beall, A. D., & Butterworth, V. C. (2002). Geomorphic classification of coastal land loss between 1932 and 1990 in the Mississippi River delta plain, southeastern Louisiana. *Gulf Coast Association of Geological Societies Transactions*, *52*, 799–807. doi: 10.3133/ofr00417

Reed, D. J. (1989). Patterns of sediment deposition in subsiding coastal salt marshes, Terrebonne Bay, Louisiana: The role of winter storms. *Estuaries*, *12*(4), 222–227.

Reed, D. J. (1995). The response of coastal marshes to sea-level rise: Survival or submergence? *Earth Surface Processes and Landforms*, *20*(1), 39–48. doi: 10.1002/esp.3290200105

Reed, D. J. (2002). Sea-level rise and coastal marsh sustainability: geological and ecological factors in the Mississippi delta plain. *Geomorphology*, *48*(1-3), 233–243. doi: 10.1016/s0169-555x(02)00183-6

Rieley, j O. (2007). Tropical peatland - The amazing dual ecosystem: coexistence and mutual benefit. In: *Proceedings of the International Symposium and Workshop on Tropical Peatland*, pp. 1–14. School of Geography, University of Nottingham, Nottingham, NG72RD, UK doi: 10.1.1.528.8670

Roberts, H. H., Bailey, A., & Kuecher, G. J. (1994). Subsidence in the Mississippi River Delta--Important Influences of Valley Filling by Cyclic Deposition, Early Diagenesis, and Primary Consolidation Phenomena, and Early Diagenesis. *Transactions of the Gulf Coast Association of Geological Societies, XLIV*, 619–629.

Rogers, J. D. (2006). History of the New Orleans Flood Protection System. Chapter Four. *Independent Levee Investigation Team Report*, Louisiana State University

Salinas, L. M., DeLaune, R. D., & Patrick, W. H. (1986). Changes Occurring along a Rapidly Submerging Coastal Area: Louisiana, USA. *Journal of Coastal Research*, 2(3), 269–284.

Sasser, C. E., Dozier, M. D., Gosselink, J. G., & Hill, J. M. (1986). Spatial and temporal changes in Louisiana's Barataria Basin marshes, 1945–1980. *Environmental Management*, 10(5), 671–680. doi: 10.1007/bf01866771

Sasser, C., Gosselink, J., Swenson, E., & Evers, D. (1995). Hydrologic, vegetation, and substrate characteristics of floating marshes in sediment-rich wetlands of the Mississippi river delta plain, Louisiana, USA. *Wetlands Ecology and Management*, 3(3). doi: 10.1007/bf00180023

Scaife, W. W., Turner, R. E., & Costanza, R. (1983). Coastal Louisiana Recent Land Loss and Canal Impacts. *Environmental Management*, 7 (5) pp 433-442

Schothorst, C. J., (1982). Drainage and behavior of peat soils. In: Proc. Symp. On Peat lands below Sea Level. *Institute for Land and Water Management Research Publ. 30*, Wageningen, The Netherlands, pp. 130-163

Shen, Z., Törnqvist, T. E., Mauz, B., Chamberlain, E. L., Nijhuis, A. G., & Sandoval, L. (2015). Episodic overbank deposition as a dominant mechanism of floodplain and delta-plain aggradation. *Geology*, 43(10), 875–878. doi: 10.1130/g36847.1

Shen, Z., Dawers, N. H., Törnqvist, T. E., Gasparini, N. M., Hijma, M. P., & Mauz, B. (2016). Mechanisms of late Quaternary fault throw-rate variability along the north central Gulf of Mexico coast: implications for coastal subsidence. *Basin Research*, 29(5), 557–570. doi: 10.1111/bre.12184

Smith III, T. J., Cahoon, D. R., (2003). Wetland sediment elevation in the Florida Everglades: response to surface water stage variation. In: Proceedings of the International Conference on Coastal Sediments 2003. *World Scientific Publishing Corp.*, East Meets West Productions, Clearwater Beach, FL.

Snowden, J. O., Simmons, B., Traugher, E. B., & Stephens, R. W. (1977). Differential Subsidence of Marshland Peat as Geologic Hazard in Greater New Orleans Area, Louisiana: Abstract. *AAPG Bulletin*, 61. doi: 10.1306/c1ea4680-16c9-11d7-8645000102c1865d

Stagg, C. L., Schoolmaster, D. R., Piazza, S. C., Snedden, G., Steyer, G. D., Fischenich, C. J., & Mccomas, R. W. (2016). A Landscape-Scale Assessment of Above- and Belowground Primary Production in Coastal Wetlands: Implications for Climate Change-Induced Community Shifts. *Estuaries and Coasts*, 40(3), 856–879. doi: 10.1007/s12237-016-0177-y

Stanley, D. J., & Warne, A. G. (1994, July 8). Worldwide Initiation of Holocene Marine Deltas by Deceleration of Sea- Level Rise. *Science*, 265(5169), 228-231. Doi: 10.1126/science.265.5169.288

Stewart, J. M., (1994). Subsidence in cultivated peatlands. In: B.Y. Aminuddin (Editor), Tropical Peat; Proc. *Int. Symp. On Tropical Peatland*, 6-10 May 1991, Kuching, Sawarak, Malaysia.

Stumpf, R. P. (1983). The process of sedimentation on the surface of a salt marsh. *Estuarine, Coastal and Shelf Science*, 17(5), 495–508. doi: 10.1016/0272-7714(83)90002-1

Syvitski, J. P., Kettner, A. J., Overeem, I., Hutton, E. W., Hannon, M. T., Brakenridge, G. R., Day, J., Vörösmarty, C., Saito, Y., Giosan, L., Nicholls, R. J. (2009). Sinking deltas due to human activities. *Nature Geoscience*, 2(10), 681-686. doi:10.1038/ngeo629

Todd M. Folse, Leigh A. Sharp, Jonathan L. West, Melissa K. Hymel, John P. Troutman, Thomas E. McGinnis, Dona Weifenbach, William M. Boshart, Laurie B. Rodrigue, Danielle C. Richardi, W. Bernard Wood, and C. Mike Miller. 2008, revised 2014. A Standard Operating Procedures Manual for the Coastwide Reference Monitoring System-Wetlands: Methods for Site Establishment, Data Collection, and Quality Assurance/Quality Control. *Louisiana Coastal Protection and Restoration Authority*. Baton Rouge, LA. 228 pp.

Törnqvist, T. E., Kidder, T. R., Autin, W. J., Borg, K. V., Jong, A. F., Klerks, C. J., Snijders, M.A., Storms, J., Dam, R., Wiemann, M. C. (1996). A Revised Chronology for Mississippi River Subdeltas. *Science*, 273(5282), 1693-1696. doi:10.1126/science.273.5282.1693

Törnqvist, T. E., Jankowski, K. L., Yong-Xiang Li, González, J. L. (2020). Tipping points of Mississippi Delta marshes due to accelerated sea-level rise. *Science. Advances*. 6, eaaz5512

Turner, R. E., R. Costanza, and W.W Scaife. (1982). Canals and wetland erosion rates in coastal Louisiana. Pages 73-84 in D.F. Boesch, ed. *Proceedings Conference on Coastal Erosion and Wetland Modification in Louisiana: Causes, Consequences, and Options*. U.S. Fish Wildlife. Ser. Biol. Serv. Program, Report FWS/OBS-82/59.

Van Asselen, S., Karssenber, D., & Stouthamer, E. (2011). Contribution of peat compaction to relative sea-level rise within Holocene deltas. *Geophysical Research Letters*, 38(24). doi: 10.1029/2011GL049835,

Van Asselen, S., Stouthamer, E., & Asch, T. V. (2009). Effects of peat compaction on delta evolution: A review on processes, responses, measuring and modeling. *Earth-Science Reviews*, 92(1-2), 35–51. doi: 10.1016/j.earscirev.2008.11.001

Visser, J. M., Sasser, C. E., Chabreck, R. H., Linscombe, R. G., (2002). The impact of a severe drought on the vegetation of a subtropical estuary. *Estuaries* 25:1184-1195.
Doi:10.1007/BF02692215

Visser, J. M., Duke-Sylvester, S. M., Carter, J., & Broussard, W. P. (2013). A Computer Model to Forecast Wetland Vegetation Changes Resulting from Restoration and Protection in Coastal Louisiana. *Journal of Coastal Research*, 67, 51–59. doi: 10.2112/si_67_4

Whelan, K. R. T., Smith III, T.J., Cahoon, D.R., Lynch J.C., Anderson, G.H., (2005). Groundwater control of mangrove surface elevation: shrink and swell varies with soil depth. *Estuaries* 28, p. 833-843

Wilson, C. A., & Allison, M. A. (2008). An equilibrium profile model for retreating marsh shorelines in southeast Louisiana. *Estuarine, Coastal and Shelf Science*, 80(4), 483–494. doi: 10.1016/j.ecss.2008.09.004

Wilson, A. M., & Gardner, L. R. (2006). Tidally driven groundwater flow and solute exchange in a marsh: Numerical simulations. *Water Resources Research*, 42(1). doi:10.1029/2005wr004302

Wiseman, W. J., Swenson, E. M., & Power, J. (1990). Salinity trends in Louisiana estuaries. *Estuaries* 13(3), 265-271

Wösten, J., Ismail, A., & Wijk, A. V. (1997). Peat subsidence and its practical implications: a case study in Malaysia. *Geoderma*, 78(1-2), 25–36. doi: 10.1016/s0016-7061(97)00013-x

Xin, P., Kong, J., Li, L., & Barry, D. (2012). Effects of soil stratigraphy on pore-water flow in a creek-marsh system. *Journal of Hydrology*, 475, 175–187. doi: 10.1016/j.jhydrol.2012.09.047

Yu, S.-Y., Törnqvist, T. E., & Hu, P. (2012). Quantifying Holocene lithospheric subsidence rates underneath the Mississippi Delta. *Earth and Planetary Science Letters*, 331-332, 21–30. doi: 10.1016/j.epsl.2012.02.021

Yuill, B., Lavoie, D., & Reed, D. J. (2009). Understanding Subsidence Processes in Coastal Louisiana. *Journal of Coastal Research*, 10054, 23–36. doi: 10.2112/si54-012.1
10.2112/si54-012.1